KTC

KENTUCKY TRANSPORTATION CENTER

SEISMIC EVALUATION OF THE CUMBERLAND RIVER BRIDGES ON I-24 IN WESTERN KENTUCKY

UK

UNIVERSITY OF KENTUCKY

College of Engineering

KTC

OUR MISSION

We provide services to the transportation community
through research, technology transfer and education.
We create and participate in partnerships
to promote safe and effective
transportation systems.

OUR VALUES

Teamwork
Listening and communicating along with
courtesy and respect for others.

Honesty and Ethical Behavior
Delivering the highest quality
products and services.

Continuous Improvement
In all that we do.

Research Report
KTC-06-25/SPR206-00-6F

SEISMIC EVALUATION OF THE CUMBERLAND RIVER BRIDGES ON I-24 IN WESTERN KENTUCKY

(KYSPR206-00-6F)

By

Wael A. Zatar
Research Professor, Kentucky Transportation Center

Wei-Xin Ren
Former Visiting Professor, Kentucky Transportation Center

Issam E. Harik
Professor of Civil Engineering and Head, Structures Section,
Kentucky Transportation Center

Kentucky Transportation Center
College of Engineering, University of Kentucky

In cooperation with

Transportation Cabinet
Commonwealth of Kentucky

and

Federal Highway Administration
U.S. Department of Transportation

September 2006

Technical Report Documentation Page

1. Report No. KTC-06-25/SPR206-00-6F	2. Government Accession No.	3. Recipient's Catalog No.
4. Title and Subtitle **SEISMIC EVALUATION OF THE CUMBERLAND RIVER BRIDGES ON I-24 IN WESTERN KENTUCKY**		5. Report Date September 2006
		6. Performing Organization Code
7. Author(s) Wael Zatar, Wei-Xin Ren, and Issam E. Harik		8. Performing Organization Report No. KTC-06-25/SPR206-00-6F
9. Performing Organization Name and Address Kentucky Transportation Center College of Engineering University of Kentucky Lexington, Kentucky 40506-0281		10. Work Unit No. (TRAIS)
		11. Contract or Grant No. KYSPR-206
12. Sponsoring Agency Name and Address Kentucky Transportation Cabinet State Office Building Frankfort, Kentucky 40622		13. Type of Report and Period Covered Final
		14. Sponsoring Agency Code
15. Supplementary Notes Prepared in cooperation with Kentucky Transportation Cabinet		

16. Abstract

   The main objective of this study is to assess the structural integrity of the I-24 parallel bridges at the Cumberland River crossing in western Kentucky. Due to its importance, the bridge is evaluated for the 250-year event and the maximum credible 500-year event. The scope of the work included: 1) Field testing of the main bridge; 2) Finite element modeling and calibration; 3) Time-history seismic response analysis for the main spans; and 4) Seismic evaluation for both the main and the approach spans.

   The seismic analysis for the 250-year event indicates that the main spans of the bridge can resist the event without yielding or loss-of-span at the supports. However, the anchor bolts on some of the piers are expected to fail in shear.   Retrofitting measures are recommended.

   The seismic analysis for the 500-year event shows that few members of the main spans would yield due to the event. Also, the capacity of the bearing shear bolts of few piers of the main and approach spans are exceeded, and retrofitting measures are recommended.

17. Key Words I-24, bridges, seismic vulnerability, seismic evaluation	18. Distribution Statement Unlimited with the approval of Kentucky Transportation Cabinet		
19. Security Classif. (of this report) Unclassified	20. Security Classif. (of this page) Unclassified	21. No. of Pages 135	22. Price

Form DOT 1700.7 (8-72) Reproduction of Completed Page Authorized

EXECUTIVE SUMMARY

Background

The need for evaluating the seismic adequacy of the existing infrastructure has come into focus following the damage and collapse of numerous bridges during recent earthquakes. For instance, the 1989 Loma Prieta earthquake and 1994 Northridge earthquake brought to the public's attention the seismic risks to bridges and elevated freeway structures. In particular, the seismic evaluation and rehabilitation of older bridges in regions of high seismicity, which were designed prior to the advent of modern seismic design codes, and have not yet been subjected to a severe earthquake, is a matter of growing concern. Many bridges in Kentucky were constructed in accordance with old code requirements that had inadequate provisions for earthquake loading.

Research Objectives

The main objective of this investigation is to assess the structural integrity of the I-24 parallel bridges at the Cumberland River crossing and the borders of Lyons and Livingston counties in western Kentucky (Figures E-1 and E-2). Due to its importance, the bridge is to be evaluated for the 250-year event and the maximum credible 500-year event. The 250-year and the 500-year events are events that have a 90 % probability of not being exceeded in 250 years and 500 years, respectively. During a 250-year event, the bridge is to remain in the elastic range without any disruption to traffic. During a 500-year event, partial damage will be permitted to the bridge, but it is to remain accessible to emergency and official vehicles. To achieve this objective, the scope of the work was divided into the following tasks: 1) Field testing of the main bridge; 2) Finite element modeling and calibration; 3) Time-history seismic response analysis; and 4) Seismic evaluation/retrofit for both the main and the approach spans of the bridges.

Field Testing of the Main Spans

The free vibration properties of the main bridge were determined through field ambient vibration testing under traffic and wind induced excitation. The purpose of the field-testing was to determine the natural frequencies and the associated mode shapes. The vibration properties were subsequently used as the basis for calibrating a finite element model that was created for seismic response analysis.

Finite Element Modeling of the Main Spans

A three-dimensional finite element model of the main bridge was used for free vibration and seismic response analysis. The model was calibrated by comparing the free vibration analysis results with the ambient vibration properties obtained from field-testing.

Seismic Evaluation of the Main Spans

After calibration of the main spans, the model was used for seismic response analysis. The three-dimensional model of the main bridge was subjected to the time histories of the projected 250-year and 500-year event to determine maximum displacements at joints, stresses in members, and forces on the bearings.

Seismic Evaluation of the Approach Spans

Simple structural models are used to idealize the approach spans depending on the type of the bearings, which are mounted on the top of the piers. The mathematical models are considered as single degree of freedom (*SDOF*) systems. The mass of the *SDOF* system is the summation of the mass of the superstructure and one-third the mass of the piers. The transverse stiffness and longitudinal stiffness of the mathematical model are calculated in accordance with the Seismic Evaluation and Retrofit of Bridges (Harik et al., 1997). Seismic response of the approach spans was carried out using the response spectrum method to determine the maximum forces and displacements.

Conclusions and Recommendations

250-Year Event

The seismic analysis indicates that the main spans of the bridge can resist the 250-year event without yielding or loss-of-span at supports. Consequently, retrofitting is not required for the main bridge members and bearings for the 250-year event (Fig. E-3).

The seismic analysis of the approach spans indicates that pier 1 can resist the 250-year event without yielding or unseating at supports. Consequently, no retrofitting is required. However, the anchor bolts of pier #2 cannot resist the applied shear forces during the 250-year and retrofit should be considered. Retrofitting can be made by increasing the capacity of the shear bolts or by providing seismic isolation bearings (Fig. E-4).

500-Year Event

The seismic analysis indicates that the bridge members # 212 (shown in Fig. E-5) of the main spans would yield due to the 500-year maximum credible event. The bearing shear bolts of both pier #4 and pier #5 would fail (Fig. E-6). Thus, retrofit has to be provided for these members and bearings. Retrofitting can be made by increasing the capacity of the shear bolts or by providing seismic isolation bearings.

The seismic analysis of the approach spans indicates that pier #1 can resist the 500-year event without yielding or unseating at supports. Consequently, no retrofitting is required. The seismic analysis of the approach spans indicates that the anchor bolts of pier #2 cannot resist the applied shear forces during the 500-year event, and retrofit should be considered (Fig. E-7). Retrofitting can be made by increasing the capacity of the shear bolts or by providing seismic isolation bearings.

NOTE: This report is the sixth (6th) in a series of seven reports for Project SRP 206: "Seismic Evaluation of I-24 Bridges". The seven reports are:	
Report Number:	**Report Title:**
(1) KTC-06-20/SPR206-00-1F	Seismic Evaluation of I-24 Bridges and Embankments in Western Kentucky – Summary Report
(2) KTC-06-21/SPR206-00-2F	Site Investigation of Bridges along I-24 in Western Kentucky
(3) KTC-06-22/SPR206-00-3F	Preliminary Seismic Evaluation and Ranking of Bridges along I-24 in Western Kentucky
(4) KTC-06-23/SPR206-00-4F	Detailed Seismic Evaluation of Bridges along I-24 in Western Kentucky
(5) KTC-06-24/SPR206-00-5F	Seismic Evaluation of the Tennessee River Bridges on I-24 in Western Kentucky
(6) KTC-06-25/SPR206-00-6F[*]	Seismic Evaluation of the Cumberland River Bridges on I-24 in Western Kentucky
(7) KTC-06-26/SPR206-00-7F	Seismic Evaluation and Ranking of Bridge Embankments along I-24 in Western Kentucky

* Denotes current report

Figure E-1 The Cumberland River Bridge

Figure E-2 Side view of the Cumberland River Bridge

Note: Capacity of bridge members and bearings of the main spans exceed demand. Consequently, no retrofit is required.

Figure E-3 Condition the of members and bearings of the main spans of the Cumberland River Bridges during the 250-year event

Bearings of Pier #2
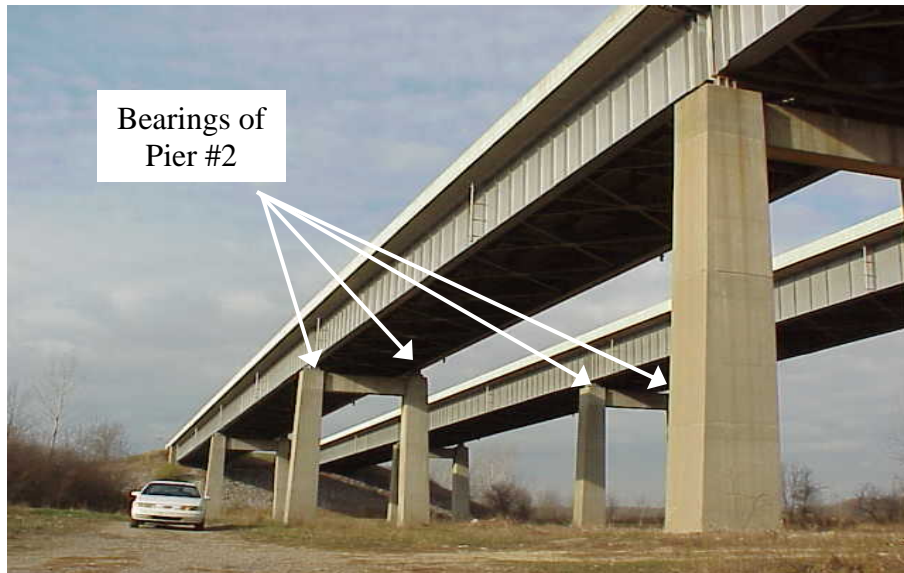
Note: Capacity of bridge members of the approach spans exceeds demand. Consequently, no retrofit is required. Demand of bearings for pier #2 of the approach spans exceeds capacity. Consequently, retrofitting of bearings for pier #2 is required by increasing the anchor bolts capacity or using seismic isolation bearings.

Figure E-4 Condition of the members and bearings of the approach spans of the Cumberland River Bridges during the 250-year event
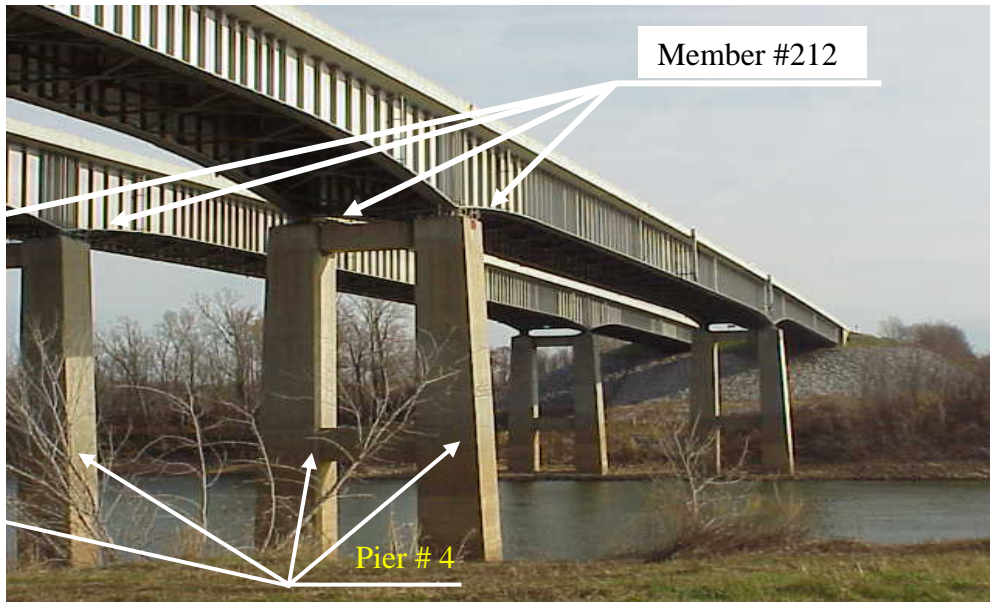
Note: Capacity of all bridge members #212 of the main spans exceed demand. Consequently retrofitting these members is required.

Figure E-5 Condition of the members of the main spans of the Cumberland River Bridges during the 500-year event
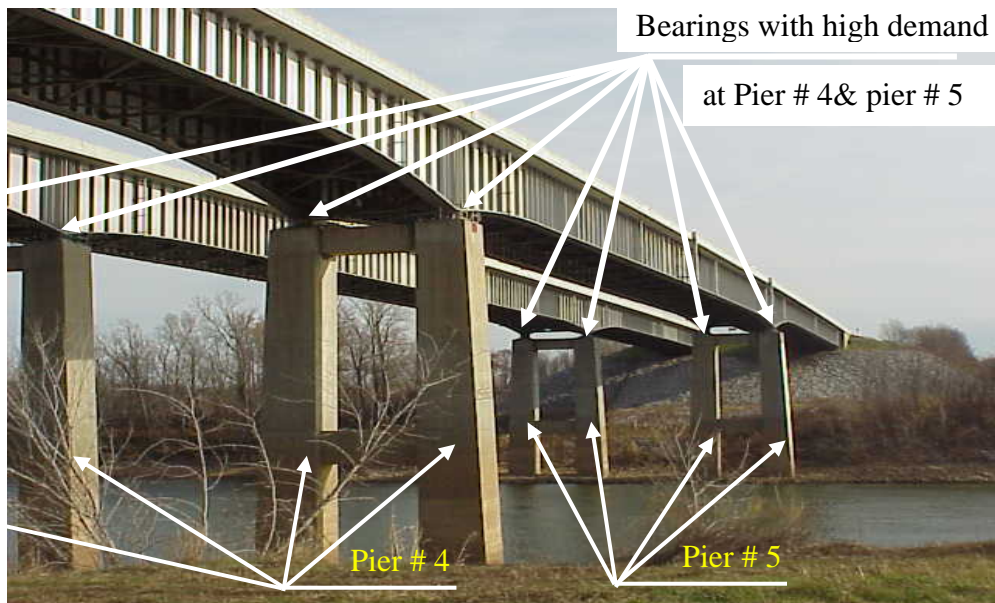
Demand of bearings for pier #4 and pier #5 of the main spans exceeds capacity. Consequently, retrofitting of bearings for pier #4, #5 is required by increasing the anchor bolts capacity or using seismic isolation bearings.

Figure E-6 Condition the bearings of the main spans of the Cumberland River Bridges during the 500-year event
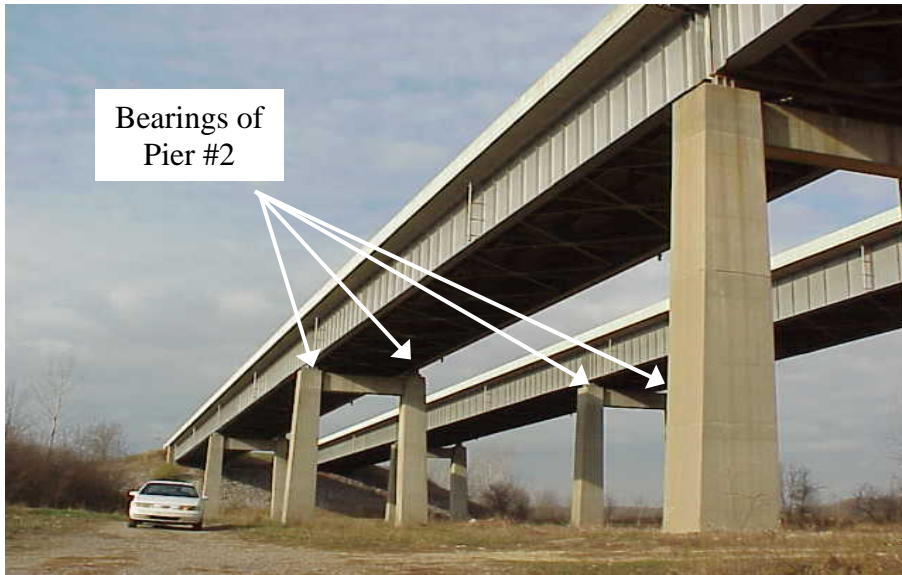
Bearings of
Pier #2

Note: Capacity of bridge members of the approach spans exceeds demand. Consequently, no retrofit is required. Demand of bearings for pier #2 of the approach spans exceeds capacity. Consequently, retrofitting of bearings for pier #2 is required by increasing the anchor bolts capacity or using seismic isolation bearings.

Figure E-7 Condition of the members and bearings of the approach spans of the Cumberland River Bridges during the 500-year event

ACKNOWLEDGEMENTS

TABLE OF CONTENTS

LIST OF TABLES

LIST OF FIGURES

1. INTRODUCTION

1.1 General

The needs for evaluating the seismic adequacy of existing infrastructure has come into focus following the damage and collapse of numerous structures during recent earthquakes. In particular, the seismic evaluation and rehabilitation of older bridges in regions of high seismicity, which were designed prior to the advent of modern seismic design codes and have not yet been subjected to a severe earthquake, is a matter of growing concern. Extensive damage to transportation facilities, including bridges, were a result of the disastrous earthquakes such as Hyogo-ken Nanbu 1995 in Japan, Loma Prieta 1989 in California, Northridge 1994 in California, Kocaeli 1999 in Turkey, Duzce 1999 in Turkey, Chi-Chi 1999 in Taiwan as well as other major earthquakes. About 17000 victims were induced in the Kocaeli earthquake, while about 2400 and more than 5000 victims were induced in the Chi-Chi and Hyogo-ken Nanbu earthquakes respectively. In the case of the Kocaeli earthquake, since the Trans-European Motorway was almost parallel to the fault responsible for this event, the fault rupture crossed the motorway at several locations causing extensive damage to the road facilities. In the case of the Hyogo-ken Nanbu earthquake, full and partial collapse occurred at nine sites while other destructive damage occurred at 16 other sites. Such bridge failures from earthquakes have brought to the public's attention the seismic risks that bridges and elevated freeway structures have. These bridge failures have also revealed that there are various critical issues in seismic design and seismic strengthening of bridges that need to be addressed. As a result, Japan took the initiative after the Hyogo-ken Nanbu earthquake to seismically retrofit more than 27000 reinforced concrete bridge columns found to have insufficient ductility. Other examples of earthquake effects on transportation facilities are the partial collapse of the San Francisco - Oakland Bay Bridge and the Cypress Viaduct portion of Interstate 880. These earthquakes resulted in a loss of life and revealed considerable problems in the transportation infrastructure. The Bay Bridge was unusable for a month and commuters were forced to commute on ferries or the crowded Bay Area Rapid Transit System. Following the Loma Prieta earthquake, the Federal Highway Administration commissioned the seismic evaluation of bridges located in seismically active regions.

After the seismic evaluation, if the bridge is found to be deficient, it will have to be retrofitted. Nevertheless, not all bridges in the highway system will have to be retrofitted simultaneously. Instead, only those bridges with the most potential danger will be retrofitted first. Also, bridges in need of retrofit will be identified by considering their structural seismic deficiencies and socio-economic aspects in order to prevent bridge failures, and thus efficiently allocating limited financial resources. It should always be remembered that seismic retrofitting is only one of several possible courses of action. Other possible actions are closing the bridge, replacing the bridge, or taking no action at all, and accepting the risk of seismic damage.

Seismic design of bridges throughout the United States is mostly governed by *AASHTO* Standard Specifications for Highway Bridges, Division I-A (1996). Generally, the *AASHTO* Standard Specifications is intended: 1) to allow the structure to yield during a major earthquake, 2) to allow damage (yielding) only in areas that are accessible (visible) and repairable, and 3) to prevent collapse even during very large earthquakes (*NHI* 1996).

The specifications given in *AASHTO* Standard Specifications (1996) and *AASHTO-LRFD* (1998) apply to bridges of conventional slab, beam girder, box girder, and truss superstructure construction with bridge spans not exceeding 500ft (150m). Suspension bridges, cable-stayed bridges, arch type and movable bridges are not covered by these specifications. In addition, the approximate seismic methods of analyses presented in AASHTO Standard Specifications are limited to bridges that are categorized as regular bridges. These regular bridges are defined by *AASHTO* Standard Specifications as bridges having less than seven spans, with no abrupt or unusual changes in weight, stiffness, or geometry, and no large changes in these parameters from span to span or support to support (abutments excluded). Any bridges not satisfying these requirements are to be identified as 'irregular bridges'. More rigorous analysis procedures, such as time history analysis, are required for bridges categorized as irregular bridges.

There are many bridges in Kentucky, which were designed before the seismic provisions were introduced into the *AASHTO* specifications. Some of them are categorized as irregular bridges according to the *AASHTO* specifications. Hence it becomes necessary to identify the appropriate seismic evaluation/retrofit procedures for different types of irregular bridges. Recently, several long span through-truss bridges over the Ohio River in Kentucky have been evaluated for seismic loading. They are the Brent-Spence Bridge on I-75 (Harik et al 1997a,b), the US-51 bridge in Ballard County (Harik et al 1998), and the US 41 Southbound and Northbound bridges in Henderson County (Harik et al 1999a,b).

The present work concentrates on the seismic evaluation of the I-24 Bridges over the Cumberland River in western Kentucky. This bridge connects I-24 across the Cumberland River between Lyons and Livingston Counties in western Kentucky. Due to its importance, the bridge is to be evaluated for the 250-year event and the maximum credible 500-year event. During a 250-year event, the bridge is to remain in the elastic range without any disruption to traffic. During a 500-year event, partial damage will be permitted on the bridge, however, it is to remain accessible to emergency and official vehicles.

1.2 Field Testing

Field-testing of bridges has become an integral part of the seismic evaluation process in order to eliminate the uncertainties and assumptions involved in analytical modeling. Full-scale dynamic tests on structures can be performed in a number of ways. Hudson (1977) describes the different types of testing as:
      (1) Free vibration tests, including
            (i)   Initial displacement as in the pullback, quick-release test
            (ii)   Initial velocity from impacts test

(2) Forced vibration tests, including
- (i)   Steady-state resonance test
- (ii)   Variable frequency excitations test including sweep, rundown, random and pulse sequences
- (iii)   Transient excitations test including earthquakes, wind, traffic, and explosions.

Shelley (1995) provides an informative discussion of the advantages and disadvantages of the various test methods used on highway bridges.

An alternative technique used to dynamically test bridges is the ambient vibration testing through measurement of the bridges response under normal traffic and wind excitations. The ambient vibration testing does not disrupt the traffic on the bridge because it uses the traffic and wind as natural excitation. This method is obviously cheaper than forced vibration testing since no extra equipment is needed to excite the structure. However, relatively long records of response measurements are required and the measurement data are highly stochastic. Consequently, the system identification results are not always that good. In the context of ambient vibration testing, only the response data of ambient vibrations are measurable while actual loading conditions are unknown. A system identification procedure will therefore need to base itself on output-only data. System identification, using ambient vibration measurements, presents a challenge requiring use of special identification techniques, which can deal with very small magnitudes of ambient vibration contaminated by noise without the knowledge of input forces. The ambient vibration testing has been used by a number of researchers (Abdel-ghaffer and Scanlan 1985a,b; Alampalli and Fu 1994; Buckland et al. 1979; Doll 1994; Farrar et al. 1995; Paultre et al. 1995; Saiidi et al. 1994; Shahawy 1995; Ventura et al. 1994; Wendichansky et al. 1995). The benchmark study on system identification through ambient vibration measurements was carried out by De Roeck et al. (2000).

For the Cumberland River Parallel Bridges, on-site dynamic testing was performed in the way of ambient vibration testing under "natural" excitation such as traffic, wind and their association. Since the main bridge is symmetric, ambient vibration measurements are carried out only on one-half of the longer spans and one-half of one of the shorter spans. The measured data taken are the acceleration-time history. The dynamic characteristics (frequencies and mode shapes) of the bridge were extracted from the peak picking of the Average Normalized Power Spectral Densities (*ANPSDs*) in frequency domain and stochastic subspace identification in time domain. These vibration properties are subsequently used as a basis for updating the original finite element model of the bridge.

1.3 Earthquake Background

The test bridge is located on the borders of Lyons and Livingston counties, in western Kentucky. This positions the bridge in the New Madrid seismic zone, site of three of the most severe earthquakes known to have occurred in American history (Johnston 1982, 1985, Johnston and Nava 1985, Street et al. 1996). The zone is named for the town of New Madrid, Missouri, which is the

epicenter of the third of the great earthquakes. All of the massive earthquakes were estimated to have had a magnitude over 8.0 on the Richter scale and each of the main shocks were followed by a protracted series of strong aftershocks. The main shocks were felt throughout all of the Central United States, most of the Eastern United States, as well as parts of Canada, and dramatically altered the region's landscape.

December 16, 1811 saw the first of the most severe earthquakes; the second of the huge quakes followed on January 23, 1812. Inhabitants reported the earth to be rolling in waves a few feet in height during the main shocks. On February 7, 1812 the third and strongest of the main shocks occurred. Denoted the "hard shock", this temblor created waterfalls on the Mississippi and caused it to flow backward, locally, for several hours. Several islands in the Mississippi disappeared altogether. Present-day Reelfoot Lake, in Kentucky and Tennessee, was created during the February hard shock. It is estimated the quake to have had a Richter magnitude of up to 8.8 (Johnston 1985b).

During the first 9 years of deployment of seismographs, which began in 1974, more than 2000 earthquakes had been instrumentally detected in the New Madrid Seismic Zone (Johnston 1985). Although 97% of the earthquakes in the region are too small to be felt, roughly a Richter magnitude of 2.5 occurs on average every 48 hours (Johnston 1982). This activity makes the New Madrid Seismic Zone the most hazardous zone east of the Rocky Mountains (Johnston and Nava 1985).

With increasing recognition of potential damage from a large New Madrid earthquake, or other less severe quake, the Kentucky Transportation Cabinet funded the research project '*Evaluation and Analysis of Innovative Concepts for Bridge Seismic Retrofit*'. Research has been conducted by the Kentucky Transportation Center at the University of Kentucky. Fundamental to this research project has been the characterization of the seismic potential affecting Kentucky from known seismic zones as well as unknown "local" events. Results from this seismological assessment of Kentucky were published in Source Zones, Recurrence Rates, and Time Histories for Earthquakes Affecting Kentucky (Street et al., 1996). In this report, three main tasks were covered: 1) definition and evaluation of earthquakes in seismic zones that have the potential to generate damaging ground motions in Kentucky, 2) specification of the source characteristics, accounting for the spreading and attenuation of the ground motions to top-of-bedrock at sites in Kentucky, and 3) determination of seismic zoning maps for the Commonwealth based on peak-particle accelerations, response spectra, and time-histories.

Time-histories generated in the aforementioned report were used in the seismic evaluation of the Cumberland River Parallel Bridges. Effects of these artificial earthquakes were calculated for bedrock elevation at the county seat of each Kentucky County. These acceleration time-histories were derived through the use of random vibration analysis and take into consideration the probability of earthquakes from nearby seismic zones, the attenuation of ground motions with distance in the Central United States, and the possibility of a random event occurring outside of the generally recognized seismic zones (Street et. al., 1996).

1.4 Scope of the Work

Due to the importance of the I-24 Bridges at Cumberland River crossing, the bridge is to be evaluated for the 250-year event and the maximum credible 500-year event. During a 250-year event, the bridge is to remain in the elastic range without any disruption to traffic. During a 500-year event, partial damage will be permitted on the bridge; however, the bridge has to remain accessible to emergency and official vehicles. In order to achieve this objective, the scope of work was divided into three tasks as: 1) field testing of the main bridge, 2) finite element modeling, and 3) time history seismic response analysis of the main bridge.

The ambient vibration properties of the main bridge are determined through field-testing under traffic and wind induced excitation. The purpose of measuring the ambient vibration properties is to determine the mode shapes and the associated natural frequencies. Full-scale ambient or forced vibration tests have been used extensively in the past to determine the dynamic characteristics of highway bridges (Abdel-ghaffer and Scanlan, 1985a,b). Then, a three dimensional finite element model of the main bridge is created for free vibration and seismic response analyses. The model is first calibrated by comparing the free vibration analysis results with ambient vibration properties from field-testing. After the calibration, the model is used for seismic response analysis to determine the maximum displacements at joints, stresses in critical members and shear forces on bearings. Checking the allowable displacements, allowable stresses in critical members and maximum capacity on bearings, the seismic safety of the bridge can then be evaluated.

2. CUMBERLAND RIVER PARALLEL BRIDGES ON THE I-24 AT LYONS AND LIVINGSTON COUNTIES IN WESTERN KENTUCKY

2.1 General

The Cumberland River Parallel Bridges on I-24 in west Kentucky is a steel plate-girder bridge, a bridge type commonly supported by the two main steel girders. Figure 2.1a to Figure 2.1d show the different views of the main bridge. This bridge was originally designed by Jolls F. Keith, Vollmer Ostrower Inc. Consulting Engineers in 1972. The steel girder bridge consists of six spans and has a total length of 1671 feet (including the approach spans). A layout of the bridge is shown in Figure 2.3. The main bridge, excluding the approach spans, is composed of three continuous spans that stretch a total length of 1020 feet. Plan and elevation views of the main bridge are shown in Figure 2.3. The lengths of the individual spans are 300, 420, and 300 feet, respectively. The distance from girder to girder is 31 feet, and the total roadway width, which consists of two 12' lanes, a 1' outside emergency lane, and a 5' 3" inside shoulder, is 39' 3". The analyzed portion is symmetric about the middle of the center span and also symmetric about the center of the roadway. The entire structure actually consists of two identical bridges; however, for simplicity, only one will be analyzed.

2.2 Bridge Superstructure

The superstructure is described in terms of two steel girders, bracings, stiffeners, and floor system. The bracing system is a combination of transverse and diagonal bracings.

The main structural support of the bridge consists of two steel girders, which varies in depth along the bridge. For the first span analyzed, the depth is 12' for most of the span. The girder tapers at the support that divides spans 4 or 6 and span 5. At 70' from the support, the girder begins tapering from the 12' in depth and continues to a depth of 20' at the support. The taper decreases from the support to a point 50' away on the center span. At this point the depth of the girder is 16', which is the depth of most of the center span. It should be noted that the main bridge is symmetric about the midpoint of the center span.

The main girders also vary in web and flange thickness, and flange widths. Most of the web of the first span is ½" thick. For the tapered section, the thickness increases to ¾". For the center span, the web is 5/8" thick. Also, the first span consists of two main flange thicknesses: 2" for the first 20' and the last 40' before the taper, and 3" for the middle section. At the taper, the flange thickness increases from 2" to 2 ¾" for 20'. For the rest of the tapered section, the flange thickness is 3 ½". After the tapered section, the thickness decreases back to 2 ¼" for 70'. The rest of the symmetrical section has a 3" flange

thickness. Finally, the flange width is 42" for all flange thickness except the 3-½" tapered section and the 3" center span section. At these locations, the flange width is 48".

The two main girders are braced in two ways. First, transverse bracing is located at 20' from each end support and at 23'-4" intervals in between. The transverse bracing consists of cross frame with W shape beams at the top and bottom, 2 sets of 2 channel beams welded back to back, and a W shape beam running vertically in the center. They connect from the top of each main girder to the center of the W shape at the bottom. The vertical W shape beam connects to the center of the W shape beams at the top and bottom of the cross frame. The size of these shapes varies somewhat throughout the bridge. The second type of bracing is diagonal bracing. Midway between each transverse bracing, the diagonal bracing connects from the bottom of the center of the transverse bracing to the main girders. Tee shape beams are used for diagonal bracing. The main shape used is a WT7×21.5, but near the supports, WT9×32 and WT9×48 beams are used.

The other key components of the superstructure are the web stiffeners and longitudinal stiffeners. Different sizes of web stiffeners are placed at varying intervals running the entire depth of the web. At the end supports, the stiffener dimensions are 1-½" by 12 ¾". At the two interior supports, the stiffener dimensions are 2 ½" by 14 ½". The rest of the web stiffeners are the same dimension throughout, which is ¾" by 12". For the bridge modeling described later in the report, the longitudinal stiffeners are ignored. A more detailed illustration of the superstructure under the roadway can be seen in Figure 2.4 and Figure 2.5.

The floor system consists of a 9 1/2" average thickness concrete slab supported by three longitudinal W24×68 stringers, which are carried by transverse built up floor beams. The width of the two-lane roadway is 39' 3". The two outside stringers are spaced at 7' 10-1/2" from the main bridge girders and the center stringer is located 7' 7 ½" from the outside stringers.

2.3 Fixed and Expansion Bearings

For the three-span main bridge, the superstructure is supported by expansion bearings at the two exterior piers, and fixed bearings at the two interior piers. The expansion bearings permit longitudinal translation and rotation, while the fixed bearings only allow longitudinal rotation. Figure 2.6 provides a view of the fixed bearing.

The fixed bearings are of standard pinned bearing design consisting of a cast steel upper shoe supported on a 5" diameter steel pin, which bears on a cast steel bottom shoe. The upper shoe is bolted to the bottom flange of the steel girder and the bottom shoe is rigidly attached to the pier via anchor bolts. The anchor bolts are 2 ½" diameter and extend 3'-3" into the pier concrete.

The expansion bearings on the exterior piers consist of pin and roller combinations to allow rotation and translation movement. The top shoe of this bearing is connected to the

bottom flange of the steel girder, which is then connected to the pin. The bottom shoe is connected to the pier through anchor bolts. There are a total of four 1 ½" diameter anchor bolts running 1'-11" into the pier concrete. The slots in the bottom flange of the steel girder allow longitudinal translation. The bottom shoe is rigidly attached to the pier via anchor bolts. A view of the expansion bearing is shown in Figure 2.6

2.4 Bridge Substructure

The three-span main bridge is supported on three concrete piers and one abutment. The first pier (Pier 3) at the end support consists of two columns connected by a pier cap beam at the top. The height of these columns is 60', which is measured from the girder bearing to the top of the pile cap. The thickness of the columns varies from 7' at the top to 9'-6" at the pile cap. The pier cap measures 6' tall by 4' wide. The second (Pier 4) and third (Pier 5) piers are identical. The heights of these columns are 96'. In addition to the 6' by 6' pier cap beam at the top, a 8' tall by 6' wide concrete beam connects the two columns at 53' above the pile cap. The columns for these piers are 10 feet wide. The thickness varies from 10' at the top to 14' at the pile cap. Finally, since the abutment (Abutment 2) will be modeled as an expansion bearing joints, no description is necessary. All the piers are constructed with reinforced concrete class 'AA'. Moreover, all the piers are supported on sheet piling foundations.

3. FIELD TESTING AND SYSTEM IDENTIFICATION

3.1 General

On-site dynamic testing of a bridge provides an accurate and reliable description of its real dynamic characteristics. There are two main types of dynamic bridge testing:

> ➢ Forced Vibration Test
> ➢ Ambient Vibration Test

In the first method, the structure is excited by artificial means such as shakers or drop weights. By suddenly dropping a load on the structure, a condition of free vibration is induced. The disadvantage of this method is that traffic has to be shut down for a rather long time, especially for large structures, e.g. long-span bridges with many test setups. It is clear that this can be a serious problem for intensively used bridges. In contrast, ambient vibration testing does not affect the traffic on the bridge because it uses the traffics and winds as natural excitations. This method is obviously cheaper than forced vibration testing since no extra equipment is needed to excite the structure. However, relatively long records of response measurements are required and the measurement data are highly stochastic. Consequently, the system identification results are not always that good.

For the Cumberland River Parallel Bridges on I-24 in west Kentucky, the field dynamic testing has been performed on the main bridge in the way of ambient vibration tests. Since the main bridge is symmetric including three spans, ambient vibration measurements are carried out on only one-half of the longer span and one-half of one of two shorter spans. Field-testing was conducted on December 02, 1999 on only the northbound lane. The bridge has two lanes of traffic, namely the northbound and southbound lanes. All measurements were taken by placing the instruments on the pavement due to the limited access to the actual floor beams and the time constraints involved. Each instrument was placed with its longitudinal axis aligned parallel to the longitudinal direction of the bridge. Ambient vibration measurements under traffic and wind induced excitations were recorded at 9 locations on both sides (right lane and left lane) of the northbound lane. The system identification is performed by both the simple peak picking method in the frequency domain and the more advanced stochastic subspace identification technique in the time domain.

3.2 Instrumentation

The equipment used to measure the acceleration-time responses of instrumentation consisted of tri-axial accelerometers (Figure 3.1) linked to its own data acquisition system (Figure 3.2). The system contained a '*Keithly MetraByte 1800HC*' digital recording strong motion accelerograph. Two units contained internal accelerometers, while the two remaining units were connected to '*Columbia Research Labs, SA-107*' force balance

accelerometers. The accelerometers are capable of measuring accelerations up to 2*g*'s, where *g* is the gravitational acceleration at frequencies up to *DC*-50*Hz*. The data was stored in a personal computer at one of the base stations for further processing. The instrumentation of testing was to set up four accelerometers on a given segment of the bridge along with fixed reference base station accelerometers at a minimum of two other locations on the bridges. The recording devices were triggered by a computer at one of the base stations to synchronize the start and stop of the accelerometers.

Sets of three accelerometers were mounted to aluminum blocks in orthogonal directions to form a tri-axial accelerometer station. A block was positioned at each station with the accelerometers oriented in the vertical, transverse and longitudinal directions. To prevent any shifting of the accelerometers during testing, 25 *lb* bags of lead shot were laid on top of the accelerometer blocks once in position. To ensure the blocks were placed in level, adjustable feet and a carpenters level were attached to each block. The accelerometers were also connected by shield cables to the data acquisition system.

Six test setups were conceived to cover the planned testing area of the bridge. As a result, a total of 18 locations (9 points per side) were measured. A reference location, hereinafter referred as the base station, was selected based on the mode shapes from the preliminary finite element model. The setup instrumentation was composed of four base tri-axial accelerometer stations and three moveable tri-axial accelerometer stations. The detailed test setups and a view on the measurement locations are shown as Figure 3.3.

3.3 Testing Procedures and Data Record

Three test setups for both the right-hand lane and left-hand lane were recorded for the whole bridge. Table 3.1 shows the distribution of the different stations (locations) per setup. The base station accelerometers remained in their original positions for each test setup. Testing began in the right lane at mid-span of the easternmost end span of the main plate-girder section of the bridge and continued until a point 50 feet past mid-span of the longest span of the bridge. The same series of tests were repeated for the left-hand lane. For each setup, the tests yielded a total of nine sets of data from moveable stations and twelve sets of base station data. The test locations, station names, and data file names are included in Table 3.2a and Table 3.2b.

The sampling frequency on site was chosen to be as high as 1000 Hz to capture the short-time transient signals of the ambient vibration in full detail. The ambient excitation of the bridge was then simultaneously recorded for 60 seconds at all accelerometers and the base stations, which results in a total of 60,000 data points per data set (channel). Once the data was collected, the moveable stations were moved to the next locations while the base stations remained stationary. This sequence was repeated six times to get measurements on all stations on the northbound lane. During all tests, normal traffic was allowed to flow over the bridge at normal speeds.

3.4 Data Processing

The raw data from the tests displayed a series of data that showed the acceleration of the bridge in one of the three axial directions with respect to time, creating a time-history record of accelerations for the bridge. This data must first be de-trended. This treatment enables the removal of the DC-components, which badly influence the identification results. Figures 3.4a, 3.5a, and 3.6a show the raw acceleration time-history of station L1 in the longitudinal, transverse, and vertical directions respectively. Figures 3.4b, 3.5b, and 3.6b show the corresponding raw power spectral densities in the longitudinal, transverse, and vertical directions in the frequency domain of station L1.

The sampling frequency on site was chosen to be as high as 1000Hz so that it could capture the transient signals of ambient vibration resulting frequency range from 0 to 500Hz. For most bridges, however, the frequency range of interest lies between 0 and 10 Hz, containing at least the first ten eigen frequencies. The re-sampling of the raw measured data is necessary since other following preprocessing steps will go much faster due to the reduced amount of data. A re-sampling and filtering from 12.5 *Hz* to 500 *Hz* is the same as decimating (=low-pass filtering and re-sampling at a lower rate) 40 times. By decimating the raw data for 40 times results in 1500 data points, where 60000/40=1500, and an excellent frequency ranging from 0 to 12.5 *Hz*. The frequency ranging from 0 to 12.5 *Hz* would result in a less sophisticated power spectral density diagram where a smaller interval would result in reducing the number of points. Figures 3.7a, 3.8a, and 3.9a show the re-sampled acceleration time-history of station L1 in the longitudinal, transverse, and vertical directions respectively. Figures 3.7b, 3.8b, and 3.9b show the corresponding re-sampled power spectral densities in the longitudinal, transverse, and vertical directions in the frequency domain of station L1. The re-sampling resulted in a noise-free signal as shown in Figure 4.7 and Figure4.8, and thus will be used for the system identification to extract the eigen frequencies and eigen mode shapes.

3.5 System Identification from Ambient Measurements

System identification was originally a topic of control engineering. However, it has received worldwide attention recently for various applications. In the context of civil engineering, structures such as bridges or buildings are considered system and identification means the extraction of modal parameters (eigen-frequencies, damping ratios and mode shapes) from dynamic measurements. These modal parameters will serve as basis or input to the finite element model updating, damage identification algorithms in detecting and locating the possible damage in structures, and safety evaluation after the structure has suffered from extensive damages such as those caused by earthquakes. These modal parameters will also be essential in the monitoring of structures in service and the controlling of structures.

In past decades, the system identification of civil engineering structures has developed very fast. Techniques such as modal testing and modal analysis have become widely available (Ewins 1986; Maia et al. 1997). Basically, the system identification

11

procedure is carried out according to both input and output measurement data through the Frequency Response Functions (*FRF*) in the frequency domain or Impulse Response Functions (*IRF*) in the time domain. For civil engineering structures there is normally no difficulty to obtain the output measurements (dynamic responses). The structural dynamic responses are the direct records of the sensors that are installed at several locations of the structure. However, the input or excitation of the real structure in the operational condition often hardly realizes. It is extremely difficult to measure the input dynamic forces acting on a large-scale structure. Although forced excitations (such as heavy shakers and drop weights) and correlated input-output measurements are sometimes available, but testing or structural complexity and achievable data quality restrict these approaches to dedicated applications. On the other hand, ambient excitations such as traffic, wave, wind, earthquake and their combination are environmental or natural excitations. The ambient vibration has the advantage of being inexpensive since no equipment is needed to excite the structure. Also the service state of the structure does not have to be interrupted by using this technique. The ambient vibration measurements have been successfully applied to many large structures, for instance, the Golden Gate Bridge (Abdel-Ghaffer and Scanlan 1985a,b) and the Brent-Spence Bridge (Harik et al. 1997a,b) to evaluate the seismic safety.

Ambient excitation does not lend itself to the calculations of the *FRF* or *IRF* because the input force cannot be measured. In this case only response data of ambient vibrations are measurable while actual loading conditions are unknown. A system identification procedure will therefore need to base itself on output-data only. System identification using ambient vibration measurements present a challenge requiring the use of special identification techniques, which can deal with very small magnitudes of ambient vibration contaminated by noise without the knowledge of input forces. There have been several ambient vibration system identification techniques available that were developed by different investigators or for different uses such as:

- Peak-picking from the power spectral densities (*PSDs*) (Bendat and Piersol 1993);

- Auto Regressive-Moving Average (*ARMA*) model based on discrete-time data (Andersen et al. 1996);

- Natural excitation technique (*NExT*) (James et al. 1995);

- Stochastic subspace methods (Van Overschee and De Moor 1996);

An extensive literature review on system identification techniques using ambient vibration measurements can be found in Van der Auweraer et al. (1999) and De Roeck et al. (2000). In fact, the mathematical background for many of these methods is often very similar, differing only from implementation aspects (data reduction, type of equation solvers, sequence of matrix operations, etc.).

In present study, both rather simple Peak Picking (*PP*) method in frequency domain and more advance stochastic subspace identification method in time domain are used to make sure the right frequencies and mode shapes. The data processing and system

12

identification are carried out by '*MACEC*', a MatLab-based program of modal analysis for civil engineering construction (De Roec'k and Peeter 1999).

3.6 Peak Picking (PP) System Identification

The peak picking system identification technique is a rather simple frequency-domain method. The raw data is to be transformed from the time domain into the frequency domain. The manner by which this was accomplished was the implementation of the Fourier Transform, which is mathematically defined using the transform equation.

$$F(\omega) = \int_{-\infty}^{\infty} f(t)e^{i\omega t}\,dt \qquad (3.1)$$

Where $f(t)$ = a function of time, $F(\omega)$ = amplitude as a function of frequency, and ω = circular frequency (radians per second). The inverse of the Fourier Transform is defined by Eq 3.2.

$$f(t) = \frac{1}{2\pi} \int_{-\infty}^{\infty} f(\omega)e^{-i\omega t}\,d\omega \qquad (3.2)$$

Using the equations above, any function that is a function of time can be converted into a function of frequency or vice versa. The only drawback associated with using these equations is that $f(t)$ must be a continuous function, which does not fit the description of the piecewise nature of digitally sampled data such as that obtained in the bridge testing. For this reason, a different form of Fourier Transform must be used, known as the Discrete Fourier Transform, which is useful when data point values are known at regularly spaced intervals, which lends itself nicely to the problem at hand. The Discrete Fourier Transform is defined by Eq 3.3.

$$F_n = \sum_{k=0}^{N-1} f_k e^{2\pi i k n / N} \qquad \text{(for n = 0 to N-1)} \qquad (3.3)$$

Where N = number of sampled points and f_k = a set of N sampled points. The inverse form of the Discrete Fourier Transform is given by Eq 3.4.

$$f_k = \frac{1}{N} \sum_{k=0}^{N-1} F_n e^{-2\pi i k n / N} \qquad \text{(for k = 0 to N-1)} \qquad (3.4)$$

This set of equations is extremely useful for engineering applications such as this, but there are still some problems. These equations require N^2 complex mathematical operations, in which, even with modern computing power, can take quite some time even for small data sets (Blevins, 1995). There is one other method that can reduce the computing time significantly. The Fast Fourier Transform, a numerical operation, can exploit the periodic and symmetric nature of trigonometric functions to greatly improve efficiency in

comparison to the Discrete Fourier Transform (*DFT*). The number of computations for the Fast Fourier Transform is reduced to $N \, log_2 \, (N)$, which is approximately 100 times faster than the Discrete Fourier Transform for a set of 1000 data points (Bracewell, 2000).

In this way the natural frequencies are simply determined from the observation of the peaks on the graphs of the Average Normalized Power Spectral Densities (*ANPSDs*). The *ANPSDs* are basically obtained by converting the measured accelerations to the frequency domain by a Discrete Fourier Transform. The peak picking method is initially based on the fact that the FRF goes through an extreme around the natural frequencies. The frequency at which this extreme occurs is a good estimate for the eigen frequency. In the context of ambient vibration measurements only the FRF is replaced by the auto spectra of the ambient outputs (Bendat and Piersol 1993). The coherence function computed for two simultaneously recorded output signals has values close to one at the natural frequency. This fact also helps to decide which frequencies can be considered as natural.

For the peak picking method, 60,000 the data points per channel are transformed to the frequency domain and averaged to estimate the power spectral densities. All the raw data is used in the PP method. The *ANPSDs* are obtained through all raw longitudinal, transverse, and vertical data, respectively. The corresponding *ANPSDs* diagrams are shown in Figure 3.10. The peak points are clearly shown, and then the eigen frequencies could be picked up. It has been noted that the figures have been proportioned to focus on the frequency range of interest. The possible frequencies picked up from the *ANPSDs* diagrams are summarized in Table 3.3. It was demonstrated that the first vertical natural frequency of the Cumberland River Parallel Bridges was about 0.88Hz, while the first transverse natural frequency was around 1.38 *Hz*. The frequency 1.4167 *Hz* was coupled with vertical vibration and longitudinal vibration, while frequency 2.35 *Hz* was coupled with three directions. The possible first longitudinal frequency would be 2.85 *Hz*. All these frequencies need to be verified by more advanced stochastic subspace identification method.

The components of the mode shapes are normally determined by the values of the transfer functions at the natural frequencies. It is important to note that in the context of ambient testing, transfer function does not mean the ratio of response over force, but rather the ratio of response measured by a roving sensor over response measured by a reference sensor. So every transfer function yields a mode shape component relative to the reference sensor.

3.7 Stochastic Subspace Identification (*SSI*)

It is beyond the scope of this paper to explain in full detail the stochastic subspace identification method. The interested reader is referred to literatures (Van Overschee and De Moor 1996; De Roeck and Peeters 1999). Here only the main ideas are discussed.

It is well known that a structural model can be describable by a set of linear, constant coefficient, second-order differential equations.

$$M\ddot{U}(t) + C\dot{U}(t) + KU(t) = F(t) \tag{3.5}$$

Where, *M, C* and *K* are the time-invariant mass, damping and stiffness matrices, respectively, of the structure associated with the *n* generalized coordinates comprising the vector $U(t)$. *F(t)* is a time-dependent vector of input forces. Equation (3.5) can be rewritten as a first-order system of differential equations in a number of ways. One commonly used reformulation is a state space representation

$$\dot{x}(t) = A_c x(t) + B_c u(t) \tag{3.6}$$

where, the state vector $x(t) = [U(t), \dot{U}(t)]^T$, the state matrix A_c and the system control influence coefficient matrix B_c are defined by Eq 3.7.

$$A_c = \begin{bmatrix} 0 & I \\ -M^{-1}K & -M^{-1}C \end{bmatrix} \qquad B_c = \begin{bmatrix} 0 \\ M^{-1}B_2 \end{bmatrix} \qquad F(t) = B_2 u(t) \tag{3.7}$$

Furthermore, the output vector of interest, $y(t)$, can be a part of, or a linear combination of system states, such as shown in Equation 3.8.

$$y(t) = C x(t) + D u(t) \tag{3.8}$$

Here *C* is a real output influence coefficient matrix and *D* is the output control influence coefficient matrix. Equations (3.6) and (3.8) constitute a continuous-time state-space model of a dynamic system. Continuous-time means that the expressions can be evaluated at each time instant, which is not realistic since the experimental data are discrete in nature. Furthermore, sample time and noise always influence the measurements. After sampling, the continuous-time state-space model looks like.

$$x_{k+1} = Ax_k + Bu_k \tag{3.9a}$$
$$y_k = C x_k + D u_k \tag{3.9b}$$

Where $x_k = x(k\Delta t)$ is the discrete time state vector; $A = \exp(A_c \Delta t)$ is the discrete state matrix; the $B = [A - I]A_c^{-1}B_c$ is the discrete input matrix. Equation (3.9) forms a discrete-time state-space model of a dynamic system.

In practice there are always system uncertainties including process and measurement noises. The process noise is due to disturbances and modeling inaccuracies, whereas the measurement noise is due to sensor inaccuracy. If the stochastic components (noise) are included Equation 3.9, it can be extended to consider process noise w_k and measurement noise v_k described as a continuous-time stochastic state-space model.

$$x_{k+1} = Ax_k + Bu_k + w_k \qquad (3.10a)$$

$$y_k = Cx_k + Du_k + v_k \qquad (3.10b)$$

It is difficult to determine accurately the individual process and measurement noise characteristics, and thus, some assumptions are required. Here the process noise w_k and measurement noise v_k are assumed to be zero-mean, white and with covariance matrices:

$$E\left[\begin{pmatrix} w_p \\ v_p \end{pmatrix}\begin{pmatrix} w_q^T & v_q^T \end{pmatrix}\right] = \begin{pmatrix} Q & S \\ S^T & R \end{pmatrix}\delta_{pq} \qquad (3.11)$$

where E is the expected value operator and δ_{pq} is the Kronrcker delta (De Roeck and Peeters 1999). The sequences w_k and v_k are assumed statistically independent of each other.

Now we come to the practical problem: in the case of ambient vibration testing the input sequence u_k remains unmeasured and disappears from Equation 3.10.

$$x_{k+1} = Ax_k + w_k \qquad (3.12a)$$

$$y_k = Cx_k + v_k \qquad (3.12b)$$

The input is now implicitly modeled by the noise terms w_k, v_k. However the white noise assumptions of these noise terms cannot be omitted. The consequence is that if this white noise assumption is violated, for instance, if the input contains additional dominant frequency components on top of white noise, these frequency components cannot be separated from the eigen frequencies of the system and they will appear as poles of the state matrix A.

Equation 3.12 constitutes the basis for the time-domain system identification through ambient vibration measurements. There have been several techniques to realize system identification algorithms based on Equation 3.12. The stochastic subspace identification algorithm is probably the most advanced method known up to date for ambient vibration measurement system identification. The subspace method identifies the state space matrices based on the measurements and by using robust numerical techniques such as *QR-factorization*, Singular Value Decomposition (*SVD*) and least squares. Loosely said, the *QR-factorization* results in a significant data reduction, whereas the *SVD* is used to reject the noise (assumed to be represented by the higher singular values). Once the mathematical description of the structure (the state space model) is found, it is straightforward to

determine the modal parameters (by an eigen value decomposition): natural frequencies, damping ratios and mode shapes.

The key element of *SSI* is the projection of the row space of the future outputs into the row space of the past outputs. The main difference with the proceeding algorithms is that the subspace algorithm is data driven instead of covariance driven so that the explicit formation of the covariance matrix is avoided. It is clear that the stochastic subspace identification is a time domain method that directly works with time data, without the need to convert them to correlations or spectra.

The stochastic subspace identification is applied to re-sampled data. The expected model order is chosen to be 90 and model order range is 2:1:100 that will be used to extract a model of order from 2 to 100. The stabilization diagrams are shown in Figure 3.11a to Figure 3.11c for the longitudinal, vertical, and transverse data respectively. The identified frequencies are listed in Table 3.4. It is demonstrated that they are almost identical to those obtained from peak picking method (Table 3.3). So the frequencies listed in Table 3.4 will be used to calibrate the finite element model.

Excellent mode shapes have been extracted by the *SSI* technique. The first three vertical mode shapes and transverse mode shapes are shown in Figure 3.12a to Figure 3.12c and Figure 3.13a to Figure 3.13c. Common to all system identification methods for ambient vibration measurements, it is not possible to obtain an absolute scaling of the identified mode shapes (e.g. mass normalization) because the input remains unknown.

3.8 Summary

Two complementary system identification methods are implemented to extract the dynamic characteristics of the Cumberland River Parallel Bridges through ambient vibration testing. It has been shown how the modal parameters can be effectively extracted from ambient vibration data only by using the frequency domain based peak picking (*PP*) method and the time domain based stochastic subspace identification (*SSI*) technique.

In the *PP* method the natural frequencies are selected as the peaks of the *ANPSDs*. This can become a quite subjective task, especially if the peaks are not very clear. For the SSI method, stabilization diagrams aid the engineer to select the true modes. One of the advantages of the SSI method is that the stabilization diagram can be constructed in an effective way. The computationally heaviest steps including the *QR-factorization* and *SVD* have to be performed only once. Then, models of increasing order are obtained by rejecting less singular values.

The advantages of the peak picking method are that it is easy to pursue and provides fast estimates. However, the damping has not been identified. In the *PP* method no modal model is fitted to the data, therefore operational deflection shapes are obtained instead of mode shapes. If the modes are well separated, this is not a major drawback, because operational deflection shapes are very similar to mode shapes.

The *SSI* technique is probably the most advanced method known up to date for ambient vibration measurement only system identification. Based on the stabilization diagram, the *SSI* technique can detect closely spaced frequencies that are possibly missed with the *PP* method. The computational load of the *SSI* technique is significantly higher than the *PP* method, the quality of the identification, however, is also higher. This fact is important since the modal parameters will serve as the key input to model updating, damage identification algorithms, structural monitoring and structural controls.

The weak point of the *PP* method is also its strong point: since no model has to be fitted to the data, the identification is very fast and it can be used on site to verify the quality of the measurements. For real applications, it is suggested that the *PP* method could be used to have a quick look at the overall dynamic behavior of the structure. Then, the *SSI* technique can be verify the results.

4. FINITE ELEMENT MODELING AND FREE VIBRATION ANALYSIS

4.1 General

Based on the general dynamic characteristics of steel-plate girder bridges and the proximity and activity of the seismic zones, the main bridge model was expected to remain elastic. Furthermore, the displacements were anticipated to be small enough to neglect the material and geometric nonlinear effects. Hence, the consideration of linear elastic and small displacement analysis was considered to be appropriate. Free vibration analysis is a key process in the dynamic analysis of a structure because the resulting natural frequency and mode shapes succinctly describe the dynamic characteristics of a complex structure. The analytical model is calibrated by comparing free vibration analysis results with ambient vibration measurements.

4.2 Finite Element Model

A three-dimensional linear elastic finite element model (Figures 4.1 and 4.2) of the three-span main bridge was developed in *SAP2000* finite element analysis software (Wilson and Habibullah, 1998). Developed for both the free vibration analysis and seismic response analysis, the model represents the structure in its current as-built configuration. All members of the superstructure are modeled using two nodes frame elements, which have three translational degrees of freedom (*DOF*) and three rotational *DOF* at each node. Based on the connection between the concrete deck and stringers, it is assumed that the deck will not contribute to the stiffness of the bridge. The weight of the concrete deck is only considered as joint forces in static analysis and as joint masses in dynamic analysis. Wall type piers are idealized as frame elements with gross cross-sectional properties. The full 3-*D* model has a total of 688 frame elements and 333 nodes. The number of material and geometric property groups are 48, and total number of active *DOF* is about 1954.

The bearings at the end piers are of expansion type and those at the interior piers are "fixed" type. The "fixed" bearings at the interior piers were modeled by simply releasing the rotational *DOF* in the vertical direction only. Pier and bearings are connected through a set of rigid elements of released rotational *DOF* at the end node to simulate the actual behavior. With the set up of rigid elements, direct output of the relative displacements between the end piers and interior piers can be obtained, and thus indicate if the translation has exceeded the expansion capacity.

The "expansion" bearings at the end piers were modeled by assigning roller restraints in the longitudinal direction and hinge restraints in the transverse direction at the joints. In other word, the *DOF* allowed are the longitudinal translation and the vertical bending rotation (the u_x and u_z *DOF*). For simplification, the end piers and the abutment are

not included in the analysis. These two structures are only modeled with roller and hinge restraints. Additionally, spring restraints are added at each joint to simulate the effect of the approach span in the longitudinal direction.

For simplification, the two steel girders are modeled as two straight lines, excluding the longitudinal and intermediate stiffeners. Also, upper and lower beams are combined into a simple straight line in the transverse direction, neglecting the vertical support and transverse bracing. Thus, the bridge is basically modeled into a flat plane that runs in a longitudinal direction with girders and stringers lines. In the transverse direction it runs with beams lines, diagonal bracing lines and with the two interior piers running in vertical direction. Moreover, the foundations of the piers are simplified and modeled as fixed end supports. Figures 4.1 and 4.2 show the isometric, side and plan view of the finite element model.

4.3 Free Vibration Analysis

An eigen value analysis is used to determine the un-damped, free vibrations of the structure. The eigen solution results in the "natural" mode shapes and frequencies of the structure. First, free vibration analysis is required to calibrate the finite element model with the field ambient vibration test measurements. Secondly, with the natural frequencies and their associated mode shapes from free vibration analysis, one can perform seismic response analysis using modal time-history method.

Generally, free vibration analysis involves the solution of the following eigen value problem:

$$[M - \omega K]u = 0 \tag{4.1}$$

where M and K are system mass and stiffness matrices, and u is modal displacement vector. The eigen value of a mode - ω^2, is the square of the circular frequency of that mode (ω), which relates to the cyclical frequency (f) by the relation $f = \omega/2\pi$, and relates to the period of vibration (T) by the equation $T = 1/f$.

SAP2000 utilizes an accelerated subspace iteration algorithm to solve the eigen value problem. The subspace iteration method was developed by Bathe in 1971. A detailed discussion of the method and its fundamentals can be found in Bathe (1982). Over years, various techniques have been used to "accelerate" the basic subspace iteration method, and the particular algorithm used in the *SAP2000* program can be found in Wilson and Tetsuji (1983).

Traditionally, mode-superposition analysis was performed using a structure's eigenvectors as the basis for the analysis. Since the finite element model is a simplified model with 688 frame elements, the exact eigenvectors system is used to perform the free vibration analysis. Even though research (Wilson et al. 1982) indicates that this is not the best starting point for a mode-superposition time-history analysis. From research, a special

set of load-dependent, orthogonal '*Ritz Vectors*' yields more accurate results than the same number of natural mode shapes, significantly reduces computing time, automatically includes the proven numerical techniques of static condensation-Guyan reduction, and static correction due to higher mode truncation. However, the exact eigenvectors are used because Ritz vectors truncate one of the important transverse mode shapes that are detected from the field. Furthermore, the finite element model is set up with the adjustments on stiffness and mass matrices, which are the same as the computing parameters of eigenvectors.

For model calibration, only 20 mode shapes are analyzed and compared with the field-testing results because all the important mode shapes in the three orthogonal directions from field-testing occur in the first 20 modes from the free vibration analysis. With 20 modes in exact eigenvectors, one can get 79%, 73% and 42% modal participating mass in longitudinal, transverse and vertical directions. It should be noted that '*Ritz Vectors*' produce the same results in mode shapes and frequencies except Ritz vectors provide slightly higher modal participating mass and the truncation of one of the important transverse mode shapes. The modal participating mass can easily be improved over 90% in all three directions if 228 modes are being analyzed.

The natural frequencies, modal participation factors and modal participating mass ratios for the lowest 20 modes are presented in Table 4.1. The natural frequency of the bridge ranges from 0.875 *Hz* to 4.714 Hz for the first 20 nodes, and the period ranges from 0.212 second to1.143 second. It should be noted that the natural frequencies listed in Table 4.1 and their mode shapes are used only to calibrate the finite element model. They are not used for the seismic response analysis.

It is seen from Table 4.1 that the modal participation factors of the first and fifth modes have higher values in vertical direction. Therefore, these two modes are treated as vertical modes. Even though the fourth mode has lower value in the vertical direction than in the longitudinal direction, it is still considered as vertical mode because the mode is curved with half-waves in vertical direction.

Figure 4.3 shows the first mode shape from the free vibration analysis in isometric and side views. The natural frequency of this mode is 0.875 *Hz*. The percentage of participating mass of this mode is about 0.356%. This mode has one half-waves on each span respectively, and they are symmetric along the centerline of the main bridge. Based on modal participation factors and the shape, this mode is identified as the first vertical mode.

Figure 4.4 shows the fourth mode shape from the free vibration analysis with a natural frequency of 1.413 *Hz* in the isometric and plan views. In this mode, one major half-wave and one minor half-wave are present in anti-symmetric shape along the centerline of the main bridge. The participating mass for this mode is 0%. Based on modal participation factors and the shape, this mode is observed as the second vertical mode with certain displacement in longitudinal direction.

Figure 4.5 shows the fifth mode shape from the free vibration analysis in isometric and side views. It has a natural frequency of 1.778 *Hz*. In this mode, three major half-waves

fall in the same direction and symmetric along the centerline of the main bridge. The participating mass for this mode is 39.668%, mainly in the vertical direction. Again, based on modal participation factors and the shape, this mode is noted as the third vertical mode. Also, this mode is one of the pure vertical modes, which is very important to contribute significantly for the vertical seismic motion.

From Table 4.1, one can see that the modal participation factors of the third, eighth and tenth modes have higher values in transverse direction direction. Therefore, these three modes are treated as transverse modes. However, only the third and eighth modes are considered to be pure transverse modes as they have high modal participation factors and participating mass.

Figure 4.6 shows the third mode shape from the free vibration analysis in isometric and plan views. The natural frequency of this mode is 1.383 *Hz*. In this mode, there is only a major half-waves in the center span of the main bridge. Based on modal participation factors and observation, it is seen that this mode is the first transverse mode. The participating mass in the transverse direction is 26.006%. This mode is one of the pure transverse modes and it is important in the event of transverse seismic motion.

Figure 4.7 shows the eighth mode shape from the free vibration analysis in isometric and plan views. It has a frequency of 1.989 *Hz*. In this mode, major half-waves are occurring at the side spans of the main bridge. The participating mass for this mode is 27.256%. Based on modal participation factors and observation, this mode is considered as the second transverse mode. This mode is another pure transverse mode that is important in the event of transverse seismic motion.

Figure 4.8 shows the tenth mode shape from the free vibration analysis in isometric and plan views. The natural frequency of this mode is 2.601 *Hz*. For this mode, there are two half-waves in the center span of the main bridge and one half-wave on each of the side span. Based on modal participation factors and observation, it is seen that this mode is the third transverse mode with displacements in longitudinal and vertical directions. The participating mass in the transverse direction is 0%.

The most important longitudinal mode in Table 4.1 is shown in Figure 4.9 in isometric and plan views. It is the eleventh mode from the free vibration analysis and has a natural frequency of 2.853 *Hz*. This mode is treated as the first longitudinal mode because of the modal participation factors and the shape. The participating mass for this mode is as high as 78.7%, and thus it is a pure longitudinal mode.

Similar observations can be made for other modes from Table 4.1. However, only the above modes are explained because of their similarities to the field test results.

4.4 Finite Element Model Calibration

A logical next step to field-testing in seismic evaluation of bridges is to create an analytical model, which will correlate well to the measured dynamic properties. Many assumptions and modeling approximations must be made when creating a practical model of a bridge. For example, a finite element model requires input of the material properties, which are inherently variable. This is one input where the analyst can only make a best estimate and later adjust to match the experimental results.

Using results from the eigen value analysis, the bridge model has to be calibrated to the experimentally determined mode shapes and frequencies. A perfectly calibrated model would match all experimentally determined mode shapes and frequencies exactly. To hope for such a perfect calibration is not realistic. Therefore, only the most structurally significant modes and frequencies are used in the model calibration process. Namely, the first three vertical modes, first three transverse modes and first longitudinal mode from field-testing are selected as calibration targets. Generally, the finite element results for the mode shapes are generated at the end nodes in the girders. On the other hand, due to the limited access to the actual floor beams, all measurements were taken by placing the instruments on the pavement just above the floor stringers. Thus, it is hard for the mode shape from the test and finite element model to match perfectly for those chosen modes.

In order to calibrate such a bridge model, a few parameters were used to correlate with the field test results: moment of inertia (I) of the frame elements, the bearing spring stiffness in the longitudinal direction, and joint masses in the transverse direction. Initial inputs were estimated based on design information and design blue prints. These estimates do not account for man-made errors and in-site material characteristics such as: 1) construction tolerances or errors that can make as-built dimensions different from design dimensions, or 2) actual strengths of materials such as the actual compressive strength of concrete, which affects its modulus of elasticity. After the initial input, a preliminary free vibration analysis was run to observe the frequencies and mode shapes. Then, the model calibration was performed by adjusting the stiffness and masses of the bridge members until an acceptable match was observed in the natural frequency and mode shape.

In this analysis, the inertial moment in the x-direction of the girder cross-section was increased by 1.862 times the original values. The joint masses used in global Y-direction are only 1.5 times of the total masses in X- and Z- directions. For the springs at the end bearings in the longitudinal direction, a value of 30650 is used for the spring stiffness. With these adjustments, a reasonable match in the natural frequency and mode shape between the finite element model and field-testing results can be obtained.

Usually, the traffic-induced excitation can produce clear acceleration records in the vertical direction, and the traffic combined with wind excitations can produce acceleration records in the transverse direction. Since there was no excitation along the longitudinal direction, clear acceleration records in the longitudinal direction were not obtained. Therefore, the matching of the frequencies is difficult for this mode. Figure 4.10 to Figure

4.15 show the comparison of the mode shape obtained from field-testing and finite element model in vertical and transverse directions.

Observing from the figures, one can see that the first two vertical modes from the finite element model and field-testing match almost perfectly. For the third vertical mode and the first transverse mode, the matching seems to be quite well at peaks locations, except there is shifting between peaks. For the last two transverse modes, the matches are not as good as the previously mentioned four modes; there is a 0.2 times differences in magnitude at the center span for the second transverse mode, and a shifting in the third transverse mode. Nevertheless, the frequencies obtained from the finite element model and field-testing are within 4% of errors. The comparisons are shown in Table 4.2.

5. SEISMIC RESPONSE ANALYSIS

5.1 General

There are a number of different analytical methods for assessing the seismic vulnerability of existing bridges, which include elastic analysis, inelastic pushover analysis, capacity spectrum analysis and nonlinear dynamic analysis (Priestly et al. 1996). Each approach incorporates different assumptions, which vary in complexity of application. The problem an engineer has is assessing the seismic vulnerability of a bridge structure is to select the most appropriate and cost-effective method for performing the assessment. Under minor ground motions, a bridge will experience little inelastic behavior and thus the linear elastic analysis is convenient and reasonable for bridge design and assessment for minor earthquakes. A limitation of the elastic analysis method is that the linear analysis offers little information regarding the inelastic response of the structure. However, there are more disadvantages of utilizing nonlinear dynamic time-history analysis. The structural elements of nonlinear models are considerably more complex than those of their linear elastic counterparts, and the numerical algorithms do not always ensure convergence to a physically valid solution. Moreover, processing and evaluating of the outputs often requires considerable effort, and the results can be extremely sensitive to input parameters and structural models. In this particular case, modal time-history analysis is used because the bridge is assumed to behave linearly elastic with small displacements under the expected earthquake loading. Modal time-history method was used instead of response spectrum method for the main bridge due to the importance of the bridge and also due to the lack of seismic considerations in its initial design. Time-history analysis is the most sophisticated analysis technique available to a structural analyst in the seismic evaluation of bridges. Using this level of analysis gives the engineer a complete description of the behavior of a structure at all times throughout an earthquake. Since no strong earthquake records are available for the Eastern U.S., time-history analyses for Kentucky bridges were performed using artificial earthquake records characteristic of the New Madrid and other nearby seismic zones.

Modal time-history method for the earthquake analysis involves the solution of the following equation of motion:

$$[M] \{ \ddot{u} \} + [C] \{ \dot{u} \} + [K] \{ u \} = -[M] \{ \ddot{u}_g \} \qquad (5.1)$$

Where $[M]$, $[C]$ and $[K]$ are global mass matrix, damping matrix and stiffness matrix, respectively. $\{\ddot{u}\}$, $\{\dot{u}\}$ and $\{u\}$ are structural system nodal acceleration, velocity and displacement vectors, respectively. $\{\ddot{u}_g\}$ is the earthquake motion for which the bridge's response has to be calculated. *SAP2000* software performs exact integration of the modal-response equations for a linear variation of the time-function between the input data time points. Therefore, the results are not dependent on the selection of a "time-integration interval" as in some other methods (Wislon and Habibullah, 1998). Damping for all the modes are assumed to be 5%.

Usually, time-histories representing the 50-year event and the 500-year event were generated for the vertical and two orthogonal horizontal directions (Street et al. 1996). Due to the importance of the I-24 Parallel Bridges at Cumberland River crossing, each bridge is to be evaluated for the 250-year event and the maximum credible 500-year event. The definition of the 250-year event is: the peak horizontal particle acceleration, at the top of rock, that has a 90% probability of not being exceeded in 250 years (i.e. 10% probability of exceedance). Likewise, the 500-year event has a 90% probability of not being exceeded in 500 years. A recurrence rate (return period) can be calculated for the earthquakes, which would produce the 250-year and the 500-year events.

For low probability of exceedance, the recurrence rate is approximately (National Highway Institute, 1996) the ratio of time and return period. Some states require even longer return periods for their earthquake design. For example, California Department of Transportation (*CalTrans*) uses a 2400-year return period, which has a 10% probability of exceedance every 250 years.

For the bridge location in this study, borders of Lyon and Livingston Counties, Kentucky, a time-history with peak horizontal acceleration of 15% gravity represents the *AASHTO* 250-year design earthquake. The time-history for the "near maximum credible earthquake" (500-year event) has a peak horizontal acceleration of 19% gravity in Lyon and Livingston Counties.

It is important to note that the main bridge in this study is analyzed based on four critical aspects in the authors' opinions. These four different aspects are stresses of critical members (compared with the yield stress of steel = 36 *ksi*), stresses of pier members (compared with the yield stress of reinforce concrete = 60 *ksi*), displacement at bearings (compared with half of the width of the bearing shoe plate), and bolt shear of the bearings anchor bolts (using Capacity/Demand ratios to check against bolt shear failure).

5.2 Seismic Response

The seismic response of the Cumberland River Parallel Bridges is calculated for the 250-year and the 500-year events. For the bridge site at Lyon and Livingston Counties, peak horizontal bedrock accelerations for the 250-year and the 500-year artificial earthquakes are 0.15g and 0.19g (Figures 5.1 and 5.2). The 250-year event and the 500-year event durations are 20.485 and 40.965 seconds consisting of 4097 and 8193 data points at 0.005-second intervals, respectively. The input motion for the 250-year and the 500-year events along the transverse, vertical and horizontal directions are presented in Figure 5.3 to Figure5.8, respectively. The peak ground accelerations for the 250-year and the 500-year events along the transverse, vertical and horizontal directions are 4.805, 5.393, 5.409, 9.486, 5.850, and 9.531 *ft/sec^2*, respectively. Since the longitudinal direction of the earthquake may not coincide with the longitudinal direction of the bridge, it is necessary to analyze the bridge under different excitation cases as described in Table 5.1. Due to the *LL*11 excitation case of the 250-year event (Table 5.1), the horizontal (longitudinal) earthquake is applied along

longitudinal direction of the bridge. Similarly, for the *LL*22, *TT*11 and *TT*22 excitation cases, only the longitudinal and transverse earthquakes are reversed in longitudinal and transverse directions. For the *L*1*T*2*V*3 and *L*2*T*1*V*3 excitation cases, all the three earthquakes are applied simultaneously in three directions. The vertical earthquake is only applied along the vertical direction of the bridge. For the 500-year event, the arrangement is exactly the same as the 250-year event, except the name is with *M*, which stands for maximum credible event.

Normally, time-history analysis produces a very large quantity of output. It is difficult to monitor the maximum forces for all the members and maximum displacements at all the joints in a modal time-history analysis for seismic excitation kind of loading. Therefore, members and joints are selected based on their proximity to critical locations. Due to the symmetry of the main bridge, only members and joints from half of the main bridge are considered. From *SAP2000* software, forces and moments are obtained for selected members. Stresses are calculated externally using simple computer programs/spreadsheets. Table 5.2 presents the cross-sectional properties of members that are selected for stresses calculation.

As an example, for the *L*1*T*2*V*3 excitation case (Table 5.1) of the 250-year event, the time history plots of longitudinal, transverse and vertical displacements at joint 90 (Figure 5.9) are presented in Figure 5.10 to Figure 5.13. It is observed that the maximum longitudinal displacement of 0.0712 *ft* occurs at 13.70 second, the maximum transverse displacement of 0.0772 *ft* occurs at 27.81 second, and the maximum vertical displacement of 0.0645 *ft* occurs at 12.44 second. The axial force time history for member 212 (Figure 5.9) under the *L*1*T*2*V*3 excitation case of the 250-year event is presented in Figure 5.14. The maximum axial force of 1009 *kips* occurs at 13.00 second.

For stress calculations, the axial stresses are calculated from P/A and bending stresses are calculated from M_{12}/Z_{13} and M_{13}/Z_{12}. M_{12} and M_{13} are the bending moments in the local 1-2 and 1-3 planes respectively. Z_{12} and Z_{13} are the section modulus about the 1-2 and 1-3 planes, respectively. Combined stresses are calculated as the sum of P/A, $M_{12}/Z_{13,}$ and M_{13}/Z_{12} directly to simplify the process. Then, members with stresses exceeding the yield strength of steel are recalculated with appropriate signs to get the maximum stresses.

Axial stress = σ_a = Axial force/Area
Bending stress in 1-2 plane at I^{th} joint = σ_{b12i}= Absolute (M_{12} at Node I / Z_{13})
Bending stress in 1-2 plane at J^{th} joint = σ_{b12j}= Absolute (M_{12} at Node J / Z_{13})
Bending stress in 1-3 plane at I^{th} joint = σ_{b13i}= Absolute (M_{13} at Node I / Z_{12})
Bending stress in 1-3 plane at J^{th} joint = σ_{b13j}= Absolute (M_{13} at Node J / Z_{12})

Combined axial and bending stress:

Stress at node $I = \sigma a + \sigma_{b12i} + \sigma_{b13i}$
Stress at node $J = \sigma a + \sigma_{b12j} + \sigma_{b13j}$

Shear stress is calculated from the shear forces in the 1-2 and 1-3 planes, i.e.,

27

Shear stress (τ) = {Square root of [$(SF_{12})^2 + (SF_{13})^2$]} / Area

The absolute maximum of stresses of all the excitation cases of the 250-year and the 500-year events and self-weight obtained from time-history analysis are presented in tabular forms (Table 5.3 to Table 5.17) and are discussed in the following section. Table 5.3 lists the stresses at selected members (Figure 5.9) due to self-weight of the main bridge. Maximum axial stress is found to be 0.013 *ksi* in members 317, 324, 332 and 339. Maximum shear stress is obtained as 1.84 *ksi* in member 219. Combined stresses from axial and bending stresses have a maximum of 18.545 *ksi* in member 185. Generally, the axial stresses are found to be larger than the bending stresses due to earthquake motion. In the tables, bending stresses are calculated and presented at the beginning node *I*, and end node *J* of the member.

Tables 5.4 and 5.10 present the member stresses due to excitation cases LL11 and *LL*11*M* of the 250-year and the 500-year events. The maximum axial stress in Table 5.4 is found to be 4.25 *ksi* in member 5. For Table 5.10, the maximum axial stress is 11.191 *ksi* in member 5. Maximum of the combined axial and bending stresses in Table 5.4 and Table 5.10 are found to be 6.35 *ksi* and 16.78 *ksi* for member 5, where both values are less than the yield strength of steel. Shear stresses are found to have a maximum of 0.134 *ksi* and 0.351 *ksi* for member 12 of Table 5.4 and Table 5.10.

Under the seismic excitation cases *LL*22 and *LL*22M of the 250-year and the 500-year events, the stresses calculated for selected members (Figure 5.9) are presented in Table 5.5 and Table 5.11. The maximum axial stresses in Table 5.5 and Table 5.11 are 2.92 *ksi* and 10.31 *ksi* for member 5. The maximum of the combined axial and bending stresses in Table 5.5 and Table 5.11 are 4.413 *ksi* and 15.585 *ksi* for member 5, where both values are far below the yield stress of steel. Shear stresses are found to have a maximum of 0.095 *ksi* and 0.35 *ksi* for member 12 in Table 5.5 and Table 5.11.

For the seismic excitation cases *TT*11 and *TT*11M of the 250-year and the 500-year events, the stresses at selected members (Figure 5.9) are presented in Table 5.6 and Table 5.12. The maximum axial stresses in Table 5.6 and Table 5.12 are 1.93 *ksi* and 6.35 *ksi* in member 339. The maximum of the combined axial and bending stresses in Table 5.6 and Table 5.12 are 6.06 *ksi* and 15.349 *ksi* for member 192, where both values are less than the yield strength of steel. Shear stresses are found to have a maximum of 0.125 *ksi* and 0.62 *ksi* for member 212 in Tables 5.6 and 5.12.

Table 5.7 and Table 5.13 list the stresses at selected members (Figure 5.9) when the seismic excitation cases *TT*22 and *TT*22*M* of the 250-year and the 500-year events are applied. The maximum axial stresses in Table 5.7 and 5.13 are found to be 2.09 *ksi* in member 87 and 5.75 *ksi* in member 339. Maximum of the combined axial and bending stresses in Tables 5.7 and 5.13 are 9.34 *ksi* in member 192 and 18.541 *ksi* in member 212, in which both are less than the yield stress of steel. The listed maximum shear stresses in Table 5.7 and Table 5.13 are 0.21 *ksi* for member 192, and 0.47 *ksi* for member 212.

Tables 5.8 and 5.14 list the stresses at selected members (Figure 5.9) when the seismic excitation cases *L*1*T*2*V*3 and *L*1*T*2*V*3*M* of the 250-year and the 500-year events are applied. In these excitation cases, three components of time histories are combined and applied on three orthogonal directions. Axial stresses in Tables 5.8 and 5.14 due to seismic forces alone are found to have a maximum of 5.23 *ksi* in member 72 and 12.38 *ksi* in member 87. The maximum combined axial and bending stresses in Table 5.8 and Table 5.14 due to seismic forces only are 14.54 *ksi* in member 192 and 29.25 *ksi* for member 212. Furthermore, these tables also present the maximum of the combined stresses from the Dead load (*DL*) ± Earthquake load (*EQ*). The maximum combined stresses are 31.17 *ksi* for member 192 (Table 5.8), and 45.89 *ksi* for member 212 (Table 5.14). The maximum combined stresses for member 192 is less than the yield stress of steel while the maximum combined stresses for member 212 exceeds the yield stress of steel. Table 5.14 shows that the combined stresses of several members including member 57, member 65, member 72, member 80, member 87, member 185, member 192 and member 212 exceed the yield stress of steel, are members. These member stresses are re-calculated and shown in Table 5.16 with appropriate sign to obtain the maximum stresses. Table 5.16 shows that only the combined stress of member 212 (-40.22 *ksi*) is actually larger than the yield strength of steel, which means that member 212 can not resist the excitation case *L*1*T*2*V*3*M* of the 500-year event. Smaller shear stresses are shown in Table 5.8 and Table 5.14, with a maximum value of 2.34 *ksi* for member 219, and 2.844 *ksi* for member 212.

Table 5.9 and Table 5.15 present the stresses at selected members (Figure 5.9) when two of the excitation directions are reversed, i.e. under *L*2*T*1*V*3 and *L*2*T*1*V*3*M* (Table 5.1) excitation cases of the 250-year and the 500-year events. Axial stresses shown in Table 5.9 and Table 5.15 due to seismic forces alone have a maximum of 3.70 *ksi* for member 87 and 10.96 *ksi* for member 5. The maximum combined axial and bending stresses in Table 5.9 and Table 5.15 due to seismic forces only are 10.66 *ksi* for member 192 and 33.90 *ksi* for member 212. Similar to Tables 5.8 and 5.14, Tables 5.9 and 5.15 also present the maximum combined stresses from the *DL* ± *EQ*. The maximum combined stresses are 27.28 *ksi* for member 192 (Table 5.9), which is less than the yield strength of steel, and 50.54 *ksi* for member 212 (Table 5.15), which exceeds the yield stress of steel. The combined stresses of members 185, 192 and 212 shown in Table 5.15 from *DL* and *EQ* exceed the yield stress of steel. These member stresses are re-calculated and shown in Table 5.17 with appropriate sign to obtain the maximum stresses. Again, Table 5.17 shows that only the combined stress of member 212 (-50.50 *ksi*) is larger than the yield strength of steel that means that member 212 cannot resist the *L*2*T*1*V*3*M* excitation case of the 500-year event. In both Tables 5.9 and 5.15, the maximum shear stresses are 2.33 *ksi* for member 219 and 2.98 *ksi* for member 212.

The displacements at selected nodes (Figure 5.9) are shown in Table 5.18 to Table 5.20 for the self-weight and different excitation cases of the 250-year and the 500-year events (Table 5.1). Table 5.21 presents the maximum displacements from the self-weight and maximum excitation cases. The maximum displacements due to the self-weight and the *L*1*T*2*V*3 and *L*1*T*2*V*3*M* excitation cases in the longitudinal direction at the exterior bearing plate (joint 1) are 0.46" and 1.10" respectively. The maximum displacements at top of the interior bearing (joint 97) in the longitudinal and transverse directions due to the self-weight and the *L*1*T*2*V*3 and *L*1*T*2*V*3*M* excitation cases are 0.86", 0.84", 2.10", and 2.72"

respectively. The maximum displacements at bottom of the interior bearing (joint 96) in the longitudinal and transverse directions due to the self-weight and the $L1T2V3$ and $L1T2V3M$ excitation cases are 0.89", 0.81", 2.14", and 2.63" respectively. All the displacements are within the limit of half the shoe plate for exterior expansion bearings (Pier 3 and Abutment 2) and interior fixed bearings (Piers 4 and 5). The limits for the exterior expansion bearings are 13.5" in the longitudinal direction and 18" in the transverse direction, while they for the interior fixed bearings are 22.5" in the longitudinal direction and 36" in the transverse direction.

The maximum relative movement between the top and bottom of the bearings over Pier 4, for example, is equal to the maximum relative longitudinal movement between the bottoms of Piers 3 and 4. For the interior fixed bearings over Piers 4 and 5 (Figure 2.2), this maximum relative movement is 1.0418". When an allowable displacement of 22.5" is considered, the loss of span at the supports over Piers 4 and 5 cannot occur.

Additionally, similar shear stress calculations at selected members above are performed on the pier members of Pier 4. Table 5.22 presents the cross-sectional properties of pier members that are selected for shear stress calculation. Table 5.23 and Table 5.24 show the pier members shear stresses of different seismic excitation cases of the 250-year and the 500- year earthquake and main bridge dead load. From Tables 5.23 and 5.24, the maximum shear stress is 2.62 ksi in pier member 196 for the $L1T2V3M$ excitation case and the self-weight of the main bridge, which is much less than the yield stress of reinforce concrete (60 ksi).

Maximum and minimum base shears and moments from different modal time histories of the 250-year and the 500-year events are obtained for the main bridge and listed in Table 5.25 to Table 5.28. These values are presented for all the different excitation cases listed in Table 5.1. Again, similar stress calculations to those discussed above are performed and summarized as the combined maximum stresses. The maximum stresses from these tables are 19.67 ksi for the $L1T2V3M$ excitation case of the 500-year event, which is less than the 60 ksi yield stress of steel in the reinforced concrete.

5.3 Capacity / Demand Ratios

Since the superstructure of the bridge is connected to the substructure through bearings, it is necessary to check these bearings against loss-of-span and anchor bolt shear failure. Table 5.29 lists the available anchor bolt shear capacity (V_c) and base shears at each pier for the 250-year and 500-year events. The anchor bolt capacity V_c is calculated by assuming the shear strength of the bolt as 26.97 ksi. The resultant of base shear is calculated as the square root of the sum of squares of the longitudinal and transverse base shears. The seismic demand (V_b) is calculated by multiplying with 1.25, as per *FHWA Retrofitting Manual.* Only Piers 4 and 5 due to the 500-year event have *C/D* ratios (r_{bf}) of 0.35. For the 250-year event the calculated *C/D* ratios are larger than 1.

5.4 Retrofit for the Main Bridge

From the previous sections, it is clear that members 212 and the symmetric part will yield due to $L1T2V3M$ and $L2T1V3M$ excitation cases of the 500-year event. It is suggested that these members be strengthened to prevent yielding.

Also, the interior fixed bearings at Piers 4 and 5 are to be strengthened to resist the 500-year event. It is suggested that additional anchor bolts may be provided to retrofit the bearings at Piers 4 and 5 in order to provide the additional 1000 *kips* of shear forces resistant. Alternatively, the bearings may be replaced with seismic isolation bearings.

6. SEISMIC EVALUATION OF THE APPROACH BRIDGE

6.1 General

Each of the two parallel bridges has three approach spans in each bound. The structural components of the bridge are two steel girders, bracings, stiffeners, and the floor system. The bracing system is a combination of transverse and diagonal bracings. The approach spans are symmetric in the transverse direction.

The main structural elements of the approach spans consist of two steel girders, each with a depth of 12'. The flange thickness and flange width varies along the length of each girder. The thickness of the web of each girder is ½". Web stiffeners are used for the girders. The two girders are braced in the transverse and longitudinal directions. The transverse bracing consists of a cross frame with W-shaped beams (W12x45) at top and bottom chords, two sets of two channel beams welded back-to-back, and a W-shaped beam, which is aligned vertically at the center. These W-shaped beams connect the top of each girder to the center of the bottom W-shaped member. The second type of bracing is a diagonal bracing, which is located midway between the transverse bracings. The beams of the diagonal bracing connect the bottom chord of the transverse bracing to the girders.

The floor system consists of a 9-1/2" thick concrete slab supported by three longitudinal W24×68 stringers, which are connected to transverse built up floor beams.

6.2 Fixed and Expansion Bearings

For the three main spans of each bridge crossing the Cumberland River, the superstructure is supported by expansion bearings at pier 2 and fixed bearings at pier 1. The expansion bearings permit longitudinal translation and rotation, and the fixed bearings only allow longitudinal rotation. Figures 6.1 and 6.2 show the details of the expansion and fixed bearings.

The fixed bearings are of standard pinned bearing-type, and consist of cast steel upper shoes supported on 5" diameter steel pins, which bear on cast steel bottom shoes. The upper shoes are bolted to the bottom flanges of the steel girders, and the bottom shoes are rigidly attached to the piers by anchor bolts. The anchor bolts are of 2-1/2" diameter, and are embedded for 3'-10" into the concrete piers.

The expansion bearings on the exterior piers consist of pin and roller combinations to allow rotation and translation. The top shoes of the bearing are connected to the bottom flanges of the steel girders, which are connected to the pins. The bottom shoes are connected to the piers through anchor bolts. A total of four 1-1/2" diameter anchor bolts, each has a length of 2'-6" are used for each bearing. Slots were made in the bottom flanges of the steel girder to permit the possible longitudinal translation.

6.3 Substructure

The approach spans are supported on three piers and one abutment. The first pier (Pier 1) at the end support consists of two columns connected by a pier cap beam at the top. The height of these columns, measured from the bottom of the bearing to the top of the pile cap is 65.8'. The thickness of the columns varies from 6' at the top to 8'-2" at the pile cap. The height of the columns of pier 2 is 74.5'. The thickness of the columns of pier 2 varies from 6' at the top to 8.5' at the pile cap. The width of the columns for all piers is 6'. All the piers are constructed with reinforced concrete of '*AA*' class.

6.4 Structural Modeling

Simple structural models are used to idealize the approach spans depending on the type of the bearings, which are mounted on the top of the piers. The mathematical models are considered as single degree of freedom (*SDOF*) systems. The mass of the *SDOF* system is the summation of the mass of the superstructure and one-third the mass of the piers. The transverse stiffness and longitudinal stiffness of the mathematical model are calculated in accordance with the Seismic Evaluation and Retrofit of Bridges (Harik et al., 1997).

Harik et al. (1999) reported that due to the unavailability of detailed site soil investigation, few representative models with maximum and minimum stiffness can be adopted for calculating the forces and displacements, respectively. The same procedure is adopted herein. For force calculations, total transverse stiffness and total longitudinal stiffness are calculated assuming that the piers are fixed at the bottom of pile caps. For displacement calculations, however, the total longitudinal stiffness is calculated by assuming that the piers are fixed at an imaginary depth beneath the pile equal to half the length of the piles. The extended parts are assumed to have similar structural properties to those of the piers. This simplified method (Figure 6.3) is adopted in this study for conservative estimations of the seismic forces and displacements.

6.5 Seismic Response Analysis

The parallel bridges at the Cumberland River crossing are located on the boundaries of Lyon and Livingston counties in western Kentucky, which is close to the New Madrid Seismic Zone. Hence, it was analyzed under the seismic motion corresponding to 0.15*g* earthquake of the 250-year event and 0.19*g* earthquake of the 500-year event. Herein, the

seismic analysis of the simplified *SDOF* models of the approach spans is carried out using the response spectrum method. The response spectra developed by Street et al (1996), and shown in Figures 6.4 through Figure 6.7, are used. Damping ratio of the response spectra is 5%. The results of the seismic analysis were utilized to determine the possibility of any unseating due to excessive longitudinal displacements at the expansion bearings or bearing failure when the shear strength of the anchor bolts is deemed inadequate.

The influence of the vertical seismic component on the longitudinal displacements was neglected. The force capacity/demand (*C/D*) ratio and the combined seismic force of the bolts under longitudinal and transverse earthquake loading are considered. Zimmerman and Brittain (1979) reported that the longitudinal seismic excitations result in more damage than that of the transverse ones for multi-span simple bridges. Therefore, for the displacement *C/D* ratio, only the longitudinal earthquake loading was considered.

In the response spectrum analysis, site soil coefficient *S* was assumed to be 1.5. The C_s is limited to 2.0*A* for soil profile type III according to Division *IA*, section 3 of *AASHTO Specifications* (2002).

6.6 Capacity/Demand Ratios

For the approach spans, the ratio between the bearing force capacity (V_c) and the demand (V_d) is called $r_{C/D}$, and is calculated in accordance with section *A*.4.3 of the Seismic Retrofitting Manual for Highway Bridges (Buckle and Friedland 1995). The anchor bolt capacity (V_c) is calculated by assuming that the nominal shear strength of each bolt is equal to 188.6 kN and 524 kN for the 1.5" and the 2.5" diameter bolts, respectively. The resultant shear force is calculated as the square of the sum of squares of the longitudinal and the transverse shear forces. According to the Seismic Retrofitting Manual for Highway Bridges (Buckle and Friedland 1995), the seismic demand (V_d) is calculated by multiplying the resultant shear force by 1.25. The V_c of one bolt of pier 1 is 524 kN, and the V_d under the 250-year seismic event is 251 kN resulting in a $r_{C/D}$ of 2.08. The V_d of pier 1 under the 500-year seismic event is 318 kN, resulting in a $r_{C/D}$ of 1.64. The V_c of one bolt of pier 2 is 188 kN, and the V_d under the 250-year seismic event is 256 kN, resulting in a $r_{C/D}$ of 0.73. The V_d of pier 2 under the 500-year seismic event is 325 kN, resulting in a $r_{C/D} = 0.58$. Therefore, the $r_{C/D}$ of the anchor bolts for pier 2 is inadequate for both the 250-year and the 500-year events, and retrofit of the bearings is recommended

For the approach spans, the expansion bearing displacement *C/D* ratios $= \dfrac{\Delta_s(c) - \Delta_i(d)}{\Delta_{eq}(d)}$ are calculated according to section *A*.4.2 of the Seismic Retrofitting Manual for Highway Bridges (Buckle and Friedland 1995), where $\Delta_s(c)$ is the available displacement. $\Delta_i(d)$ is the maximum possible displacement due to a 32°C (90°F) maximum differential temperature effect, and $\Delta_{eq}(d)$ is the maximum displacement due to earthquake. The calculated *C/D* ratios are greater than 1.0 and hence loss-of-span could not occur due to the displacement considerations.

7. Conclusions and Recommendations

7.1 General

The I-24 Parallel Bridges at the Cumberland River crossing may be subjected to earthquakes in the future. Therefore, it is important to evaluate the bridge under the projected seismic motion. In this work, since the bridge is located at the borders of Lyons and Livingston Counties at Kentucky, the effect of projected earthquake events with accelerations of 0.15g and 0.19g for the 250-year and the 500-year events is investigated.

7.2 Main Bridge

The seismic evaluation of the main bridge consisted of field ambient vibration testing, finite element modeling and seismic response analysis using the modal time-history method. Field-testing was mainly carried out to identify the natural frequencies and mode shapes of the main bridge. These frequencies and mode shapes were compared with the results from the finite element model to calibrate the finite element model. Comparisons were performed for three vertical modes, three transverse modes and one longitudinal mode.

The three-dimensional finite element model was developed with frame elements, joint restraints and spring restraints. The model was calibrated utilizing the field test results for the natural frequencies and mode shapes. Frequencies obtained from field-testing for the first modes in the vertical, transverse and longitudinal directions are 0.875 Hz, 1.382 Hz, and 2.850 Hz, respectively. Frequencies obtained from the finite element model for the first modes in the vertical, transverse and longitudinal directions are 0.875 Hz, 1.383 Hz, and 2.853 Hz, respectively. Reasonable agreement between the field test and finite element model results was obtained.

Moreover, seismic response analyses were carried out using modal time-history method. Displacements of selected joints and stresses for selected members were calculated. The results are presented in tabular forms for different seismic excitation by cases. Stresses for pier members are also presented. For the bearings, the maximum displacements in the transverse and longitudinal directions are within the limit of the shoe plates, so no loss of span is expected.

7.3 Approach Spans

Simple structural models were used to idealize the approach spans depending on the type of the bearings, which are mounted on the top of the piers. The mathematical models are considered as single degree of freedom (*SDOF*) systems. The mass of the *SDOF* system is the summation of the mass of the superstructure and one-third the mass of the piers. The transverse stiffness and longitudinal stiffness of the mathematical model are calculated in

accordance with the Seismic Evaluation and Retrofit of Bridges (Harik et al., 1997). Seismic response of the approach spans was carried out using the response spectrum method to determine the maximum forces and displacements.

7.4 250-year Event

The seismic analysis indicates that the main spans of the bridge can resist the 250-year event without yielding or loss-of-span at supports. Consequently, retrofitting is not required for the main bridge members and bearings for the 250-year event.

The seismic analysis of the approach spans indicates that pier #1 can resist the 250-year event without yielding or unseating at supports. Consequently, no retrofitting is required. However, the anchor bolts of pier #2 cannot resist the applied shear forces during the 250-year and retrofit should be considered. Retrofitting can be made by increasing the capacity of the shear bolts or by providing seismic isolation bearings.

7.5 500-year Event

The seismic analysis of the main spans indicates that the maximum combined axial and bending stresses were 50.495 ksi for member # 212 and the symmetric members, which are located on the bottom chords adjacent to pier #4 on the span that connect pier #4 and pier#5. This stress is larger than the yield stress of steel and hence this particular member and the symmetric members have to be replaced in order to prevent material yielding. Shear stresses of the pier members, base shears and moments were also calculated and presented in tabular forms. It was found that the stresses are within the yield strength of reinforced concrete and thus failure is unlikely to occur.

The seismic analysis of the approach spans indicates that pier #1 can resist the 500-year event without yielding or unseating at supports. Consequently, no retrofitting is required. The seismic analysis of the approach spans indicates that the anchor bolts of pier #2 cannot resist the applied shear forces during the 500-year event, and retrofit should be considered. Retrofitting can be made by increasing the capacity of the shear bolts or by providing seismic isolation bearings.

REFERENCES

AASHTO (1996), *Standard Specifications for Highway Bridges*, 16th Edition, American Association of State Highway and Transportation Officials, Washington D.C.

AASHTO (1998), *LRFD Bridge design Specifications*, Second Edition, American Association of State Highway and Transportation Officials, Washington D.C.

Abdel-ghaffer, A.M. and R. H. Scanlan (1985a), *Ambient Vibration Studies of Golden Gate Bridge: I. Suspended Structure*, ASCE J. of Engrg. Mech., 111(4), 463-482.

Abdel-ghaffer, A.M. and R. H. Scanlan (1985b), *Ambient Vibration Studies of Golden Gate Bridge: II.* ASCE J. of Engrg. Mech., 111(4).

Alampalli, S., and Fu, G., (1994), *"Instrumentation for Remote and Continuous Monitoring of Structural Condition,"* Paper No.940261 Presented at the Transportation Research Board's 73rd Annual Meeting, Washington D.C..

Andersen, P., Brincker, R. and Kirkegaard, P.H. (1996). "Theory of Covariance Equivalent ARMAV Models of Civil Engineering Structures." *Proceedings of IMAC14, the 14th International Modal Analysis Conference,* Dearborn, MI, 518-524.

Bathe, K.J., (1982), Finite *Element Procedures in Engineering Analysis*, Prentice-Hall, Inc., Englewood Cliffs, New Jersey, Chapter 12.

Bendat, J.S. and Piersol, A.G. (1993). *Engineering Applications of Correlation and Spectral Analysis.* 2nd edition, John Wiley & Sons, New York.

Blevins, Robert D., (1995), *Formulas for Natural Frequency and Mode Shape*, Krieger Publishing Company, Malabar, Florida.

Bracewell, Ronald N., (2000), *The Fourier Transform and Its Applications*, Third Edition McGraw Hill.

Buckland, P.G., et al., (1979), "Suspension Bridge Vibrations: Computed and Measured," *Journal of the Structural Division*, Vol. 105, No. ST5, 859-874.

Buckle, I.G. and I. M. Friedland (editors, 1995), Seismic Retrofitting Manual for Highway Bridges, Report No. FHWA-RD-94-052, Federal Highway Administration.

Chapra, S.C., and Canale, R.P., (1988), *Numerical Methods for Engineers*, 2nd Edition, McGraw-Hill, Inc., New York, New York, Chapter 13.

De Roeck, G. and Peeter, B. (1999). *MACEC2.0 – Modal Analysis on Civil Engineering Constructions*, Department of Civil Engineering, Catholic University of Leuven, Belgium. http://www.bwk.kuleuven.ac.be/bwk/mechanics/macec

De Roeck, G., Peeters, B. and Ren, W.X. (2000). "Benchmark Study on System Identification through Ambient Vibration Measurements." *Proceedings of IMAC-XVIII*, the 18th International Modal Analysis Conference, San Antonio, Texas, 1106-1112.

Doll, H., (1994), "Eigenfrequencies and Normal Modes of the Norderelb Bridge Near Hamburg: Numerical and Measuring Investigations," Proceedings of *the 12th International Modal Analysis Conference*, Honolulu, Hawaii, 449-455.

EERI (1990), Loma Prieta Earthquake Resistance Report, Earthquake Spectra, Special supplement to Vol.6, 448.

EERI (1995), Northbridge Earthquake Resistance Report, Earthquake Spectra, Special supplement to Vol.11, 116.

Ewins, D.J. (1986). *Modal Testing: Theory and Practice*. Research Studies Press Ltd., England.

Farrar, C., White, K., and Mayes, R., (1995), "Vibration Testing of the I-40 Bridge Before and after the Introduction of Damage," Presented at the North-American Workshop on Instrumentation and Vibration Analysis of Highway Bridges, Cincinnati, Ohio.

Harik, I.E., D. Dietz, C. Hill and M.W. Guo (1997), Seismic Evaluation and Retrofit of Bridges, Research Report KTC-96-5, Kentucky Transportation Center, University of Kentucky.

Harik, I.E., D. L. Allen, R. L. Street, M.W. Guo, R.C. Graves, J. Harrison and M. J. Gawry (1997a), Free and Ambient Vibration of Brent-Spence Bridge, ASCE J. of Struct. Engrg., 123(9), 1262-1268.

Harik, I.E., D. L. Allen, R. L. Street, M. W. Guo, R.C. Graves, J. Harrison, and M. J. Gawry(1997b), Seismic Evaluation of Brent-Spence Bridge, ASCE J. of Struct. Engrg., 123(9), 1269-1275.

Harik, I.E., Madasamy, C., Chen, D.L., Zhou, L.N., Sutterer, K. Street, R.L., and Allen, D.L. (1998), Seismic Evaluation of the Ohio River Bridge on US51 at Wickliffe, Kentucky, Research Report, KTC-98-20, Kentucky Transportation Center, University of Kentucky.

Harik, I.E., Madasamy, C., Chen, D.L., Zhou, L.N., Sutterer, K. Street, R.L., and Allen, D.L. (1999a), Seismic Evaluation of the US41 Northbound Bridge over the Ohio River

at Henderson, KY, Research Report, KTC-99-16, Kentucky Transportation Center, University of Kentucky.

Harik, I.E., Vasudevan, K., Madasamy, C., Chen, D.L., Zhou, L.N., Sutterer, K. Street, R.L., and Allen, D.L. (1999b), Seismic Evaluation of the US41 Southbound Bridge over the Ohio River at Henderson, KY, Research Report, KTC-99-17, Kentucky Transportation Center, University of Kentucky.

Hudson, D.E., (1977), "Dynamic Tests of Full-Scale Structures", Journal of the Engineering Mechanics Division, Vol. 103, No.EM6, 1141-1157.

Jacob, K., (1995), "Geotechnical and Seismological Aspects of New York Seismic Code Provisions," *National Center for Earthquake Engineering Research Bulletin*, Vol. 9, No. 3.

James III, G.H., Carne, T.G. and Lauffer, J.P. (1995). "The Natural Excitation Technique (NExT) for Modal Parameter Extraction from Operating Structures*." International Journal of Analytical and Experimental Modal Analysis,* 10(4), 260-277.

Johnston, A.C., (1982), "A Major Earthquake Zone on the Mississippi*," Scientific American*, Vol. 246, No. 4, 60-68.

Johnston, A.C., (1985), "A Brief Overview of the Geology, Seismicity and Seismic Hazard of the Central Mississippi Valley Area," Presented at A Regional Seminar on Earthquake Fundamentals for the Mississippi Valley, Memphis, Tennessee.

Johnston, A.C. and Nava, S.J. (1985), "Recurrence Rates and Probability Estimates for the New Madrid Seismic Zone", Journal *of Geophysical Research*, Vol. 90, No. B8, 6737-6753.

Maia, N.M.M. and Silva, J.M.M. Edited. (1997), *Theoretical and Experimental Modal Analysis.* Research Studies Press Ltd., England.

Mayes, R.L., et al., (1992), "AASHTO Seismic Isolation Design Requirements for Highway Bridges," *Journal of Structural Engineering*, Vol. 118, No. 1, 284-304.

Morteza A. M., M. Torkamani and H. E. Lee, (2002). "Dynamic Behavior of Steel Deck Tension-Tied Arch Bridges to Seismic Excitation", *Journal of Bridge Engineering*, Vol. 7, No.1, 57-67.

National Highway Institute (NHI) Course No. 13063, (1996), "Seismic Bridge Design Applications," Notes from Sessions 1 & 2.

Paultre, P., Proulx, J., and Talbot, M., (1995), "Dynamic Testing Procedures for Highway Bridges Using Traffic Loads," *Journal of Structural Engineering*, Vol. 121, No. 2, 362-376.

Priestly, M.J.N., F. Seible and G. M. Calvi, Seismic Design and Retrofit of Bridges, John-Wiley & Sons, Inc., 1996.

Saiidi, M., Douglas, B., and Feng, S. (1994), "Prestress Force Effect on Vibration Grequency of Concrete Bridges," *Journal of Structural Engineering*, Vol. 120, No. 7, 2233-2241.

Shahawy, M.A., (1995), "Non-destructive Strength Evaluation of Florida Bridges," Proceedings of SPIE Nondestructive Evaluation of Aging Infrastructure Conference, Oakland, California.

Shama, A. A., J. B. Mander, S. S. Chen and A. J. Aref, (2001). "Ambient Vibration and Seismic Evaluation of a Cantilever Truss Bridge", *Engineering Structures*, 23(2001), 1281-1292

Shelley, S.J., et al., (1995), "Dynamic Testing (Vibration Analysis) of Highway Bridges," Notes Presented at the *North-American Workshop on Instrumentation and Vibration Analysis of Highway Bridges*, Cincinnati, Ohio.

Street, R., Z. Wang, I. E. Harik, D. L. Allen and J. J. Griffin (1996), Source Zones, Recurrence Rates, and Time Histories for Earthquakes Affecting Kentucky, Report No.KTC-96-4, Kentucky Transportation Center, University of Kentucky.

Van der Auweraer, H. and Hermans, L. (1999). "Structural Modal Identification from Real Operating Conditions." *Sound and Vibration*, 33(1), 34-41.

Van Overschee, P. and De Moor, B. (1996). *Subspace Identification for Linear Systems: Theory, Implementation and Applications,* Kluwer Academic Publishers, Dordrecht, Netherlands

Ventura, C.E., Felber, A.J., and Prion, G.L., (1994). "Seismic Evaluation of a Long Span Bridge by Modal Testing", Proceedings of the *12th International Modal Analysis Conference*, Honolulu, Hawaii, 1309-1315.

Wendichansky, D.A., Chen, S.S., and Mander, J.B., (1995). "In-Situ Performance of Rubber Bearing Retrofits," Presented at National Seismic Conference on Bridges and Highways, San Diego, California.

Wilson, E.L. and A. Habibullah (1998), SAP2000 - Structural Analysis Users Manual, Computers and Structures, Inc.

Wilson, E.L., M.W. Yuvan, and J.M. Dickens (1982), Dynamic Analysis by Direct Superposition of Ritz Vectors, Earthquake Engineering and Structural Dynamics, 10, 813-823.

Wilson, E.L., and Tetsuji, I.J., (1983), "An Eigensolution Strategy for Large Systems," *Computers and Structures*, Vol. 16, 259-265.

Zimmerman, R. M. and Brittain, R. D. (1979), Seismic Response of Multi-simple Span Highway Bridges, Proceedings of the 3rd Canadian Conference on Earthquake Engineering, Montreal, 1091-1120.

Table 3.1   Different points per setup

Setup	Moveable Stations	Base Stations
SL1	L1, L2, L3	L1, L6, L8, R8
SL2	L4, L5, L6	L1, L6, L8, R8
SL3	L7, L8, L9	L1, L6, L8, R8
SR1	R1, R2, R3	R1, R6, R8, L8
SR2	R4, R5, R6	R1, R6, R8, L8
SR3	R7, R8, R9	R1, R6, R8, L8

Table 3.2a   The Cumberland River Bridge accelerometer layout – right lane

Station	Filename	Accelerometer Block	Channel Number (XX)	Orientation
1	**F1chXX.dat**	Green	0	Horizontal
			1	Transverse
			2	Vertical
2		Orange	3	Horizontal
			4	Transverse
			5	Vertical
6		Red - Base 2	6	Horizontal
			7	Transverse
			8	Vertical
3		White	9	Horizontal
			10	Transverse
			11	Vertical
1		Blue - Base 3	12	Horizontal
			13	Transverse
			14	Vertical
8 - Left Lane	**E1chXX.dat**	Black – Base 1	0	Horizontal
			1	Transverse
			2	Vertical
8 - Right Lane		Yellow – Base 1	3	Horizontal
			4	Transverse
			5	Vertical
4	**F2chXX.dat**	Green	0	Horizontal
			1	Transverse
			2	Vertical
5		Orange	3	Horizontal
			4	Transverse
			5	Vertical
6		Red - Base 2	6	Horizontal
			7	Transverse
			8	Vertical
6		White	9	Horizontal
			10	Transverse
			11	Vertical
1		Blue - Base 3	12	Horizontal
			13	Transverse
			14	Vertical
8 - Left Lane	**E2chXX.dat**	Black – Base 1	0	Horizontal
			1	Transverse
			2	Vertical
8 - Right Lane		Yellow – Base 1	3	Horizontal
			4	Transverse
			5	Vertical
7	**F3chXX.dat**	Green	0	Horizontal
			1	Transverse
			2	Vertical
8		Orange	3	Horizontal
			4	Transverse
			5	Vertical
6		Red - Base 2	6	Horizontal
			7	Transverse
			8	Vertical
9		White	9	Horizontal
			10	Transverse
			11	Vertical
1		Blue - Base 3	12	Horizontal
			13	Transverse
			14	Vertical
8 - Left Lane	**E3chXX.dat**	Black – Base 1	0	Horizontal
			1	Transverse
			2	Vertical
8 - Right Lane		Yellow – Base 1	3	Horizontal
			4	Transverse
			5	Vertical

Table 3.2b   Cumberland River Bridge Accelerometer Layout – Left Lane

Station	Filename	Accelerometer Block	Channel Number (XX)	Orientation
1	**H1chXX.dat**	Green	0	Horizontal
			1	Transverse
			2	Vertical
2		Orange	3	Horizontal
			4	Transverse
			5	Vertical
6		Red - Base 2	6	Horizontal
			7	Transverse
			8	Vertical
3		White	9	Horizontal
			10	Transverse
			11	Vertical
1		Blue - Base 3	12	Horizontal
			13	Transverse
			14	Vertical
8 - Left Lane	**G2chXX.dat**	Black – Base 1	0	Horizontal
			1	Transverse
			2	Vertical
8 - Right Lane		Yellow – Base 1	3	Horizontal
			4	Transverse
			5	Vertical
4	**H2chXX.dat**	Green	0	Horizontal
			1	Transverse
			2	Vertical
5		Orange	3	Horizontal
			4	Transverse
			5	Vertical
6		Red - Base 2	6	Horizontal
			7	Transverse
			8	Vertical
6		White	9	Horizontal
			10	Transverse
			11	Vertical
1		Blue - Base 3	12	Horizontal
			13	Transverse
			14	Vertical
8 - Left Lane	**G3chXX.dat**	Black – Base 1	0	Horizontal
			1	Transverse
			2	Vertical
8 - Right Lane		Yellow – Base 1	3	Horizontal
			4	Transverse
			5	Vertical
7	**H3chXX.dat**	Green	0	Horizontal
			1	Transverse
			2	Vertical
8		Orange	3	Horizontal
			4	Transverse
			5	Vertical
6		Red - Base 2	6	Horizontal
			7	Transverse
			8	Vertical
9		White	9	Horizontal
			10	Transverse
			11	Vertical
1		Blue - Base 3	12	Horizontal
			13	Transverse
			14	Vertical
8 - Left Lane	**G4chXX.dat**	Black – Base 1	0	Horizontal
			1	Transverse
			2	Vertical
8 - Right Lane		Yellow – Base 1	3	Horizontal
			4	Transverse
			5	Vertical

Table 3.3   Possible sequent frequencies from peak picking

Full Data	Longitudinal Data	Vertical Data	Transverse Data
0.866	-	0.886	1.383
1.416	1.416	1.416	1.9
1.783	-	1.783	2.183
2.35	2.35	2.35	2.35
2.466	-	2.45	2.466
2.633	2.85	2.65	2.633
3.05	-	3.05	2.863
3.15	3.2	3.15	3.233
3.833	-	-	3.833
4.25	4.25	4.25	4.366
4.65	4.65	2.65	4.65

Table 3.4   Possible frequencies from stochastic subspace identification

Order	Longitudinal Data		Vertical Data		Transverse Data	
	f(Hz)	ξ (%)	f(Hz)	ξ (%)	f(Hz)	ξ (%)
1	2.85	3.4	0.875	0.6	1.382	1.2
2	-	-	1.417	1.6	1.915	1.1
3	-	-	1.780	1.3	2.625	1.0

Table 4.1 Natural frequencies, modal participation factors and modal participating mass ratios of the main bridge (exact eigenvectors system)

Mode Number	Circular Frequency (Hz)	Angular Frequency (rad/s)	Period (sec)	Modal Participation Factors			Modal Participating Mass Ratios					
							Individual Mode (Percent)			Cumulative Sum (Percent)		
				X-DIR	Y-DIR	Z-DIR	X-DIR	Y-DIR	Z-DIR	X-DIR	Y-DIR	Z-DIR
1	0.875	5.498	1.143	4.640E-07	1.160E-06	1.325E+00	0	0	0.356	0	0	0.356
2	1.107	6.957	0.903	5.910E-07	-9.823E-02	1.940E-05	0	0.003	0	0	0.003	0.356
3	1.383	8.692	0.723	-3.920E-05	-8.942E+00	2.540E-05	0	26.006	0	0	26.009	0.356
4	1.413	8.875	0.708	-9.287E-02	-2.730E-05	-1.480E-04	0.002	0	0	0.002	26.009	0.356
5	1.778	11.169	0.563	-1.030E-05	-3.560E-05	1.400E+01	0	0	39.668	0.002	26.009	40.023
6	1.816	11.413	0.551	-3.140E-06	1.800E-05	-3.210E-05	0	0	0	0.002	26.009	40.023
7	1.931	12.135	0.518	-1.930E-05	-2.580E-05	3.960E-05	0	0	0	0.002	26.009	40.023
8	1.989	12.495	0.503	-3.700E-05	9.155E+00	4.180E-05	0	27.256	0	0.002	53.265	40.023
9	2.293	14.410	0.436	-1.480E-05	-1.413E-01	5.820E-05	0	0.007	0	0.002	53.271	40.023
10	2.601	16.346	0.384	-5.620E-05	-4.380E-04	3.970E-04	0	0	0	0.002	53.271	40.023
11	2.853	17.923	0.351	1.980E+01	2.930E-05	-4.360E-05	78.708	0	0	78.710	53.271	40.023
12	2.939	18.468	0.340	8.773E-01	-2.280E-04	1.540E-04	0.155	0	0	78.864	53.271	40.023
13	2.968	18.648	0.337	7.310E-05	-7.325E+00	-1.460E-04	0	17.452	0	78.864	70.723	40.023
14	3.656	22.968	0.274	-1.340E-04	-1.210E-04	-1.132E+00	0	0	0.260	78.864	70.723	40.283
15	3.718	23.359	0.269	-2.150E-04	2.210E-04	-8.600E-04	0	0	0	78.864	70.723	40.283
16	3.842	24.137	0.260	-1.225E-03	-1.241E-03	1.238E-03	0	0	0	78.864	70.723	40.283
17	4.036	25.360	0.248	-3.830E-05	1.526E-03	-1.409E-03	0	0	0	78.864	70.723	40.283
18	4.410	27.706	0.227	4.670E-04	-4.060E-05	-3.190E+00	0	0	2.060	78.864	70.723	42.343
19	4.655	29.247	0.215	-2.900E-04	-2.509E+00	-5.980E-04	0	2.047	0	78.864	72.770	42.343
20	4.714	29.618	0.212	-1.131E-02	-2.610E-04	-1.520E-04	0	0	0	78.864	72.770	42.343

Table 4.2 Comparisons of Frequencies between FE Model and Field-testing

Mode	FE Freq. (Hz)	Field-testing Freq. (Hz)	Difference (%)
1st Vertical	0.875	0.875	0
2nd Vertical	1.413	1.417	0.28
3rd Vertical	1.778	1.780	0.11
1st Transverse	1.383	1.382	0.07
2nd Transverse	1.989	1.915	3.86
3rd Transverse	2.601	2.625	0.91
1st Longitudinal	2.853	2.850	0.11

Table 5.1 Description of Seismic Excitation Cases

Seismic Excitation Cases	Description
LL11 / LL11M*	Horizontal Component of 250- / 500- year Earthquake Applied Along Longitudinal Direction of the Bridge.
LL22 / LL22M*	Transverse Component of 250- / 500- year Earthquake Applied Along Longitudinal Direction of the Bridge.
TT11 / TT11M*	Horizontal Component of 250- / 500- year Earthquake Applied Along Transverse Direction of the Bridge
TT22 / TT22M*	Transverse Component of 250- / 500- year Earthquake Applied Along Transverse Direction of the Bridge
L1T2V3 / L1T2V3M*	Horizontal, Vertical and Transverse Components of 250- / 500-year Earthquakes are Applied Along Longitudinal, Vertical and Transverse Directions of the Bridge, respectively.
L2T1V3 / L2T1V3M*	Horizontal, Vertical and Transverse Components of 250- / 500- year Earthquakes are Applied Along Transverse, Vertical and Longitudinal Directions of the Bridge, respectively.

*M means the maximum credible event.

Table 5.2 Cross Sectional Properties of Member for Stress Calculation

Element Number	Area, A (in^2)	Moment of Inertia, I$_{13}$ (in^4)	Section Modulus, Z$_{13}$ (in^3)	Moment of Inertia, I$_{12}$ (in^4)	Section Modulus, Z$_{12}$ (in^3)
5	240	1020010	13784	24703	1176
12	282	1251229	16795	30866	1470
20	282	1251229	16795	30866	1470
27	324	1486072	19814	37045	1764
50	324	1486072	19814	37045	1764
57	324	1486072	19814	37045	1764
65	324	1486072	19814	37045	1764
72	324	1486072	19814	37045	1764
80	324	1486072	19814	37045	1764
87	324	1486072	19814	37045	1764
170	453	2374817	29139	64524	2689
177	477	3511963	35947	64526	2689
185	477	3511963	35947	64526	2688
192	516	5845416	47331	64528	2689
212	516	5845416	47331	64528	2689
219	489	4148048	39318	64526	2689
227	489	4148048	39318	64526	2689
234	480	3653544	36719	64526	2689
317	408	3106773	31382	55301	2304
324	408	3106773	31382	55301	2304
332	408	3106773	31382	55301	2304
339	408	3106773	31382	55301	2304

Table 5.3 Self-Weight Induced Stresses (ksi)

Element Number	Stresses due to Self-Weight							
	Axial Stress	Bending Stress in 1-2		Bending Stress in 1-3		Combined Stress		Shear Stress
		Node I	Node J	Node I	Node J	Node I	Node J	
5	0.006	0.001	0.003	9.58E-05	3.391	0.007	3.400	1.639
12	0.005	0.002	0.002	2.786	5.441	2.793	5.448	1.335
20	0.006	0.001	0.001	5.441	7.980	5.448	7.986	1.100
27	0.005	0.001	0.001	6.764	8.748	6.770	8.754	0.891
50	0.005	2.72E-04	4.08E-04	11.466	12.188	11.472	12.194	0.335
57	0.005	4.08E-04	0.001	12.189	12.747	12.194	12.753	0.264
65	0.005	2.04E-04	3.40E-04	12.747	12.758	12.753	12.764	0.025
72	0.005	3.40E-04	4.76E-04	12.758	12.606	12.764	12.612	0.080
80	0.005	2.04E-04	3.40E-04	12.606	11.905	12.611	11.911	0.326
87	0.005	3.40E-04	4.76E-04	11.905	11.041	11.911	11.047	0.397
170	0.004	0.002	0.005	12.043	15.427	12.049	15.436	1.574
177	0.004	0.005	0.014	12.505	15.363	12.515	15.382	1.557
185	0.004	0.014	0.004	15.363	18.537	15.382	18.545	1.727
192	0.004	0.004	0.043	14.079	16.581	14.087	16.628	1.659
212	0.011	0.046	0.008	16.581	13.856	16.638	13.875	1.806
219	0.011	0.008	0.013	16.679	13.504	16.698	13.529	1.843
227	0.011	0.013	0.005	13.504	10.620	13.528	10.637	1.676
234	0.011	0.005	0.002	11.372	8.403	11.388	8.416	1.642
317	0.013	0.001	0.001	11.333	12.111	11.347	12.124	0.447
324	0.013	0.001	0.001	12.111	12.771	12.125	12.784	0.382
332	0.013	0.001	0.001	12.771	13.069	12.784	13.083	0.184
339	0.013	0.001	0.001	13.069	13.250	13.083	13.264	0.119

Table 5.4 Members Stresses (ksi) due to Seismic Excitation Case LL11 (250-year event)

| Element Number | Axial Stress | Stresses due to LL11 Earthquake (250 years) | | | | | | Shear Stress |
| | | Bending Stress in 1-2 | | Bending Stress in 1-3 | | Combined Stress | | |
		Node I	Node J	Node I	Node J	Node I	Node J	
5	4.248	1.038	1.977	2.52E-06	0.120	5.286	6.345	0.070
12	4.001	1.607	1.276	0.098	0.195	5.706	5.472	0.134
20	4.025	0.794	0.535	0.195	0.295	5.015	4.856	0.065
27	3.641	0.451	0.615	0.250	0.331	4.342	4.586	0.054
50	3.696	0.266	0.310	0.435	0.452	4.397	4.457	0.023
57	3.707	0.311	0.351	0.452	0.459	4.469	4.517	0.026
65	3.683	0.249	0.273	0.459	0.432	4.391	4.388	0.024
72	3.665	0.273	0.282	0.432	0.397	4.371	4.344	0.027
80	3.628	0.255	0.252	0.397	0.332	4.281	4.212	0.035
87	3.591	0.252	0.230	0.332	0.260	4.174	4.080	0.037
170	2.036	0.169	0.087	0.443	0.472	2.648	2.595	0.017
177	1.869	0.087	0.016	0.382	0.404	2.338	2.288	0.012
185	1.794	0.150	0.111	0.404	0.418	2.348	2.323	0.015
192	1.583	0.109	0.068	0.318	0.328	2.010	1.979	0.012
212	1.408	0.196	0.072	0.255	0.158	1.859	1.638	0.066
219	1.384	0.068	0.020	0.190	0.093	1.642	1.498	0.068
227	1.303	0.172	0.120	0.093	0.095	1.568	1.518	0.063
234	1.226	0.115	0.012	0.102	0.206	1.443	1.444	0.061
317	0.371	0.171	0.019	0.409	0.317	0.952	0.708	0.051
324	0.266	0.018	0.135	0.317	0.221	0.601	0.622	0.053
332	0.159	0.158	0.008	0.221	0.111	0.538	0.278	0.061
339	0.054	0.006	0.149	0.111	3.86E-04	0.171	0.203	0.061

Table 5.5 Members Stresses (ksi) due to Seismic Excitation Case LL22 (250-year event)

Element Number	Axial Stress	Bending Stress in 1-2		Bending Stress in 1-3		Combined Stress		Shear Stress
		Node I	Node J	Node I	Node J	Node I	Node J	
5	2.924	0.710	1.390	2.02E-06	0.099	3.634	4.413	0.056
12	2.729	1.129	0.866	0.082	0.162	3.940	3.758	0.095
20	2.701	0.578	0.369	0.162	0.245	3.441	3.315	0.050
27	2.436	0.311	0.424	0.208	0.275	2.954	3.134	0.040
50	2.560	0.192	0.217	0.362	0.376	3.114	3.153	0.016
57	2.597	0.219	0.272	0.376	0.383	3.191	3.251	0.019
65	2.610	0.171	0.199	0.383	0.360	3.163	3.169	0.018
72	2.622	0.200	0.227	0.360	0.331	3.183	3.180	0.022
80	2.621	0.175	0.191	0.331	0.279	3.127	3.090	0.028
87	2.616	0.191	0.190	0.279	0.223	3.085	3.029	0.030
170	1.530	0.146	0.071	0.375	0.410	2.050	2.011	0.019
177	1.399	0.071	0.018	0.332	0.359	1.802	1.776	0.015
185	1.336	0.136	0.095	0.359	0.382	1.831	1.813	0.016
192	1.168	0.094	0.046	0.290	0.307	1.552	1.521	0.013
212	1.301	0.177	0.059	0.263	0.176	1.742	1.536	0.058
219	1.280	0.054	0.023	0.212	0.109	1.547	1.412	0.060
227	1.207	0.162	0.111	0.109	0.110	1.478	1.429	0.056
234	1.138	0.107	0.011	0.118	0.189	1.363	1.338	0.054
317	0.348	0.168	0.019	0.333	0.259	0.850	0.626	0.042
324	0.250	0.017	0.134	0.259	0.180	0.526	0.564	0.044
332	0.150	0.156	0.008	0.180	0.091	0.486	0.248	0.049
339	0.050	0.006	0.147	0.091	3.14E-04	0.147	0.198	0.050

Table 5.6 Members Stresses (ksi) due to Seismic Excitation Case TT11 (250-year event)

Element Number	Axial Stress	Bending Stress in 1-2		Bending Stress in 1-3		Combined Stress		Shear Stress
		Node I	Node J	Node I	Node J	Node I	Node J	
5	0.677	0.235	0.464	1.09E-06	0.038	0.911	1.179	0.022
12	0.329	0.385	1.114	0.031	0.062	0.745	1.505	0.035
20	0.332	1.244	0.331	0.062	0.096	1.638	0.758	0.043
27	0.697	0.274	0.714	0.081	0.108	1.052	1.519	0.026
50	1.103	0.965	0.909	0.151	0.167	2.220	2.179	0.008
57	1.378	0.905	1.199	0.167	0.179	2.450	2.756	0.015
65	1.382	1.150	0.990	0.179	0.185	2.712	2.558	0.007
72	1.537	0.988	1.302	0.185	0.188	2.711	3.027	0.013
80	1.542	1.265	1.077	0.188	0.183	2.994	2.802	0.011
87	1.615	1.076	1.335	0.183	0.174	2.874	3.124	0.012
170	0.756	0.822	0.757	0.136	0.155	1.714	1.668	0.028
177	0.678	0.755	1.726	0.126	0.140	1.559	2.544	0.045
185	0.679	1.657	2.154	0.140	0.156	2.476	2.989	0.035
192	0.733	2.152	5.189	0.119	0.137	3.004	6.059	0.120
212	0.817	4.300	1.165	0.151	0.131	5.268	2.112	0.125
219	0.696	1.172	0.692	0.157	0.136	2.024	1.523	0.036
227	0.692	0.711	0.564	0.136	0.115	1.539	1.371	0.016
234	0.534	0.574	1.062	0.123	0.101	1.230	1.696	0.024
317	1.678	1.288	1.272	0.144	0.156	3.110	3.106	0.008
324	1.863	1.269	1.585	0.156	0.166	3.288	3.614	0.014
332	1.867	1.547	1.415	0.166	0.171	3.579	3.453	0.006
339	1.933	1.414	1.649	0.171	0.173	3.518	3.755	0.010

Table 5.7 Members Stresses (ksi) due to Seismic Excitation Case TT22 (250-year event)

Element Number	Axial Stress	Bending Stress in 1-2		Bending Stress in 1-3		Combined Stress		Shear Stress
		Node I	Node J	Node I	Node J	Node I	Node J	
5	0.901	0.323	0.665	1.34E-06	0.050	1.224	1.617	0.033
12	0.355	0.543	1.432	0.041	0.082	0.939	1.868	0.044
20	0.347	1.542	0.623	0.082	0.126	1.971	1.096	0.060
27	0.875	0.522	1.065	0.107	0.142	1.503	2.082	0.036
50	1.439	1.301	1.181	0.197	0.215	2.937	2.835	0.011
57	1.827	1.175	1.538	0.215	0.228	3.217	3.593	0.017
65	1.830	1.464	1.231	0.228	0.233	3.523	3.294	0.010
72	2.047	1.228	1.527	0.233	0.232	3.508	3.805	0.016
80	2.045	1.505	1.189	0.232	0.222	3.782	3.456	0.014
87	2.092	1.189	1.449	0.222	0.206	3.503	3.747	0.017
170	0.828	0.967	0.688	0.131	0.162	1.926	1.678	0.042
177	0.490	0.685	1.958	0.131	0.165	1.306	2.613	0.069
185	0.487	1.844	2.990	0.165	0.204	2.496	3.680	0.056
192	0.578	2.982	8.572	0.155	0.187	3.715	9.337	0.210
212	0.646	4.290	1.088	0.210	0.177	5.146	1.911	0.125
219	0.549	1.094	0.591	0.213	0.176	1.856	1.316	0.039
227	0.546	0.585	0.516	0.176	0.144	1.307	1.205	0.021
234	0.460	0.519	0.889	0.154	0.122	1.132	1.470	0.025
317	1.698	1.144	1.137	0.136	0.149	2.979	2.984	0.009
324	1.869	1.134	1.435	0.149	0.159	3.152	3.462	0.013
332	1.872	1.401	1.281	0.159	0.164	3.432	3.317	0.006
339	1.931	1.280	1.501	0.164	0.166	3.376	3.599	0.009

Table 5.8 Members Stresses (ksi) due to Seismic Excitation Case L1T2V3 (250-year event) and Dead Load

| Element Number | Stresses due to L1T2V3 Earthquake (250 years) | | | | | | | | | Maximum Stresses from DL & EQ* | | |
| | Axial Stress | Bending Stress in 1-2 | | Bending Stress in 1-3 | | Combined Stress | | Shear Stress | Combined Stress | | Shear Stress |
		Node I	Node J	Node I	Node J	Node I	Node J		Node I	Node J	
5	5.000	1.270	2.424	3.48E-05	0.971	6.270	8.395	0.468	6.278	11.794	2.108
12	4.203	1.969	2.491	0.798	1.552	6.969	8.245	0.405	9.763	13.693	1.740
20	4.223	2.183	1.066	1.552	2.253	7.958	7.541	0.316	13.406	15.528	1.416
27	4.217	0.897	1.627	1.910	2.457	7.024	8.301	0.261	13.794	17.055	1.152
50	4.751	1.539	1.439	3.186	3.458	9.476	9.648	0.174	20.948	21.842	0.510
57	5.102	1.434	1.797	3.458	3.813	9.994	10.712	0.159	22.188	23.466	0.423
65	5.070	1.660	1.452	3.907	3.953	10.637	10.476	0.097	23.390	23.240	0.122
72	5.230	1.449	1.698	3.953	4.054	10.633	10.981	0.087	23.396	23.593	0.167
80	5.184	1.677	1.389	4.054	3.936	10.915	10.508	0.108	23.526	22.419	0.434
87	5.166	1.388	1.607	3.936	3.762	10.490	10.535	0.122	22.400	21.581	0.520
170	2.611	1.015	0.747	2.711	3.453	6.337	6.811	0.368	18.387	22.248	1.943
177	2.182	0.743	1.948	2.799	3.480	5.724	7.610	0.373	18.239	22.992	1.930
185	2.107	1.851	3.043	3.480	4.263	7.439	9.413	0.439	22.820	27.958	2.167
192	2.102	3.034	8.578	3.238	3.863	8.374	14.543	0.481	22.461	31.171	2.140
212	1.956	4.221	1.139	3.842	3.122	10.019	6.217	0.511	26.657	20.092	2.318
219	1.863	1.142	0.590	3.758	2.931	6.763	5.384	0.499	23.461	18.913	2.342
227	1.779	0.650	0.546	2.931	2.352	5.360	4.676	0.430	18.888	15.313	2.107
234	1.549	0.547	0.891	2.518	2.337	4.614	4.777	0.413	16.002	13.193	2.055
317	1.851	1.156	1.143	2.818	2.992	5.824	5.986	0.181	17.171	18.110	0.628
324	1.888	1.140	1.479	2.992	3.177	6.020	6.544	0.166	18.145	19.329	0.549
332	1.825	1.400	1.284	3.177	3.254	6.402	6.362	0.108	19.187	19.445	0.292
339	1.916	1.282	1.550	3.254	3.309	6.452	6.775	0.091	19.535	20.039	0.210

*Note: DL means dead load, EQ means earthquake load.

Table 5.9 Members Stresses (ksi) due to Seismic Excitation Case L2T1V3 (250-year event) and Dead Load

Element Number	Stresses due to L2T1V3 Earthquake (250 years)								Maximum Stresses from DL & EQ*		
	Axial Stress	Bending Stress in 1-2		Bending Stress in 1-3		Combined Stress		Shear Stress	Combined Stress		Shear Stress
		Node I	Node J	Node I	Node J	Node I	Node J		Node I	Node J	
5	3.513	0.820	1.643	3.48E-05	1.072	4.333	6.228	0.514	4.340	9.627	2.154
12	2.891	1.336	1.608	0.881	1.708	5.108	6.206	0.425	7.901	11.655	1.759
20	2.864	1.433	0.612	1.708	2.454	6.005	5.931	0.326	11.453	13.917	1.426
27	2.772	0.512	1.059	2.080	2.657	5.364	6.488	0.257	12.134	15.242	1.148
50	3.140	1.095	1.043	3.367	3.533	7.602	7.716	0.171	19.074	19.910	0.506
57	3.447	1.040	1.411	3.533	3.755	8.019	8.612	0.156	20.213	21.366	0.420
65	3.461	1.279	1.109	3.755	3.889	8.494	8.459	0.090	21.247	21.223	0.115
72	3.657	1.107	1.434	3.889	3.979	8.653	9.069	0.076	21.417	21.681	0.156
80	3.655	1.394	1.094	3.979	3.861	9.028	8.610	0.115	21.639	20.521	0.441
87	3.701	1.094	1.437	3.861	3.702	8.656	8.839	0.132	20.566	19.886	0.529
170	1.926	0.830	0.803	2.801	3.514	5.557	6.242	0.366	17.606	21.678	1.940
177	1.786	0.799	1.715	2.849	3.482	5.434	6.983	0.370	17.949	22.365	1.927
185	1.733	1.612	2.195	3.482	4.214	6.827	8.142	0.431	22.209	26.687	2.158
192	1.707	2.191	5.158	3.200	3.791	7.098	10.656	0.440	21.185	27.284	2.100
212	1.877	4.318	1.207	3.827	3.096	10.022	6.180	0.495	26.660	20.054	2.301
219	1.746	1.211	0.700	3.727	2.887	6.684	5.333	0.484	23.382	18.862	2.327
227	1.681	0.796	0.642	2.887	2.356	5.365	4.679	0.423	18.893	15.316	2.099
234	1.390	0.646	1.070	2.522	2.225	4.558	4.686	0.409	15.947	13.102	2.051
317	1.836	1.315	1.274	2.859	3.076	6.010	6.186	0.175	17.357	18.311	0.623
324	1.935	1.271	1.617	3.076	3.256	6.282	6.808	0.159	18.407	19.593	0.542
332	1.904	1.567	1.416	3.256	3.302	6.727	6.622	0.095	19.512	19.705	0.278
339	1.939	1.415	1.684	3.302	3.319	6.656	6.942	0.077	19.739	20.206	0.196

*Note: DL means dead load, EQ means earthquake load.

Table 5.10 Members Stresses (ksi) due to Seismic Excitation Case LL11M (500-year event)

| Element Number | Stresses due to LL11M Earthquake (500 years) | | | | | | | |
| | Axial Stress | Bending Stress in 1-2 | | Bending Stress in 1-3 | | Combined Stress | | Shear Stress |
		Node I	Node J	Node I	Node J	Node I	Node J	
5	11.191	2.546	5.296	5.85E-06	0.292	13.737	16.779	0.180
12	10.455	4.303	3.320	0.240	0.477	14.998	14.252	0.351
20	10.354	2.184	1.412	0.477	0.722	13.014	12.488	0.170
27	9.223	1.190	1.500	0.612	0.809	11.024	11.531	0.135
50	9.019	0.726	0.755	1.070	1.113	10.816	10.887	0.060
57	9.037	0.758	0.908	1.113	1.135	10.908	11.081	0.066
65	8.980	0.654	0.679	1.135	1.073	10.770	10.732	0.059
72	8.984	0.681	0.747	1.073	0.997	10.738	10.728	0.068
80	8.951	0.628	0.641	0.997	0.849	10.576	10.440	0.084
87	8.920	0.641	0.619	0.849	0.685	10.409	10.224	0.090
170	5.157	0.468	0.234	1.102	1.203	6.728	6.594	0.057
177	4.722	0.232	0.059	0.975	1.052	5.929	5.833	0.046
185	4.518	0.431	0.306	1.052	1.118	6.001	5.942	0.049
192	3.964	0.302	0.166	0.849	0.897	5.114	5.026	0.040
212	4.085	0.562	0.194	0.723	0.481	5.370	4.760	0.164
219	4.018	0.179	0.065	0.579	0.291	4.776	4.374	0.168
227	3.787	0.504	0.349	0.291	0.353	4.582	4.489	0.157
234	3.566	0.335	0.038	0.378	0.562	4.280	4.166	0.151
317	1.087	0.516	0.058	0.962	0.747	2.565	1.891	0.121
324	0.780	0.052	0.411	0.746	0.519	1.579	1.709	0.126
332	0.467	0.479	0.024	0.519	0.262	1.464	0.752	0.143
339	0.157	0.018	0.450	0.262	0.001	0.437	0.608	0.145

Table 5.11 Members Stresses (ksi) due to Seismic Excitation Case LL22M (500-year event)

Element Number	Stresses due to LL22M Earthquake (500 years)							
	Axial Stress	Bending Stress in 1-2		Bending Stress in 1-3		Combined Stress		Shear Stress
		Node I	Node J	Node I	Node J	Node I	Node J	
5	10.310	2.512	4.832	8.71E-06	0.443	12.822	15.585	0.234
12	9.701	3.928	3.088	0.364	0.723	13.992	13.511	0.352
20	9.697	1.963	1.299	0.723	1.093	12.383	12.089	0.199
27	8.782	1.096	1.490	0.927	1.224	10.804	11.497	0.164
50	8.969	0.656	0.754	1.616	1.679	11.241	11.402	0.060
57	9.017	0.757	0.873	1.679	1.712	11.453	11.603	0.065
65	8.980	0.604	0.669	1.712	1.618	11.296	11.268	0.069
72	8.956	0.670	0.708	1.618	1.495	11.245	11.159	0.080
80	8.883	0.618	0.623	1.495	1.263	10.996	10.770	0.115
87	8.807	0.623	0.582	1.263	1.007	10.693	10.396	0.123
170	5.027	0.432	0.221	1.629	1.757	7.088	7.005	0.066
177	4.610	0.218	0.053	1.424	1.521	6.253	6.184	0.054
185	4.420	0.389	0.283	1.521	1.598	6.330	6.302	0.050
192	3.893	0.279	0.163	1.214	1.270	5.387	5.327	0.041
212	3.627	0.507	0.183	1.090	0.720	5.224	4.530	0.246
219	3.566	0.170	0.062	0.867	0.435	4.603	4.063	0.256
227	3.354	0.441	0.308	0.435	0.415	4.231	4.078	0.236
234	3.156	0.296	0.032	0.447	0.805	3.899	3.993	0.230
317	0.953	0.452	0.050	1.495	1.159	2.900	2.163	0.186
324	0.684	0.045	0.361	1.159	0.806	1.888	1.851	0.195
332	0.409	0.420	0.021	0.806	0.406	1.634	0.836	0.220
339	0.138	0.016	0.396	0.405	0.001	0.559	0.534	0.224

Table 5.12 Members Stresses (ksi) due to Seismic Excitation Case TT11M (500-year event)

Element Number	Stresses due to TT11M Earthquake (500 years)							
	Axial Stress	Bending Stress in 1-2		Bending Stress in 1-3		Combined Stress		Shear Stress
		Node I	Node J	Node I	Node J	Node I	Node J	
5	1.678	0.666	1.091	2.34E-06	0.091	2.345	2.861	0.065
12	1.336	0.881	1.960	0.075	0.149	2.291	3.444	0.060
20	1.339	2.062	1.558	0.149	0.229	3.549	3.125	0.099
27	1.976	1.296	2.286	0.194	0.258	3.467	4.520	0.064
50	2.798	2.519	2.151	0.356	0.388	5.673	5.338	0.023
57	3.297	2.143	2.659	0.388	0.411	5.828	6.367	0.023
65	3.295	2.566	2.034	0.411	0.418	6.272	5.747	0.023
72	3.504	2.031	2.389	0.418	0.416	5.953	6.310	0.025
80	3.494	2.386	1.755	0.416	0.398	6.297	5.648	0.027
87	3.445	1.757	1.942	0.398	0.371	5.600	5.758	0.027
170	2.103	1.814	1.319	0.182	0.225	4.099	3.646	0.060
177	1.787	1.311	3.011	0.184	0.228	3.282	5.025	0.106
185	1.785	2.795	4.398	0.228	0.280	4.807	6.463	0.078
192	1.878	4.381	13.215	0.213	0.256	6.472	15.349	0.334
212	2.223	20.982	4.440	0.341	0.280	23.546	6.942	0.621
219	1.651	4.481	1.805	0.337	0.268	6.468	3.724	0.144
227	1.641	1.875	1.443	0.268	0.205	3.784	3.289	0.046
234	0.793	1.473	2.953	0.220	0.169	2.486	3.915	0.071
317	5.615	3.899	3.809	0.330	0.353	9.844	9.777	0.021
324	6.149	3.800	4.749	0.353	0.371	10.302	11.269	0.040
332	6.158	4.638	4.221	0.371	0.381	11.168	10.761	0.019
339	6.345	4.218	4.932	0.381	0.385	10.945	11.663	0.029

Table 5.13 Members Stresses (ksi) due to Seismic Excitation Case TT22M (500-year event)

| Element Number | Stresses due to TT22M Earthquake (500 years) | | | | | | | |
| | Axial Stress | Bending Stress in 1-2 | | Bending Stress in 1-3 | | Combined Stress | | Shear Stress |
		Node I	Node J	Node I	Node J	Node I	Node J	
5	1.712	0.709	1.268	2.20E-06	0.100	2.421	3.080	0.067
12	1.161	1.038	2.567	0.082	0.163	2.281	3.891	0.078
20	1.167	2.807	1.282	0.163	0.250	4.137	2.699	0.116
27	2.024	1.064	2.574	0.212	0.281	3.301	4.880	0.073
50	2.951	3.014	2.641	0.384	0.416	6.349	6.008	0.021
57	3.519	2.632	3.308	0.416	0.436	6.567	7.264	0.034
65	3.526	3.207	2.614	0.436	0.438	7.169	6.578	0.025
72	3.848	2.611	3.101	0.438	0.429	6.897	7.378	0.031
80	3.845	3.109	2.377	0.429	0.400	7.384	6.623	0.033
87	3.846	2.380	2.830	0.400	0.363	6.626	7.039	0.033
170	2.190	2.322	2.142	0.333	0.361	4.845	4.693	0.070
177	2.186	2.134	4.303	0.293	0.327	4.613	6.817	0.118
185	2.194	4.081	5.268	0.327	0.390	6.602	7.852	0.091
192	2.308	5.289	13.716	0.296	0.346	7.892	16.370	0.316
212	2.607	15.486	3.973	0.449	0.388	18.541	6.968	0.469
219	2.117	4.004	2.098	0.467	0.396	6.588	4.611	0.119
227	2.106	2.146	1.758	0.396	0.328	4.647	4.191	0.047
234	1.312	1.783	3.194	0.351	0.280	3.446	4.786	0.074
317	5.057	3.844	3.807	0.371	0.403	9.271	9.267	0.023
324	5.560	3.798	4.752	0.403	0.429	9.762	10.741	0.041
332	5.569	4.638	4.249	0.429	0.442	10.635	10.261	0.019
339	5.749	4.246	4.951	0.442	0.449	10.438	11.148	0.029

Table 5.14 Members Stresses (ksi) due to Seismic Excitation Case L1T2V3M (500-year event) and Dead Load

Element Number	Stresses due to L1T2V3M Earthquake (500 years)								Maximum Stresses from DL & EQ*		
	Axial Stress	Bending Stress in 1-2		Bending Stress in 1-3		Combined Stress		Shear Stress	Combined Stress		Shear Stress
		Node I	Node J	Node I	Node J	Node I	Node J		Node I	Node J	
5	11.800	2.954	6.044	6.09E-05	2.171	14.754	20.015	1.049	14.761	23.415	2.688
12	11.150	4.907	5.171	1.783	3.472	17.840	19.793	0.916	20.633	25.241	2.250
20	11.060	4.358	2.360	3.472	5.227	18.889	18.648	0.796	24.337	26.634	1.897
27	9.956	1.986	3.765	4.431	5.902	16.373	19.623	0.664	23.143	28.377	1.555
50	10.955	3.569	2.911	8.174	8.851	22.697	22.716	0.367	34.169	34.910	0.702
57	11.598	2.906	3.868	8.851	9.419	23.355	24.886	0.327	35.550	37.639[a]	0.590
65	11.631	3.702	2.923	9.419	9.508	24.752	24.061	0.180	37.505[a]	36.825[a]	0.205
72	12.173	2.922	3.485	9.508	9.473	24.603	25.132	0.152	37.367[a]	37.743[a]	0.232
80	12.155	3.572	2.755	9.473	9.005	25.201	23.915	0.247	37.812[a]	35.826	0.573
87	12.375	2.758	3.391	9.005	8.477	24.138	24.242	0.300	36.048[a]	35.288	0.697
170	6.496	2.507	2.257	6.970	8.399	15.973	17.152	0.784	28.022	32.589	2.358
177	6.048	2.251	4.321	6.808	7.974	15.108	18.343	0.793	27.622	33.725	2.350
185	5.849	3.910	5.435	7.974	9.189	17.733	20.473	0.914	33.115	39.018[a]	2.642
192	5.231	5.417	13.664	6.979	7.915	17.627	26.811	0.939	31.714	43.439[a]	2.598
212	5.622	15.307	4.126	8.318	7.311	29.246	17.060	1.038	45.885[a]	30.934	2.844
219	5.215	4.146	2.084	8.801	7.660	18.162	14.959	0.939	34.859	28.487	2.782
227	4.998	2.461	1.873	7.660	6.566	15.119	13.437	0.809	28.647	24.074	2.486
234	4.155	1.893	3.202	7.031	5.922	13.079	13.279	0.791	24.467	21.695	2.434
317	5.898	4.154	3.808	6.246	6.659	16.298	16.364	0.407	27.645	28.488	0.854
324	6.130	3.795	4.984	6.659	6.983	16.583	18.096	0.370	28.707	30.880	0.753
332	5.865	4.933	4.264	6.983	6.993	17.781	17.122	0.247	30.565	30.205	0.430
339	5.843	4.257	5.227	6.993	7.269	17.093	18.339	0.209	30.176	31.603	0.328

*Note: DL means dead load, EQ means earthquake load.
[a]These values need to be recalculated with appropriate signs to get maximum stress.

Table 5.15 Members Stresses (ksi) due to Seismic Excitation Case L2T1V3M (500-year event) and Dead Load

Element Number	Stresses due to L2T1V3M Earthquake (500 years)								Maximum Stresses from DL & EQ*		
	Axial Stress	Bending Stress in 1-2		Bending Stress in 1-3		Combined Stress		Shear Stress	Combined Stress		Shear Stress
		Node I	Node J	Node I	Node J	Node I	Node J		Node I	Node J	
5	10.963	2.472	4.988	6.96E-05	2.251	13.436	18.202	1.084	13.443	21.602	2.723
12	10.011	4.053	4.122	1.849	3.602	15.913	17.736	0.929	18.706	23.184	2.264
20	9.963	3.285	2.223	3.602	5.237	16.850	17.422	0.777	22.297	25.409	1.877
27	8.763	1.865	3.300	4.439	5.714	15.067	17.778	0.662	21.837	26.532	1.553
50	8.935	2.920	2.193	8.026	8.806	19.881	19.935	0.355	31.353	32.129	0.691
57	9.486	2.192	3.267	8.807	9.469	20.484	22.221	0.312	32.678	34.975	0.576
65	9.479	2.961	2.031	9.469	9.606	21.909	21.115	0.195	34.662	33.879	0.220
72	9.693	2.033	2.901	9.606	9.604	21.331	22.197	0.164	34.095	34.809	0.244
80	9.670	2.807	1.740	9.604	9.081	22.080	20.491	0.252	34.692	32.402	0.578
87	9.599	1.746	2.379	9.081	8.517	20.425	20.495	0.309	32.336	31.542	0.706
170	5.273	1.949	1.424	7.218	8.614	14.440	15.311	0.770	26.489	30.747	2.344
177	4.945	1.416	2.981	6.983	8.120	13.344	16.046	0.756	25.859	31.428	2.313
185	4.773	2.843	4.505	8.120	9.250	15.736	18.528	0.882	31.118	37.073[a]	2.609
192	4.310	4.487	13.136	7.025	7.992	15.822	25.437	0.914	29.909	42.065[a]	2.574
212	4.608	21.087	4.416	8.209	7.037	33.904	16.062	1.173	50.542[a]	29.936	2.980
219	4.071	4.442	1.853	8.471	7.216	16.984	13.141	1.009	33.681	26.670	2.852
227	3.894	2.110	1.667	7.216	6.153	13.220	11.713	0.878	26.748	22.350	2.554
234	3.309	1.689	2.960	6.588	5.548	11.586	11.817	0.855	22.974	20.233	2.497
317	6.342	4.182	3.824	6.532	6.783	17.057	16.949	0.469	28.403	29.073	0.916
324	6.572	3.814	4.859	6.783	6.943	17.168	18.374	0.441	29.293	31.158	0.823
332	6.349	4.844	4.227	6.943	6.800	18.137	17.376	0.326	30.921	30.459	0.510
339	6.282	4.222	5.047	6.800	7.086	17.304	18.415	0.287	30.388	31.679	0.406

*Note: DL means dead load, EQ means earthquake load.
[a]These values need to be recalculated with appropriate signs to get maximum stresses.

Table 5.16 Recalculation of Members Stresses (ksi) due to Seismic Excitation Cases L1T2V3M (500-year event) and Dead Load

Element Number	Stresses due to L1T2V3M Earthquake (500 years)							Maximum Stresses from DL & EQ*		
	Axial Stress	Bending Stress in 1-2		Bending Stress in 1-3		Combined Stress		Shear Stress	Combined Stress		Shear Stress
		Node I	Node J	Node I	Node J	Node I	Node J		Node I	Node J	
57	11.598	-2.906	-3.868	-8.851	-9.419	-11.757	-13.287	0.327	-11.757	-13.287	0.590
65	11.631	-3.702	-2.923	-9.419	-9.508	-13.121	-12.430	0.180	-13.121	12.753	0.205
72	12.173	-2.922	-3.485	-9.508	-9.473	-12.430	-12.958	0.152	12.753	-12.958	0.232
80	12.155	-3.572	-2.755	-9.473	-9.005	-13.045	12.155	0.247	-13.045	24.766	0.573
87	12.375	-2.758	-3.391	-9.005	-8.477	12.375	12.375	0.300	24.986	24.286	0.697
185	5.849	-3.910	5.435	7.974	9.189	13.823	20.473	0.914	-15.377	20.473	2.642
192	5.231	5.417	13.664	6.979	7.915	17.627	26.811	0.939	17.627	26.811	2.598
212	5.622	-15.307	4.126	-8.318	7.311	-23.625	17.060	1.038	<mark>-40.217</mark>	17.06	2.844

Table 5.17 Recalculation of Members Stresses (ksi) due to Seismic Excitation Cases L2T1V3M (500-year event) and Dead Load

Element Number	Stresses due to L2T1V3M Earthquake (500 years)							Maximum Stresses from DL & EQ*		
	Axial Stress	Bending Stress in 1-2		Bending Stress in 1-3		Combined Stress		Shear Stress	Combined Stress		Shear Stress
		Node I	Node J	Node I	Node J	Node I	Node J		Node I	Node J	
185	-4.773	-2.843	4.505	8.120	9.250	8.120	13.755	0.882	-15.377	-18.541	2.609
192	-4.310	4.487	13.136	7.025	-7.992	11.512	13.136	0.914	-14.083	-16.581	2.574
212	-4.608	-21.087	-4.416	-8.209	-7.037	-33.904	-16.062	1.173	<mark>-50.495</mark>	-29.936	2.980

*Note: DL means dead load, EQ means earthquake load.

Table 5.18 Displacements (in) due to Self-Weight

Node	Self-Weight		
	U_x	U_y	U_z
1 (EB)[*]	0.0005	0	0
6	0.0005	0	-0.4416
8	0.0006	0	-0.8700
13	0.0006	0	-1.3332
43	0.0008	0	-2.9124
48	0.0009	0	-2.7564
50	0.0009	0	-2.5500
85	0.0012	0.0001	-0.0401
90	0.0012	0.0005	-0.0122
97 (IBT)[*]	0.0012	0.0009	-0.0512
96 (IBB)[*]	-0.0295	0.0001	-0.0512
107	0.0012	0.0005	-0.2556
109	0.0011	0	-0.5184
158	0.0001	0	-5.0220
163	0.0001	0	-5.1012
165	0	0	-5.1288

[*]EB means exterior bearing, IBT means top of interior bearing, and IBB means bottom of interior bearing.

Table 5.19 Displacement (in) Due to Self-weight and Seismic Excitation Cases of 250-year Earthquake

Node	L1T2V3			L2T1V3			LL11			LL22			TT11			TT22		
	U_x	U_y	U_z	U_x	U_y	U_z	U_x	U_y	U_z	U_x	U_y	U_z	U_x	U_y	U_z	U_x	U_y	U_z
1 (EB)[*]	0.4620	0	0	0.3288	0	0	0.3924	0	0	0.2724	0	0	0.0645	0	0	0.0860	0	0
6	0.4824	0.2688	0.1368	0.3432	0.1836	0.1404	0.4104	0.0188	0.0115	0.2844	0.0132	0.0098	0.0672	0.1752	0.0063	0.0898	0.2592	0.0079
8	0.5004	0.5232	0.2700	0.3552	0.3600	0.2760	0.4272	0.0076	0.0225	0.2952	0.0053	0.0192	0.0675	0.3588	0.0125	0.0896	0.5256	0.0156
13	0.5208	0.8556	0.4140	0.3684	0.5904	0.4224	0.4464	0.0079	0.0343	0.3084	0.0055	0.0292	0.0677	0.5928	0.0194	0.0898	0.8592	0.0242
43	0.6420	2.4948	1.0392	0.4332	1.9452	1.0212	0.6000	0.0018	0.0409	0.4068	0.0014	0.0370	0.0430	1.9464	0.0479	0.0506	2.4972	0.0577
48	0.6516	2.5440	1.0140	0.4380	1.9284	0.9924	0.6168	0.0035	0.0304	0.4164	0.0027	0.0287	0.0424	1.9296	0.0463	0.0443	2.5464	0.0558
50	0.6624	2.5584	0.9720	0.4452	1.8768	0.9552	0.6336	0.0018	0.0190	0.4260	0.0015	0.0196	0.0412	1.8768	0.0438	0.0375	2.5596	0.0536
85	0.8436	1.0872	0.1428	0.5916	0.9816	0.1488	0.7932	0.0012	0.0198	0.5364	0.0011	0.0166	0.0755	0.9828	0.0178	0.0890	1.0884	0.0193
90	0.8544	0.9264	0.0774	0.5988	0.9384	0.0784	0.8016	0.0014	0.0102	0.5424	0.0012	0.0086	0.0756	0.9384	0.0167	0.0898	0.9264	0.0172
97 (IBT)[*]	0.8616	0.8400	0.0281	0.6060	0.9168	0.0303	0.8088	0.0002	0.0007	0.5484	0.0002	0.0005	0.0751	0.9168	0.0164	0.0898	0.8400	0.0156
96 (IBB)[*]	0.8556	0.8112	0.0281	0.6012	0.8868	0.0303	0.8100	0.0001	0.0007	0.5496	0.0001	0.0005	0.0753	0.8868	0.0164	0.0901	0.8112	0.0156
107	0.8688	0.8400	0.0774	0.6132	0.9480	0.0755	0.8160	0.0009	0.0145	0.5532	0.0008	0.0118	0.0758	0.9480	0.0183	0.0900	0.8400	0.0171
109	0.8748	0.8556	0.1452	0.6192	1.0104	0.1404	0.8220	0.0010	0.0289	0.5592	0.0008	0.0235	0.0764	1.0104	0.0203	0.0897	0.8556	0.0194
158	0.8904	2.2032	1.0368	0.6312	2.6460	1.0584	0.8880	0.0003	0.0334	0.6204	0.0003	0.0267	0.0183	2.6460	0.0622	0.0184	2.2020	0.0616
163	0.8904	2.2608	1.0692	0.6264	2.7096	1.0704	0.8892	0.0004	0.0169	0.6204	0.0004	0.0135	0.0093	2.7096	0.0632	0.0093	2.2596	0.0625
165	0.8892	2.2800	1.0884	0.6216	2.7324	1.0800	0.8892	0.0003	0	0.6216	0.0004	0	0	2.7324	0.0636	0	2.2800	0.0629

[*]EB means exterior bearing, IBT means top of interior bearing, and IBB means bottom of interior bearing.

Table 5.20 Displacement (in) Due to Self-weight and Seismic Excitation Cases of 500-year Earthquake

Node	L1T2V3M			L2T1V3M			LL11M			LL22M			TT11M			TT22M		
	U_x	U_y	U_z	U_x	U_y	U_z	U_x	U_y	U_z	U_x	U_y	U_z	U_x	U_y	U_z	U_x	U_y	U_z
1 (EB)[*]	1.0968	0	0	1.0176	0	0	1.0404	0	0	9.5640	0	0	0.1584	0	0	0.1632	0	0
6	1.1448	0.4812	0.3120	1.0632	0.3996	0.3048	1.0872	0.0503	0.0293	0.9984	0.0460	0.0437	0.1656	0.3960	0.0140	0.1704	0.4596	0.0132
8	1.1916	0.9360	0.6180	1.1040	0.7884	0.6036	1.1304	0.0201	0.0577	1.0380	0.0184	0.0860	0.1680	0.7968	0.0276	0.1704	0.9300	0.0260
13	1.2444	1.5180	0.9540	1.1520	1.2756	0.9336	1.1808	0.0209	0.0879	1.0848	0.0192	0.1308	0.1692	1.2852	0.0427	0.1716	1.5120	0.0401
43	1.6428	4.2228	2.2488	1.5084	3.2484	2.2272	1.5600	0.0046	0.1182	1.4520	0.0045	0.1704	0.1620	3.2508	0.1025	0.1416	4.2228	0.0962
48	1.6824	4.1388	2.1504	1.5444	3.1908	2.1372	1.5984	0.0089	0.0947	1.4904	0.0086	0.1320	0.1656	3.1956	0.0964	0.1428	4.1376	0.0932
50	1.7184	3.9900	2.0184	1.5804	3.1536	2.0100	1.6356	0.0048	0.0699	1.5276	0.0046	0.0915	0.1668	3.1536	0.0914	0.1440	3.9888	0.0890
85	2.0544	2.6748	0.2040	1.9332	2.0880	0.2364	1.9800	0.0034	0.0495	1.9152	0.0031	0.0754	0.2592	2.0868	0.0430	0.2244	2.6748	0.0485
90	2.0784	2.6784	0.1107	1.9548	2.0088	0.1236	1.9992	0.0039	0.0256	1.9368	0.0036	0.0389	0.2652	2.0064	0.0402	0.2244	2.6784	0.0475
97 (IBT)[*]	2.1000	2.7204	0.0586	1.9752	2.0160	0.0544	2.0160	0.0005	0.0015	1.9548	0.0005	0.0024	0.2724	2.0160	0.0395	0.2256	2.7204	0.0478
96 (IBB)[*]	2.1096	2.6340	0.0586	1.9788	1.9380	0.0544	2.0220	0.0004	0.0015	1.9584	0.0004	0.0024	0.2724	1.9380	0.0395	0.2256	2.6340	0.0478
107	2.1180	2.9172	0.1174	1.9908	2.3148	0.1175	2.0256	0.0025	0.0348	1.9716	0.0024	0.0537	0.2796	2.3136	0.0461	0.2268	2.9160	0.0493
109	2.1336	3.1980	0.2040	2.0040	2.7660	0.2232	2.0340	0.0027	0.0692	1.9884	0.0025	0.1072	0.2856	2.7648	0.0535	0.2340	3.1980	0.0512
158	2.1816	8.7108	2.0844	2.1636	10.237	2.0388	2.1660	0.0010	0.0779	2.1588	0.0009	0.1224	0.0603	10.237	0.1620	0.0546	8.7108	0.1584
163	2.1648	8.8860	2.1468	2.1636	10.416	2.1000	2.1672	0.0012	0.0394	2.1612	0.0011	0.0617	0.0306	10.415	0.1632	0.0277	8.8860	0.1608
165	2.1684	8.9472	2.1816	2.1624	10.478	2.1396	2.1684	0.0011	0.0001	2.1612	0.0010	0.0001	0	10.478	0.1644	0.0001	8.9472	0.1620

[*]EB means exterior bearing, IBT means top of interior bearing, and IBB means bottom of interior bearing.

Table 5.21 Maximum Displacement (in) from Self-weight & Seismic Excitation Cases

Node	Self-weight + L1T2V3			Self-weight + L2T1V3			Self-weight + L1T2V3M			Self-weight + L2T1V3M		
	U_x	U_y	U_z	U_x	U_y	U_z	U_x	U_y	U_z	U_x	U_y	U_z
1 (EB)[*]	0.4625	0	0	0.3293	0	0	1.0973	0	0	1.0181	0	0
6	0.4829	0.2688	0.5784	0.3437	0.1836	0.5820	1.1453	0.4812	0.7536	1.0637	0.3996	0.7464
8	0.5010	0.5232	1.1400	0.3558	0.3600	1.1460	1.1922	0.9360	1.4880	1.1046	0.7884	1.4736
13	0.5214	0.8556	1.7472	0.3690	0.5904	1.7556	1.2450	1.5180	2.2872	1.1526	1.2756	2.2668
43	0.6428	2.4948	3.9516	0.4340	1.9452	3.9336	1.6436	4.2228	5.1612	1.5092	3.2484	5.1396
48	0.6525	2.5440	3.7704	0.4389	1.9284	3.7488	1.6833	4.1388	4.9068	1.5453	3.1908	4.8936
50	0.6633	2.5584	3.5220	0.4461	1.8768	3.5052	1.7193	3.9900	4.5684	1.5813	3.1536	4.5600
85	0.8448	1.0873	0.1829	0.5928	0.9817	0.1889	2.0556	2.6749	0.2441	1.9344	2.0881	0.2765
90	0.8556	0.9269	0.0896	0.6000	0.9389	0.0906	2.0796	2.6789	0.1229	1.9560	2.0093	0.1358
97 (IBT)[*]	0.8628	0.8409	0.0792	0.6072	0.9177	0.0814	2.1012	2.7213	0.1097	1.9764	2.0169	0.1055
96 (IBB)[*]	0.8851	0.8113	0.0792	0.6307	0.8869	0.0814	2.1391	2.6341	0.1097	2.0083	1.9381	0.1055
107	0.8700	0.8405	0.3330	0.6144	0.9485	0.3311	2.1192	2.9177	0.3730	1.9920	2.3153	0.3731
109	0.8759	0.8556	0.6636	0.6203	1.0104	0.6588	2.1347	3.1980	0.7224	2.0051	2.7660	0.7416
158	0.8905	2.2032	6.0588	0.6313	2.6460	6.0804	2.1817	8.7108	7.1064	2.1637	10.237	7.0608
163	0.8905	2.2608	6.1704	0.6265	2.7096	6.1716	2.1649	8.8860	7.2480	2.1637	10.416	7.2012
165	0.8892	2.2800	6.2172	0.6216	2.7324	6.2088	2.1684	8.9472	7.3104	2.1624	10.478	7.2684

[*]EB means exterior bearing, IBT means top of interior bearing, and IBB means bottom of interior bearing.

Table 5.22 Cross Sectional Properties of Piers Members for Stresses Calculation

Pier Member	Area, A (in^2)	Moment of Inertia, I_{13} (in^4)	Section Modulus, Z_{13} (in^3)	Moment of Inertia, I_{12} (in^4)	Section Modulus, Z_{12} (in^3)
199	1281.876	21063865	328641	18459015	307650
198	1397.496	27293028	390599	20123942	335399
197	1521.876	35248270	1826251	5558656	365250
196	1631.256	43407660	1957507	6386391	4698017

Table 5.23 Piers Members Stresses (ksi) due to Seismic Excitation Cases of 250-year Earthquake and Dead Load (DL)

Pier Member	L1T2V3 + DL Shear Stress	L2T1V3 + DL Shear Stress	LL11 + DL Shear Stress	LL22 + DL Shear Stress	TT11 + DL Shear Stress	TT22 + DL Shear Stress
199	0.3951	0.3804	0.2226	0.2510	0.2901	0.3319
198	0.3815	0.3880	0.2190	0.1826	0.3406	0.3183
197	0.5697	0.5798	0.3586	0.4213	0.4063	0.4329
196	0.8263	0.8238	0.5887	0.6936	0.4657	0.5850

Table 5.24 Piers Members Stresses (ksi) due to Seismic Excitation Cases of 500-year Earthquake and Dead Load (DL)

Pier Member	L1T2V3M + DL Shear Stress	L2T1V3M + DL Shear Stress	LL11M + DL Shear Stress	LL22M + DL Shear Stress	TT11M + DL Shear Stress	TT22M + DL Shear Stress
199	1.0847	1.0648	0.6702	0.6506	0.8307	0.8472
198	1.1104	0.9341	0.5589	0.5271	0.7813	0.9460
197	1.8485	1.6489	1.3283	1.2256	1.0354	1.3192
196	2.6232	2.5121	2.0474	1.9814	1.4702	1.6666

Table 5.25 Maximum and Minimum Base Shear (kips) and Combined Stresses (ksi) from Modal Time-History for 250-year Event

Seismic Excitation Case	Longitudinal Direction				Transverse Direction				Vertical Direction				Combined Maximum Stresses
	Maximum		Minimum		Maximum		Minimum		Maximum		Minimum		
	Shear	Time	Shear	Time	Shear	Time	Shear	Time	Shear	Time	Shear	Time	
LL11	8361	14.05	-8280	16.33	0.4821	5.49	-0.4806	4.77	0.2249	5.045	-0.2467	5.325	4.9768
LL22	7289	11.74	-7418	11.57	0.636	10.3	-0.6123	10.91	0.3131	11.52	0.2993	11.8	4.4155
TT11	0.4821	5.49	-0.4806	4.77	2635	11.29	-2511	34.71	0.0861	12.29	-0.0869	17.18	1.5685
TT22	0.636	10.3	-0.6123	10.91	3201	16.53	-3141	19.75	0.1444	9.4	-0.1441	9.65	1.9054
L1T2V3	8361	14.05	-8280	16.33	3201	16.53	-3141	19.75	2133	14.1	-2177	12.72	5.3291
L2T1V3	7289	11.74	-7418	11.57	2635	11.29	-2511	34.71	2134	14.1	-2178	12.72	4.6858

Table 5.26 Maximum and Minimum Base Moment (kip-ft) and Combined Stresses (ksi) from Modal Time-History for 250-year Event

Seismic Excitation Case	Longitudinal Direction				Transverse Direction				Vertical Direction				Combined Maximum Stresses
	Maximum		Minimum		Maximum		Minimum		Maximum		Minimum		
	Moment	Time	Moment	Time	Moment	Time	Moment	Time	Moment	Time	Moment	Time	
LL11	20.65	5.045	-22.05	4.77	168400	5.1	-159100	4.935	937600	16.33	-946800	14.05	1.0325
LL22	30.93	10.97	-29.04	11.24	185900	11.69	-181200	11.69	839700	11.57	-825100	11.74	1.1399
TT11	70740	12.3	-74760	7.43	93.92	33.88	-84.89	17.61	1431000	11.29	-1364000	34.71	0.1916
TT22	92370	9.405	-86290	19.75	18.1	9.48	-17.76	17.19	1739000	16.53	-1707000	19.75	0.2361
L1T2V3	299600	13.55	-300100	13.28	1134000	12.16	-1142000	14.1	2305000	31.07	-2551000	29.83	9.0631
L2T1V3	279500	12.98	-267800	17.17	1236000	12.7	-1215000	12.98	1821000	21.37	-1891000	14.52	9.5873

Table 5.27 Maximum and Minimum Base Shear (kips) and Combined Stresses (ksi) from Modal Time-History for 500-year Event

Seismic Excitation Case	Longitudinal Direction				Transverse Direction				Vertical Direction				Combined Maximum Stresses
	Maximum		Minimum		Maximum		Minimum		Maximum		Minimum		
	Shear	Time	Shear	Time	Shear	Time	Shear	Time	Shear	Time	Shear	Time	
LL11M	25520	14.74	-26330	14.91	1.798	10.52	-1.824	10.46	0.9144	11.08	0.865	13.24	15.6726
LL22M	22180	19.72	-22310	19.89	1.836	15.17	-1.736	15.23	0.8544	15.28	-0.8619	15.56	13.2798
TT11M	1.798	10.52	-1.825	10.46	6519	18.72	-7171	18.48	0.4297	10.62	-0.4268	10.7	4.2685
TT22M	1.836	15.17	-1.737	15.23	8621	11.28	-7294	14.51	0.3826	11.28	-0.3363	11.19	5.1315
L1T2V3M	25530	14.74	-26340	14.91	8622	11.28	-7292	14.51	4524	7.885	-4505	8.16	16.4972
L2T1V3M	22180	19.72	-22320	19.89	6521	18.72	-7170	18.48	4524	7.885	-4505	8.16	13.9544

Table 5.28 Maximum and Minimum Base Moment (kip-ft) and Combined Stresses (ksi) from Modal Time-History for 500-year Event

Seismic Excitation Case	Longitudinal Direction				Transverse Direction				Vertical Direction				Combined Maximum Stresses
	Maximum		Minimum		Maximum		Minimum		Maximum		Minimum		
	Moment	Time	Moment	Time	Moment	Time	Moment	Time	Moment	Time	Moment	Time	
LL11M	98.97	10.52	-92.57	10.8	512600	10.35	-525800	10.52	2980000	14.91	-2889000	14.74	3.2241
LL22M	83.13	14.17	-84.15	15.56	603700	16.67	-609700	16.83	2525000	19.89	-2510000	19.72	3.7383
TT11M	208700	11.61	-226100	10.37	491.1	10.36	-511.2	10.62	3542000	18.72	-3896000	18.48	0.5809
TT22M	255200	11.28	-233200	14.5	391	14.34	-393.2	11.28	4684000	11.28	-3963000	14.51	0.6545
L1T2V3M	552200	7.315	-651600	13.17	2499000	8.145	-2438000	7.87	5027000	18.38	-5654000	19.62	19.6767
L2T1V3M	583000	14.59	-592900	19.47	2402000	20.01	-2377000	19.18	5456000	20.22	-5421000	15.5	18.9321

Table 5.29 Capacity/demand ratios of the bearing under the 250 & 500-Year excitations

Seismic Case	Pier #	Anchor Bolt Capacity, (Vc)			Seismic Force (kips)			Seismic [a] Demand (kips)	C/D [b] ratio	Required [c] Additional Capacity (kips)
		# of Bolts	Area (in^2)	Capacity (kips)	Longitudinal H_L	Transverse H_T	Resultant H_R			
250-Year	4	4 Dia 2.5"	19.64	529.56	283.07	278.36	397.01	496.26	1.07	-
	5	4 Dia 2.5"	19.64	529.56	293.15	267.15	397.77	496.97	1.07	-
500-Year	4	4 Dia 2.5"	19.64	529.56	916.29	795.08	1213.15	1516.44	0.35	986.89 [d]
	5	4 Dia 2.5"	19.64	529.56	910.87	785.02	1202.47	1503.09	0.35	973.54 [d]

[a]: Seismic Demand = 1.25 x H_R (kips)
[b]: C/D ratio = Capacity/Demand
[c]: Minimum required additional capacity of bolts to have C/D ratio $\geq$ 1
[d]: Alternate retrofitting by replacing the existing bearings with seismic isolation bearings may be utilized.

Figure 2.1a Orthogonal view of the Cumberland River Bridge

Figure 2.1b Side view of Cumberland River Bridge

Figure 2.1c Bottom view showing the main span of Cumberland River Bridge

Figure 2.1d View showing the roadway of Cumberland River Bridge

PLAN

ELEVATION

TYPICAL SECTION

216'-0"
SPAN 1

216'-0"
SPAN 3

300'-0"
SPAN 4

420'-0"
SPAN 5

300'-0"
SPAN 6

WESTBOUND

EASTBOUND

SPAN 2

CUMBERLAND RIVER

SPAN 1   SPAN 2   SPAN 3   SPAN 4   SPAN 5   SPAN 6

2:1 SLOPE

1:1

1:1

3

ABUTMENT 1   PIER 1   PIER 2   PIER 3

APPROX. RIVER BED

NORMAL POOL EL. 302.0

2:1 SLOPE

1
3

ABUTMENT 2

APPROX. TOP OF ROCK

PIER 4   PIER 5

42'-6 1/2"

31'-0"
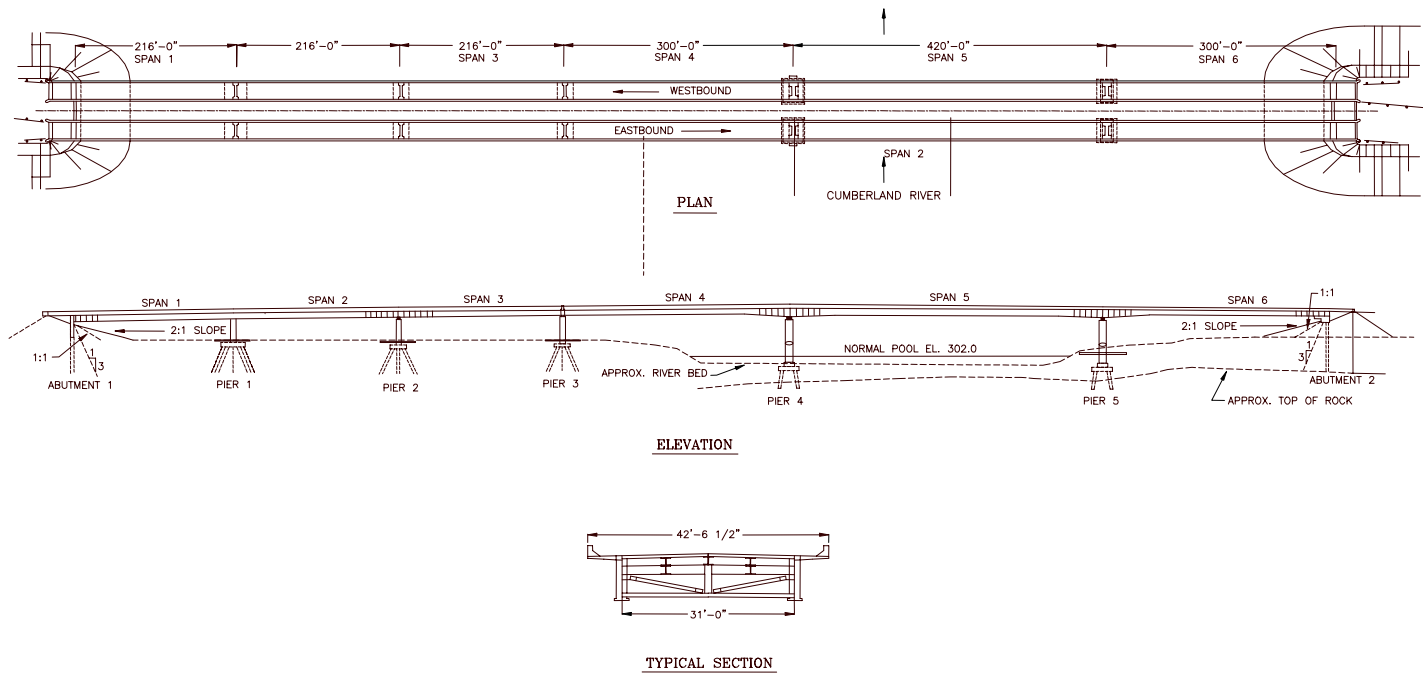
Figure 2.2 Layout of Cumberland River Bridge

73

CUMBERLAND RIVER

| 300'-0" SPAN 4 | 420'-0" SPAN 5 | 300'-0" SPAN 6 |

WESTBOUND

EASTBOUND

PLAN

SPAN 4   SPAN 5   SPAN 6

1:1

2:1 SLOPE

NORMAL POOL EL. 302.0

1
3

APPROX. RIVER BED

PIER 3

PIER 4

PIER 5

APPROX. TOP OF ROCK

ABUTMENT 2
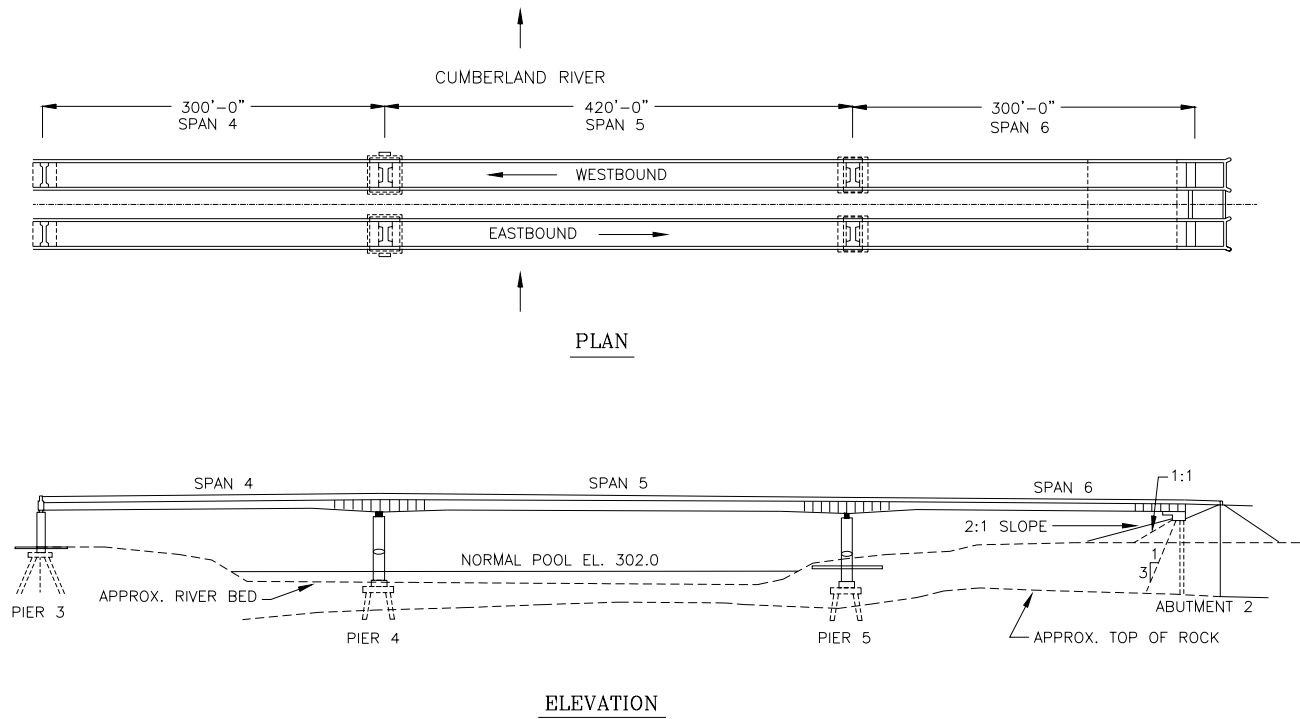
ELEVATION

Figure 2.3 Main Span Plan and Elevation Views of Cumberland River Bridge

Figure 2.4 Plan view showing part of the superstructure

Figure 2.5 Elevation view showing part of the superstructure
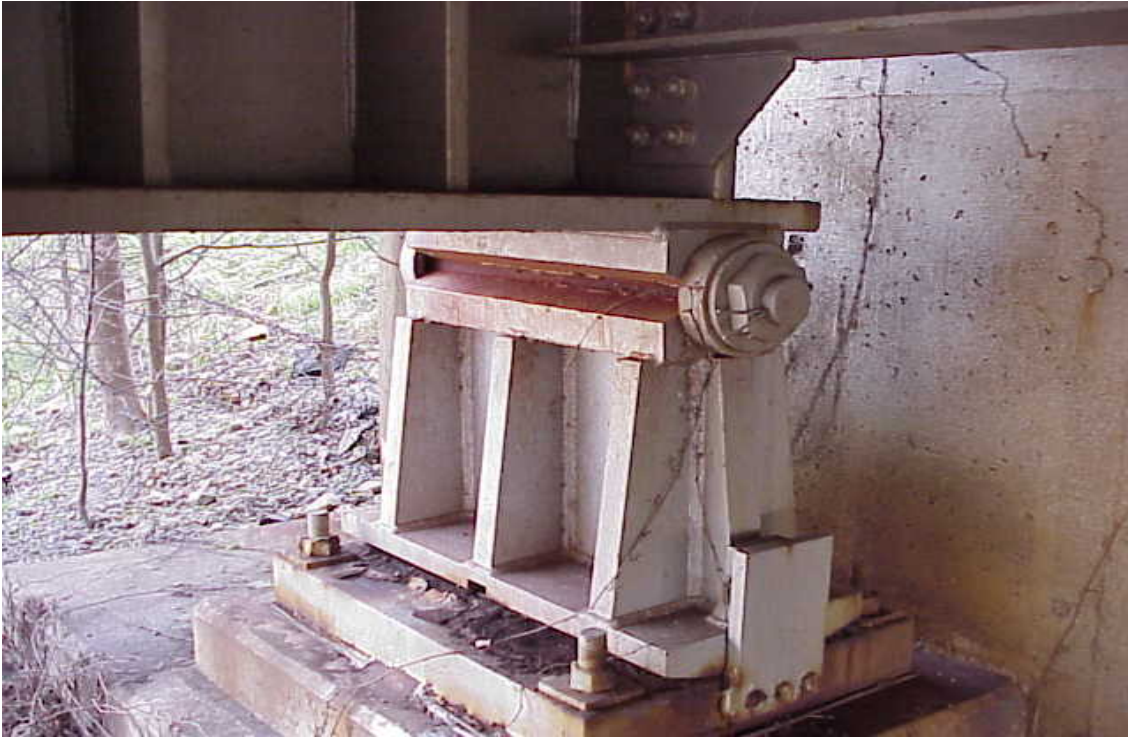
Figure 2.6 View of fixed bearing
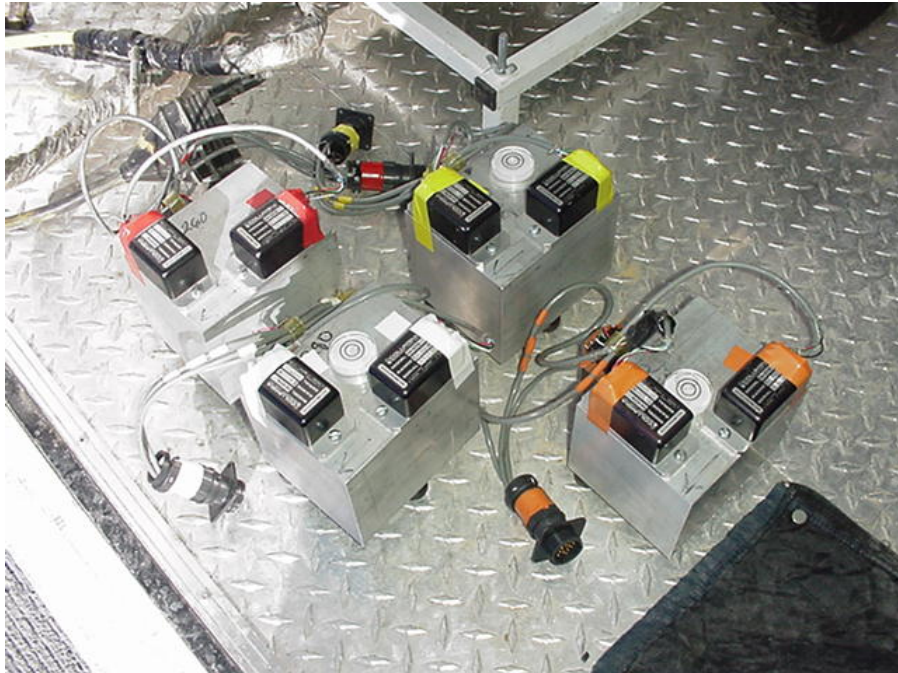
Figure 3.1 Tri-axial accelerometers mounted on the aluminum block

Figure 3.2 On-site data acquisition system
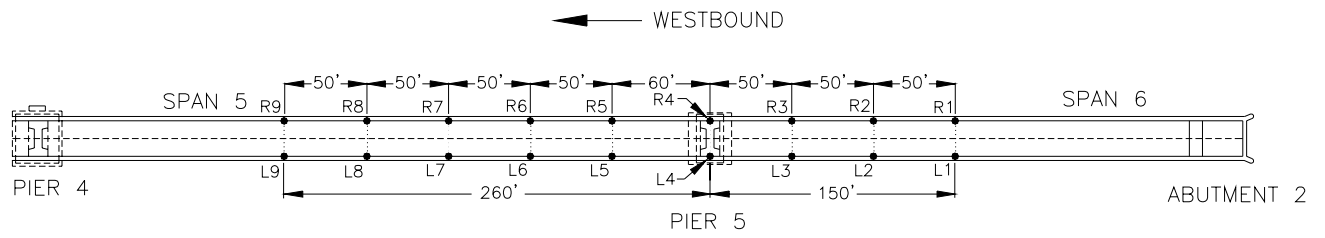
Figure 3.3 Test setup and a view on the measurement locations
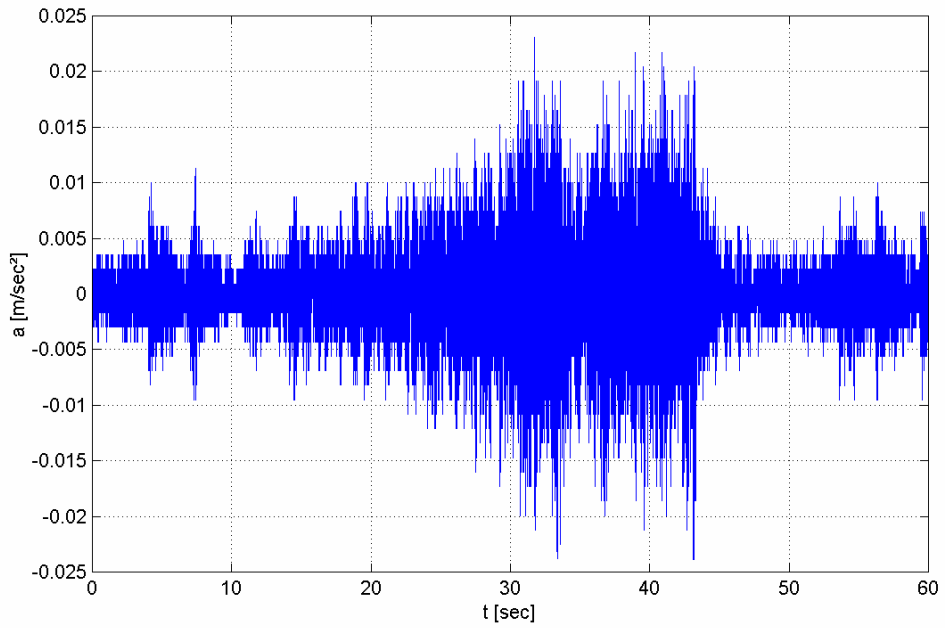
Figure 3.4a Raw longitudinal time history data at station $L1$
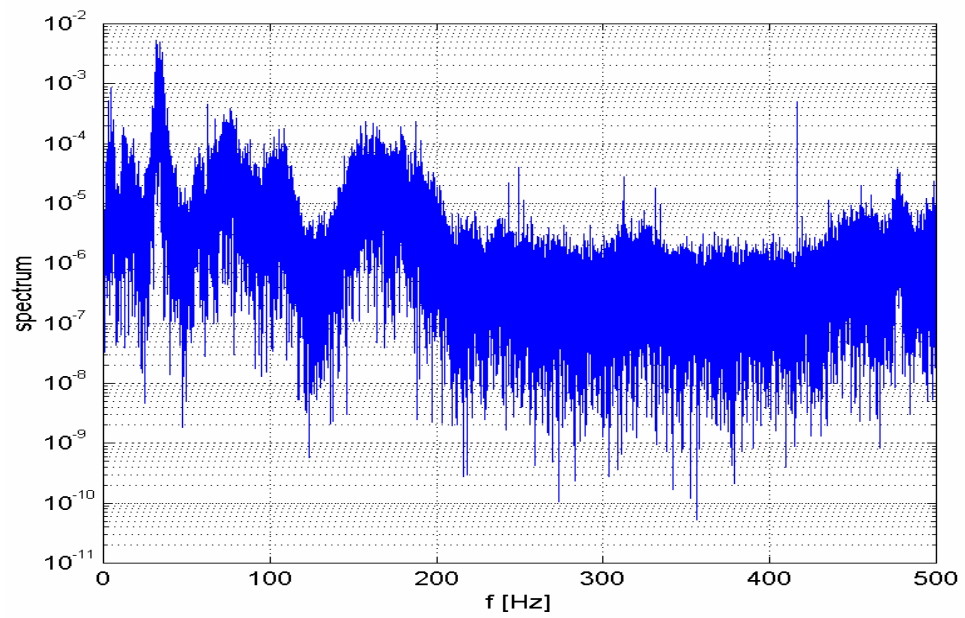
Figure 3.4b Raw longitudinal power spectral density at station $L1$
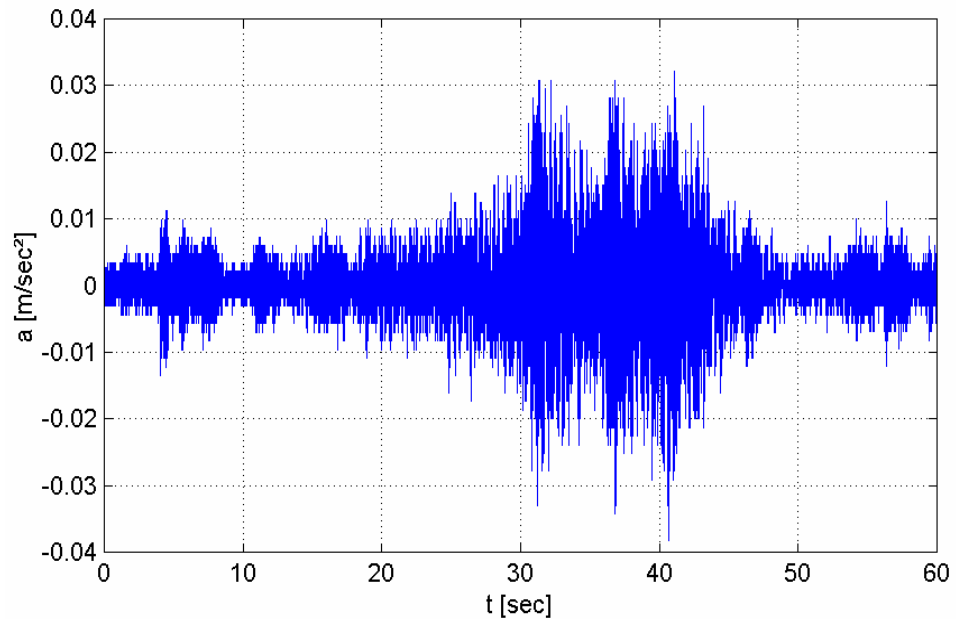
Figure 3.5a Raw transverse time history data at station $L1$
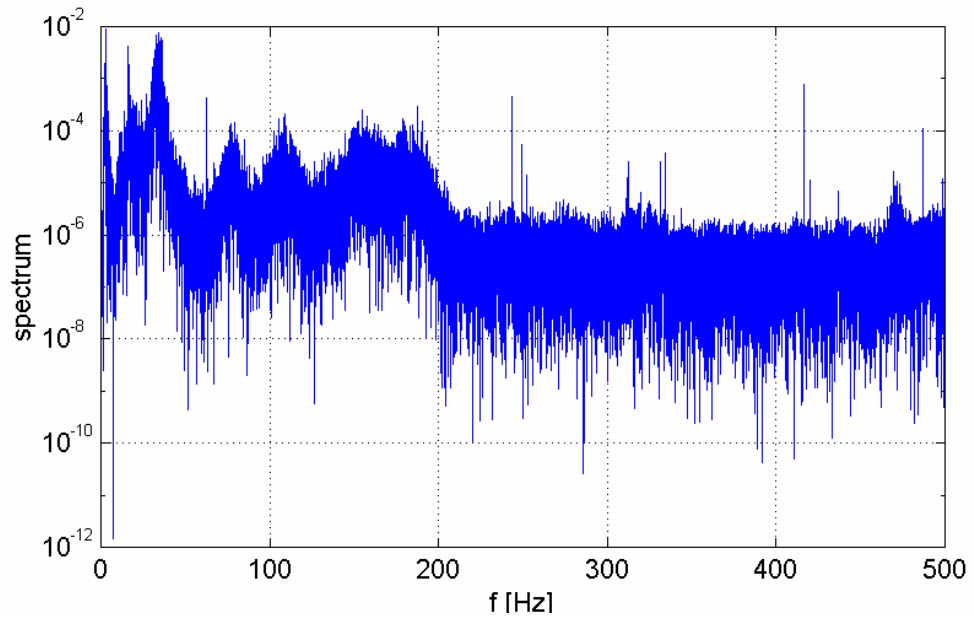
Figure 3.5b Raw transverse power spectral density at station $L1$
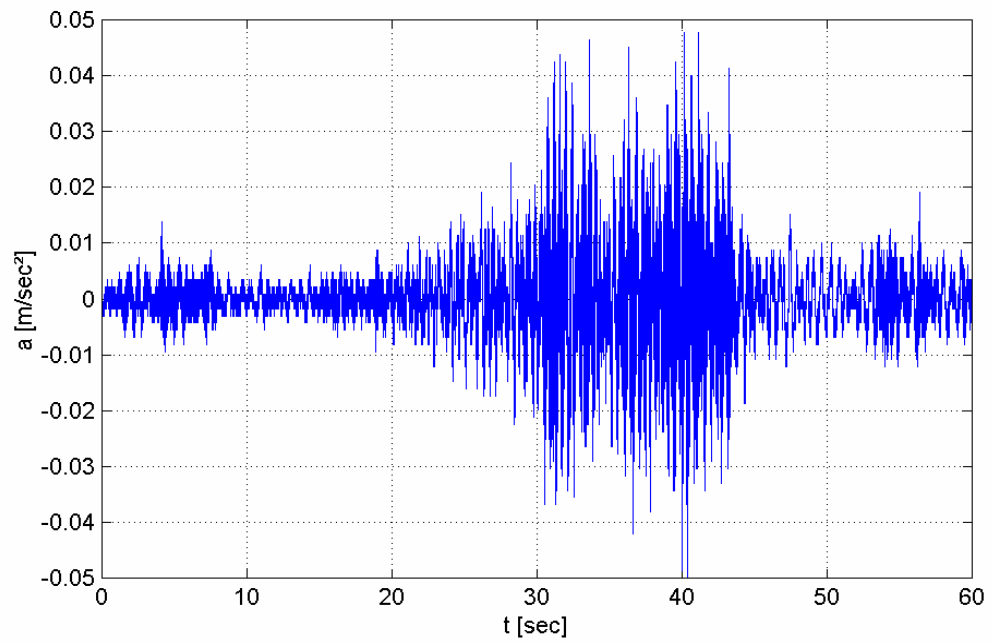
Figure 3.6a Raw vertical time history data at station *L*1
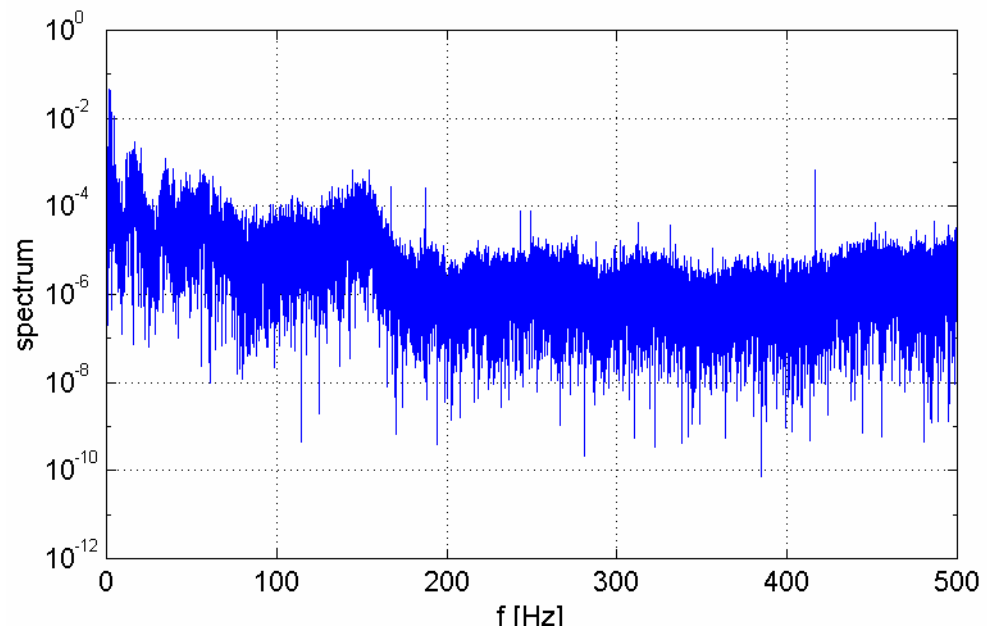
Figure 3.6b Raw vertical power spectral density at station *L*1
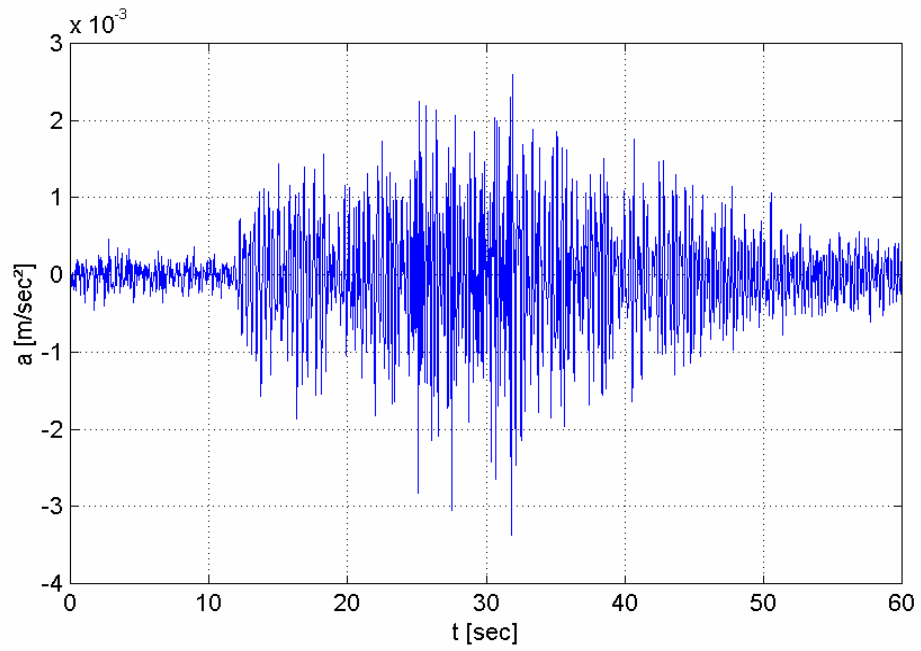
Figure 3.7a Re-sample longitudinal time history data at station *L*1
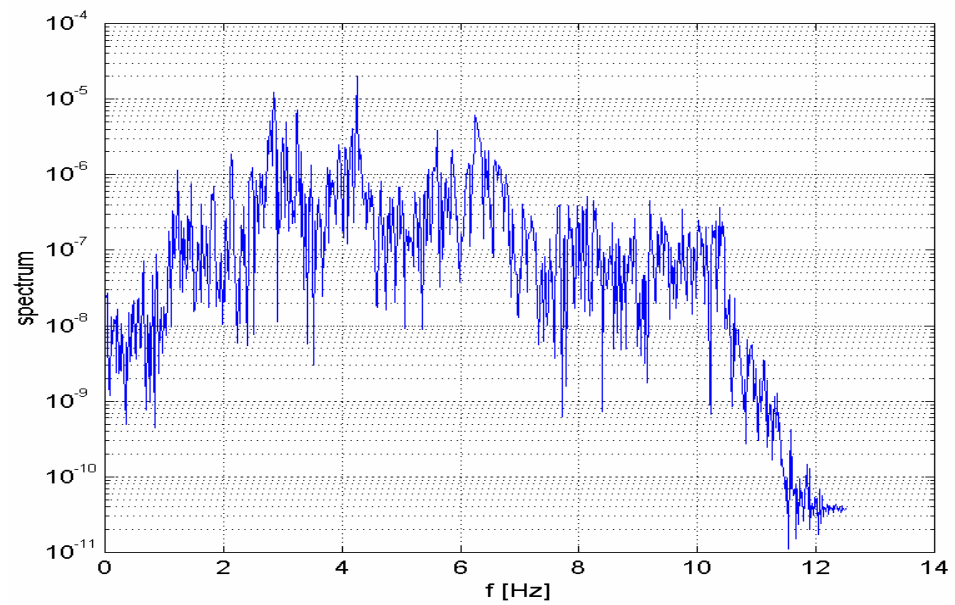
Figure 3.7b Re-sample longitudinal power spectral density at station *L*1

83
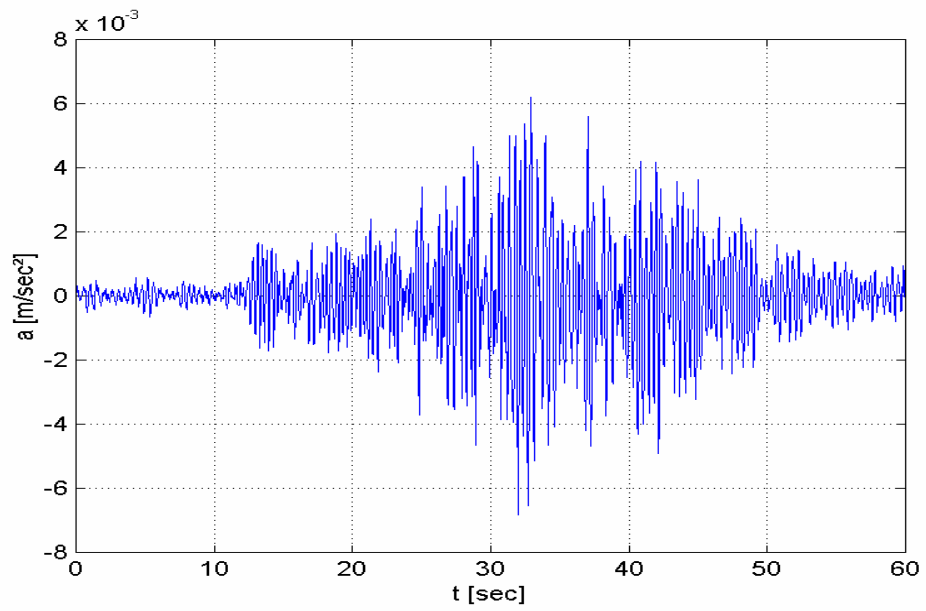
Figure 3.8a Re-sample transverse time history data at station $L1$
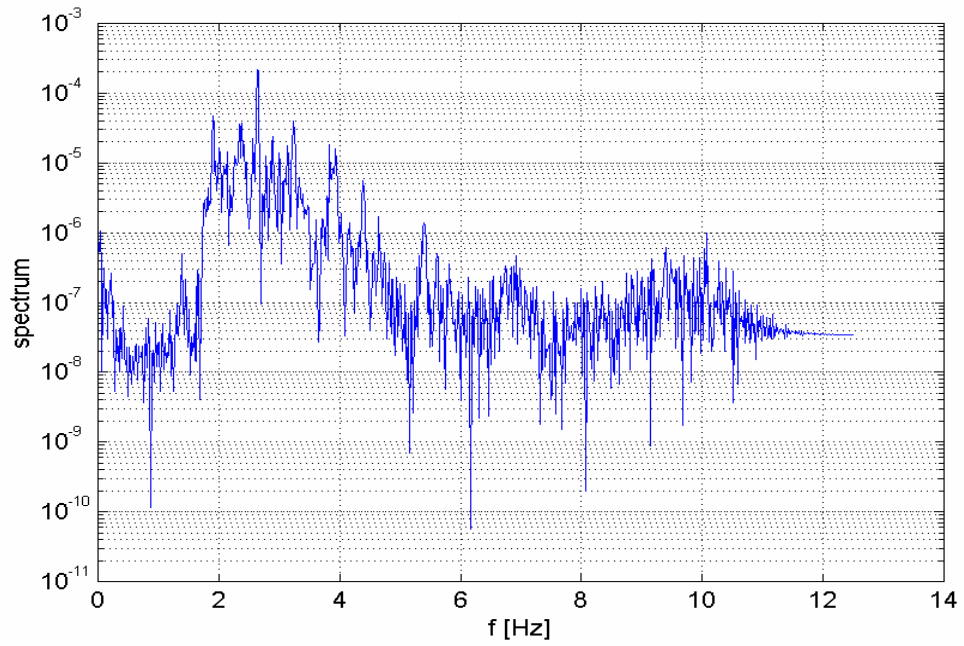
Figure 3.8b Re-sample transverse power spectral density at station $L1$
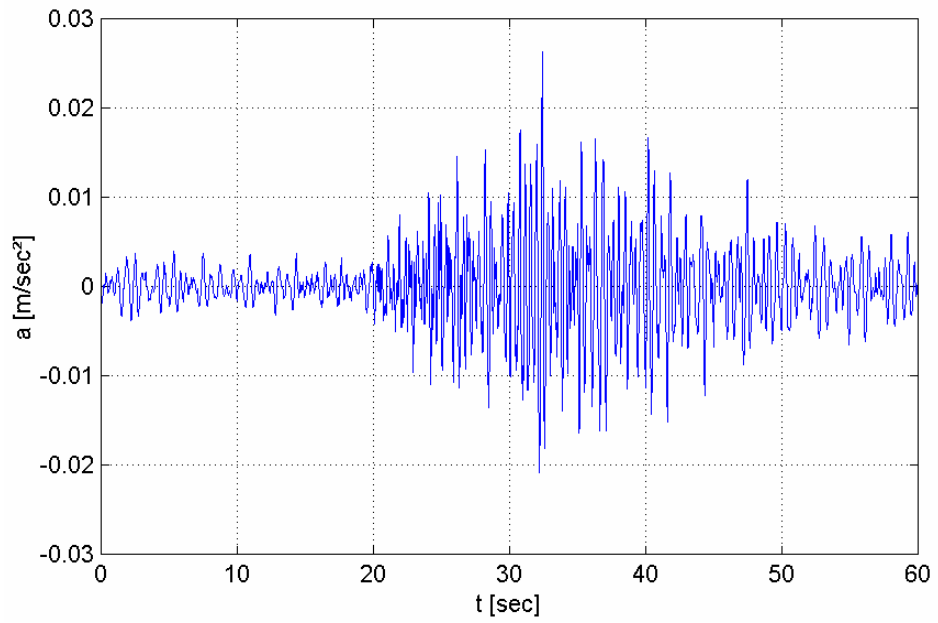
Figure 3.9a Re-sample vertical time history data at station *L*1
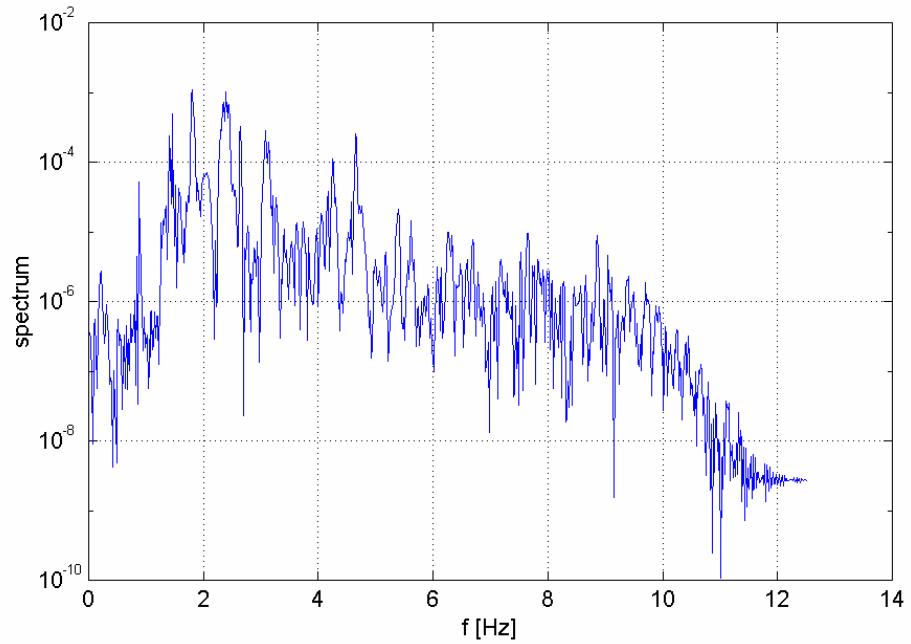
Figure 3.9b Re-sample vertical power spectral density at station *L*1
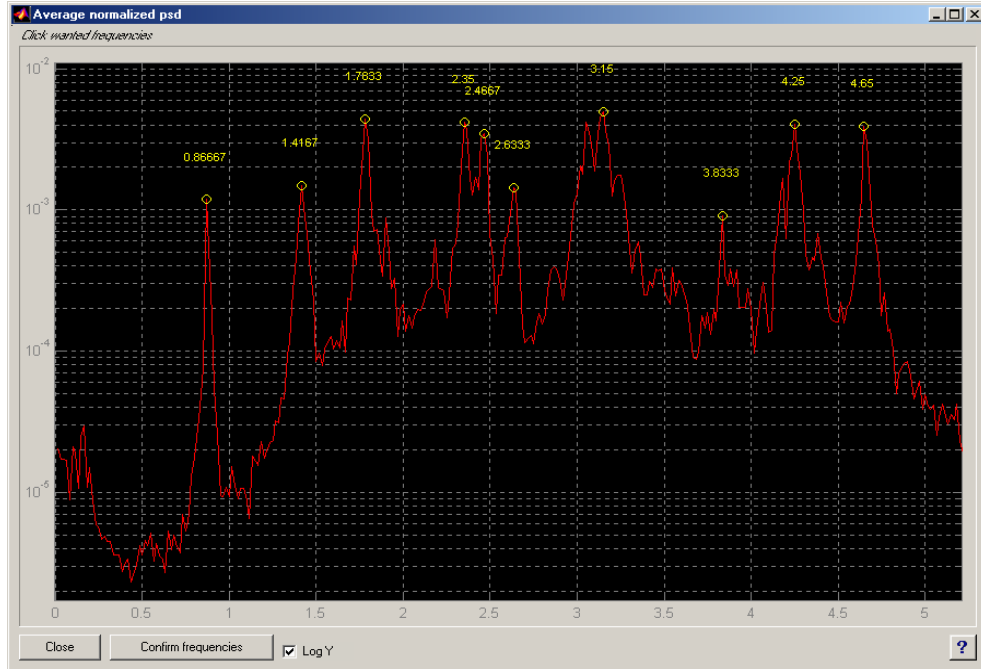
Figure 3.10a Full average normalized power spectral density
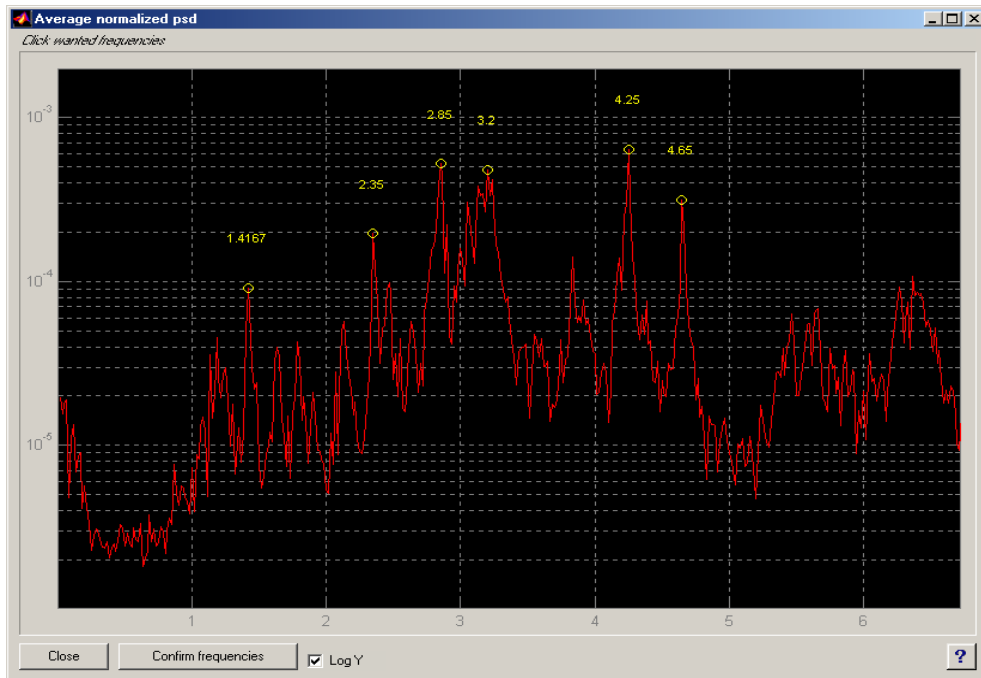
Figure 3.10b Longitudinal average normalized power spectral density

86
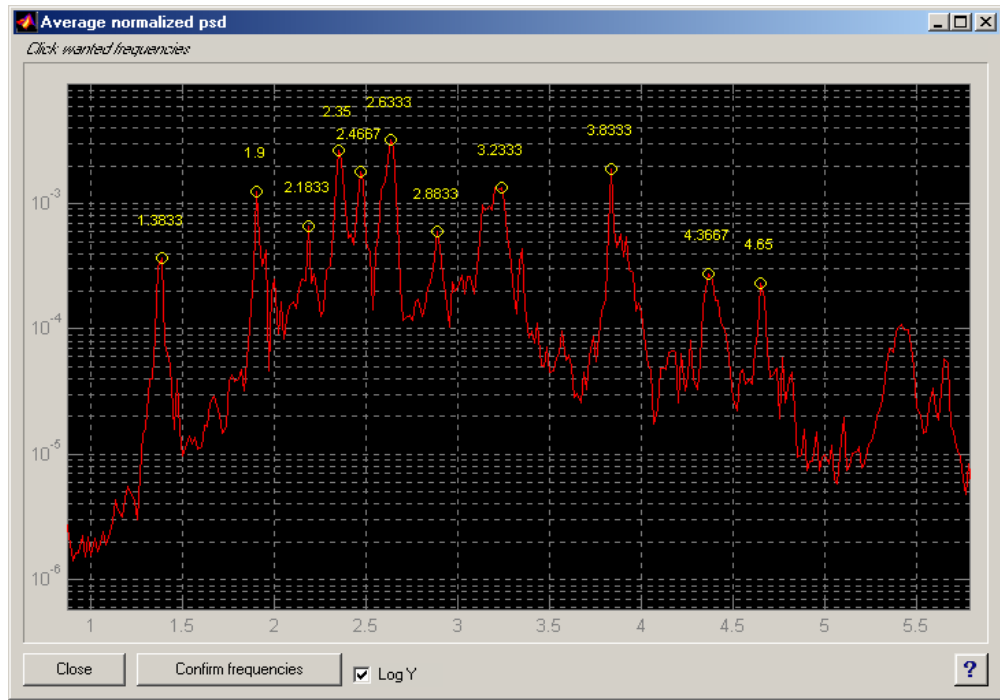
Figure 3.10c Transverse average normalized power spectral density
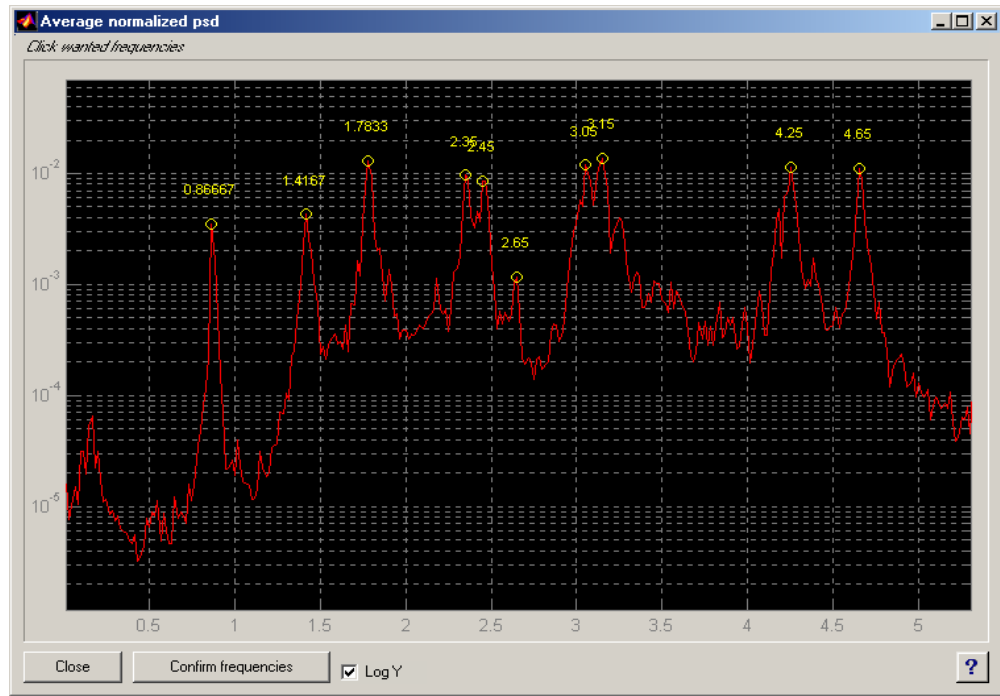
Figure 3.10d Vertical average normalized power spectral density
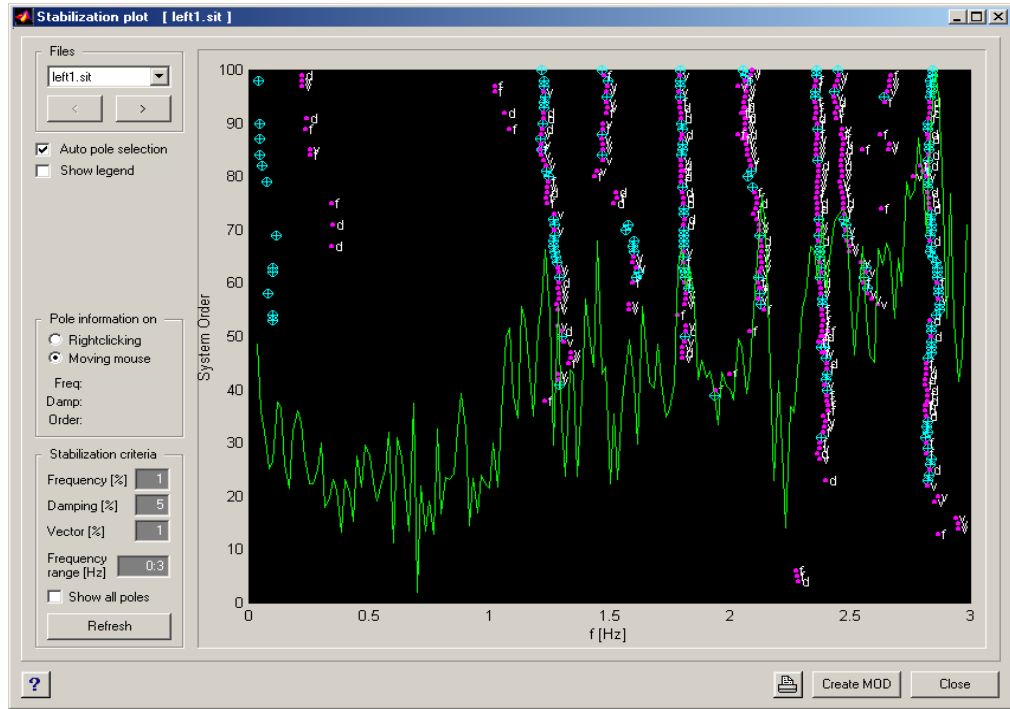
Figure 3.11a Stabilization diagram of longitudinal data
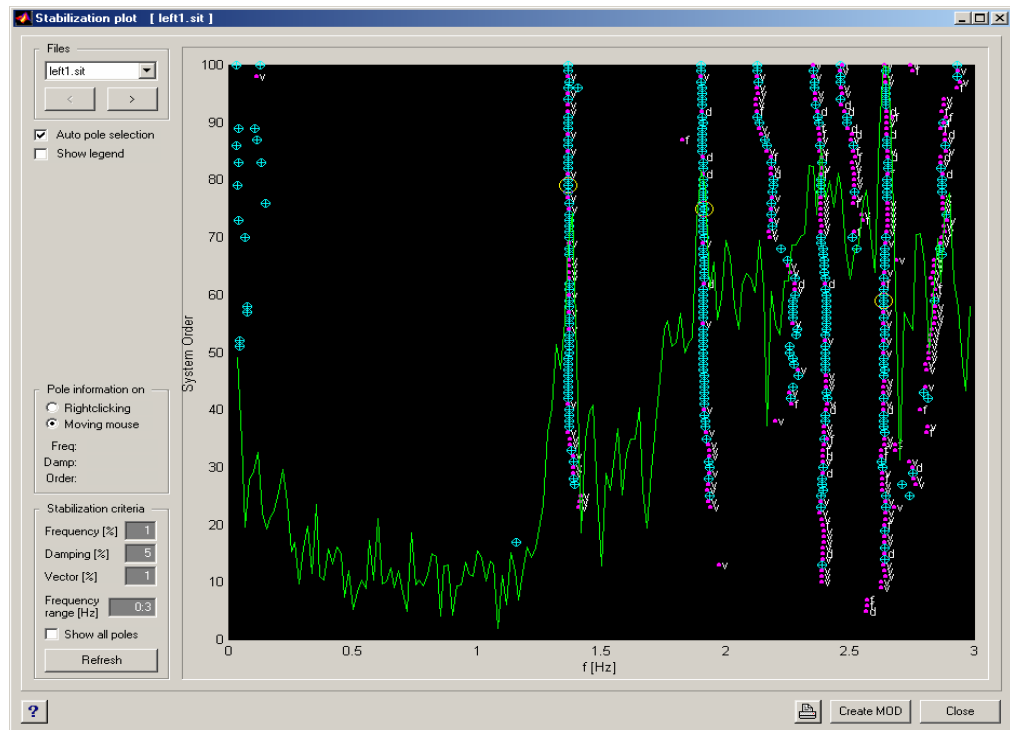
Figure 3.11b Stabilization diagram of transverse data
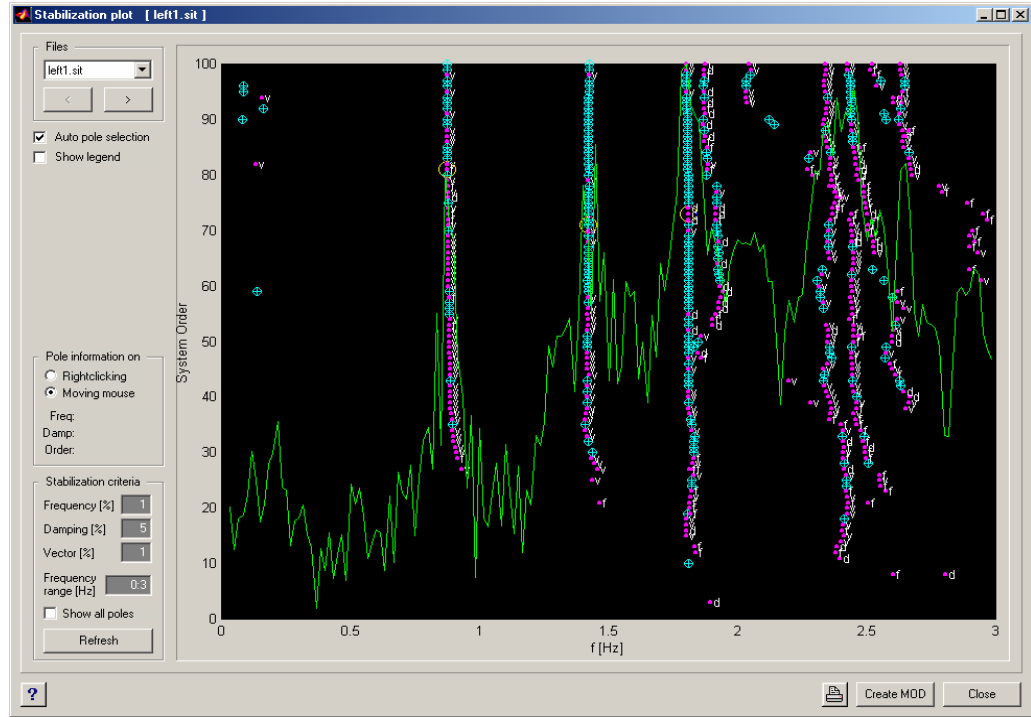
Figure 3.11c Stabilization diagram of vertical data
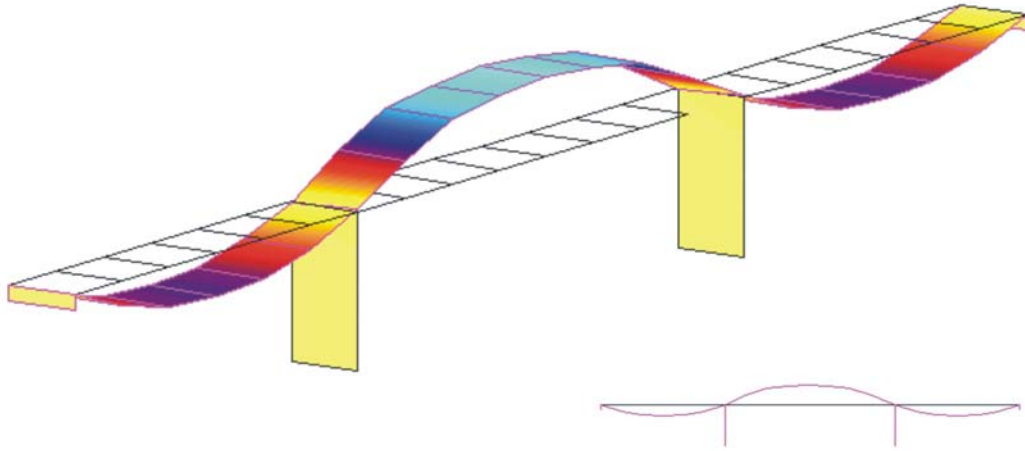
Figure 3.12a First vertical mode shape ($f = 0.875$ *Hz*, damping ratio = 0.6%)
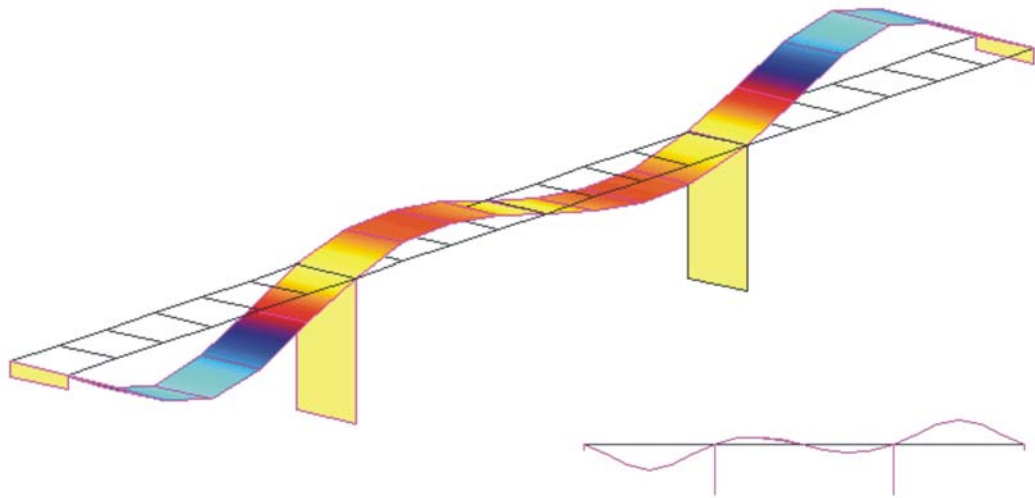
Figure 3.12b Second vertical mode shape ($f = 1.417\ Hz$, damping ratio = 1.6%)
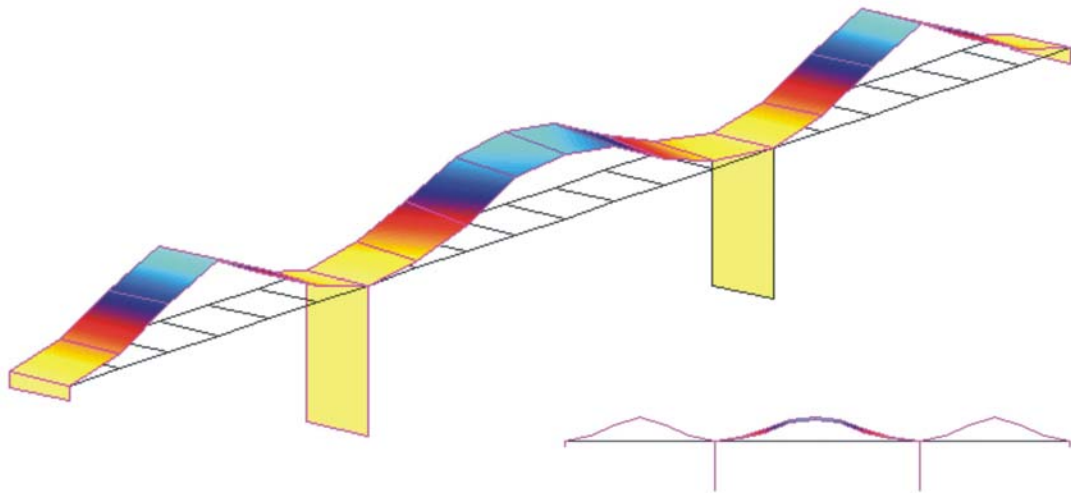
Figure 3.12c Third vertical mode shape (f = 1.780 *Hz*, damping ratio = 1.3%)
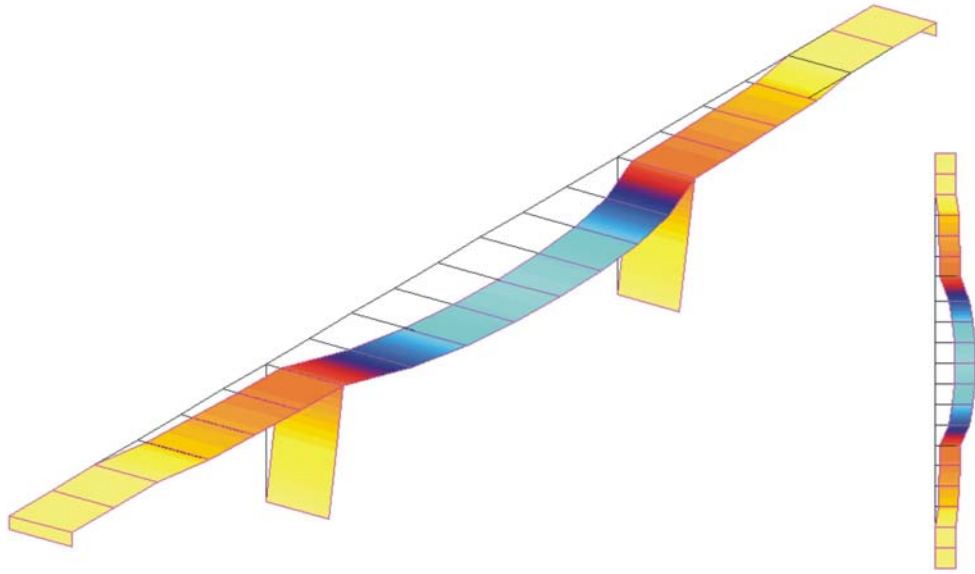
Figure 3.13a First transverse mode shape ($f = 1.382\ Hz$, damping ratio = 1.2%)
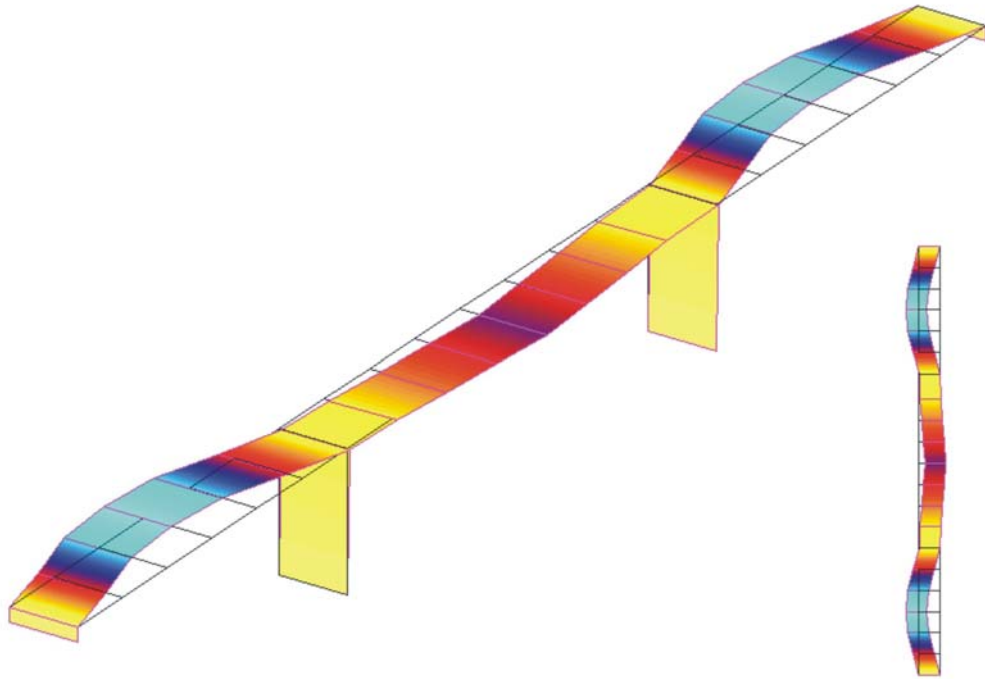
Figure 3.13b Second transverse mode shape (f = 1.915 Hz, damping ratio = 1.1%)
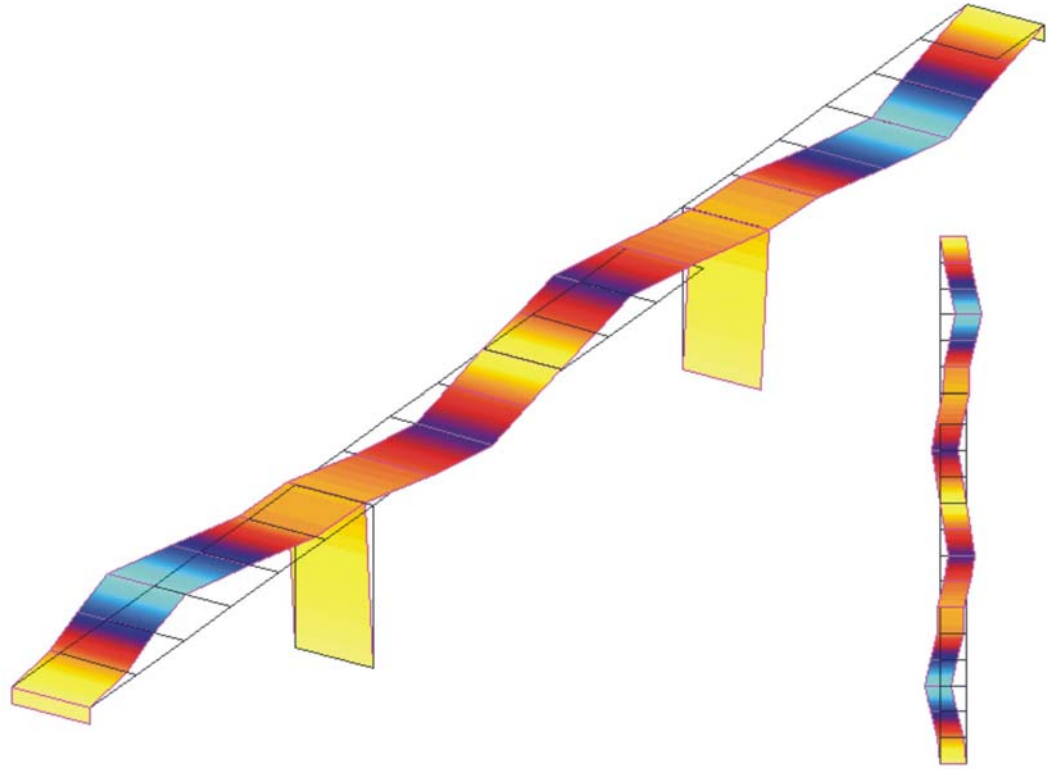
Figure 3.13c Third transverse mode shape (f = 2.625 Hz, damping ratio = 1.0 %)
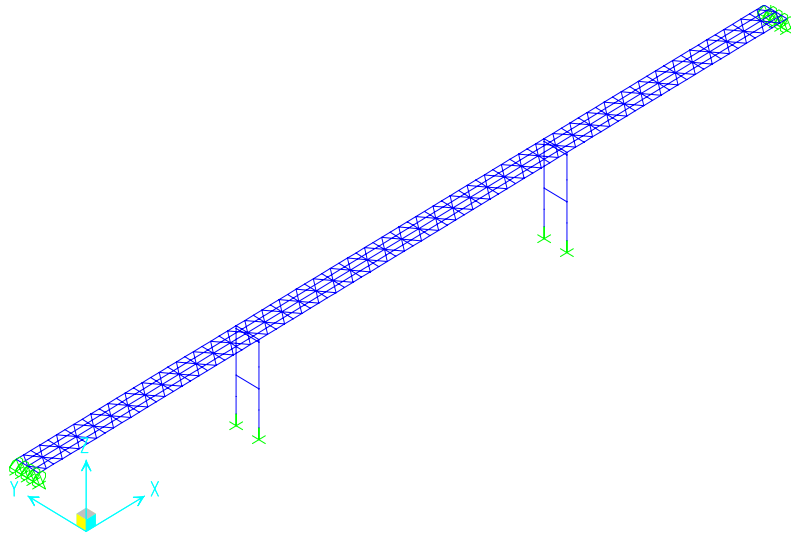
Figure 4.1 Isometric view of finite element model
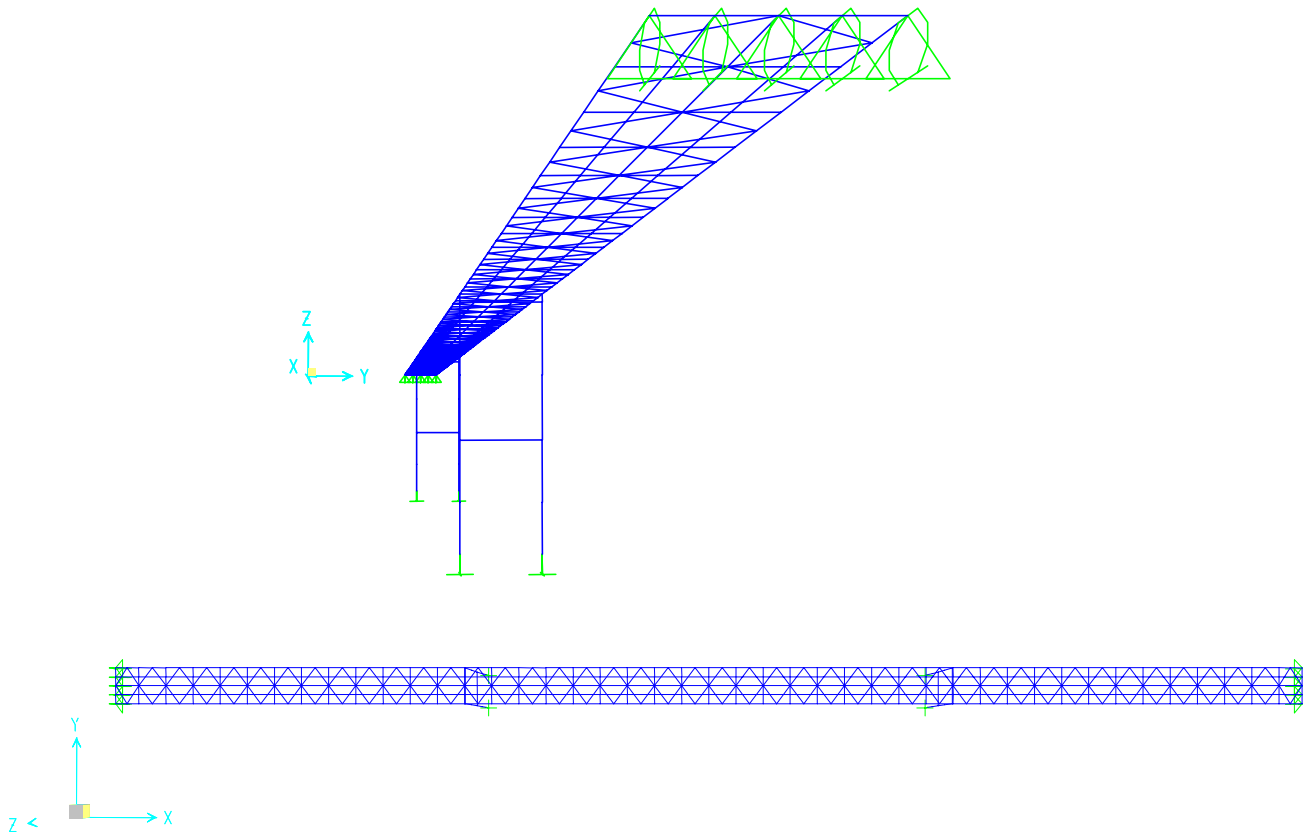
Figure 4.2 Side and plan views of finite element model

96
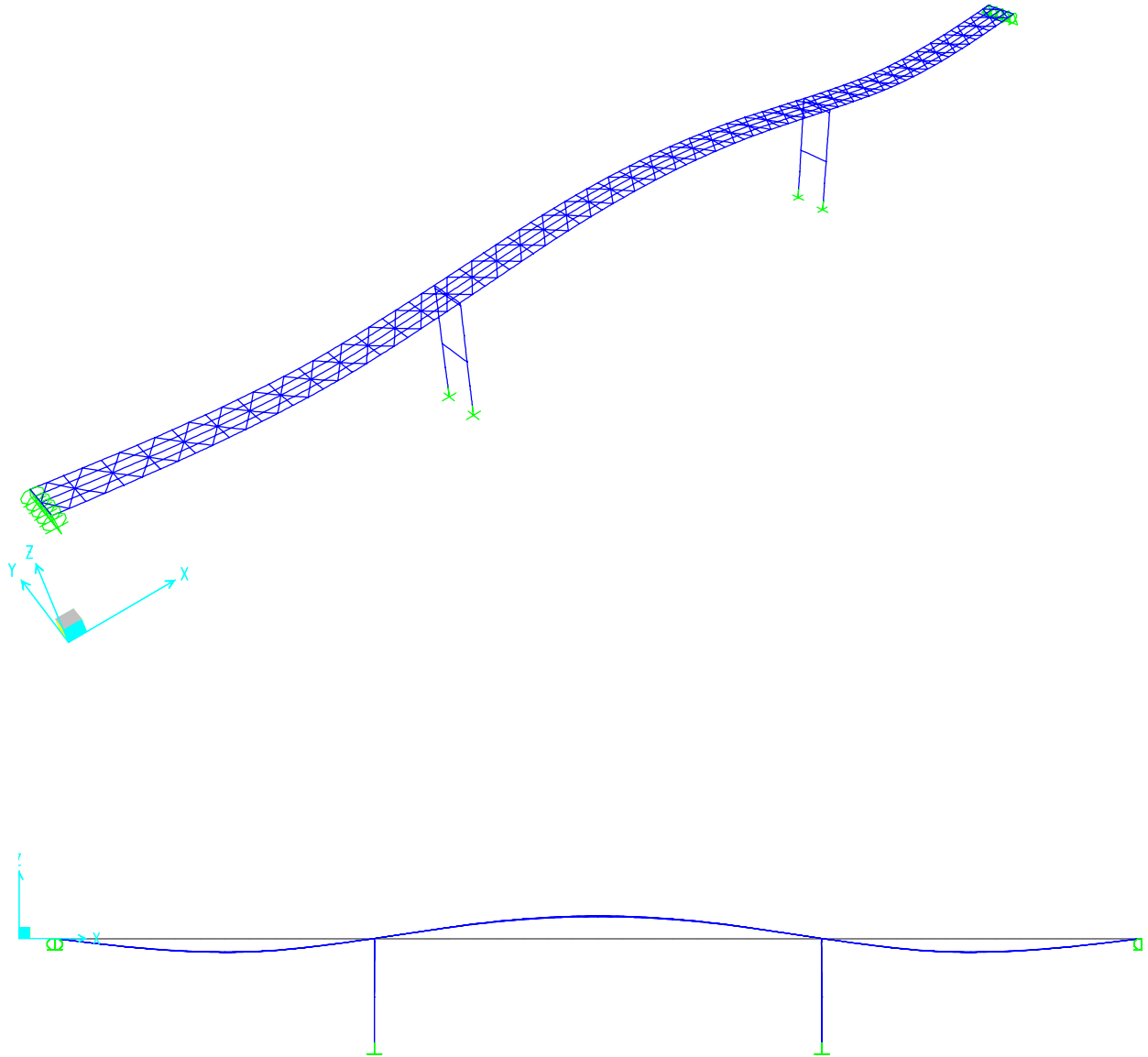
Figure 4.3 Isometric and side views of the first vertical mode shape (0.876 Hz)
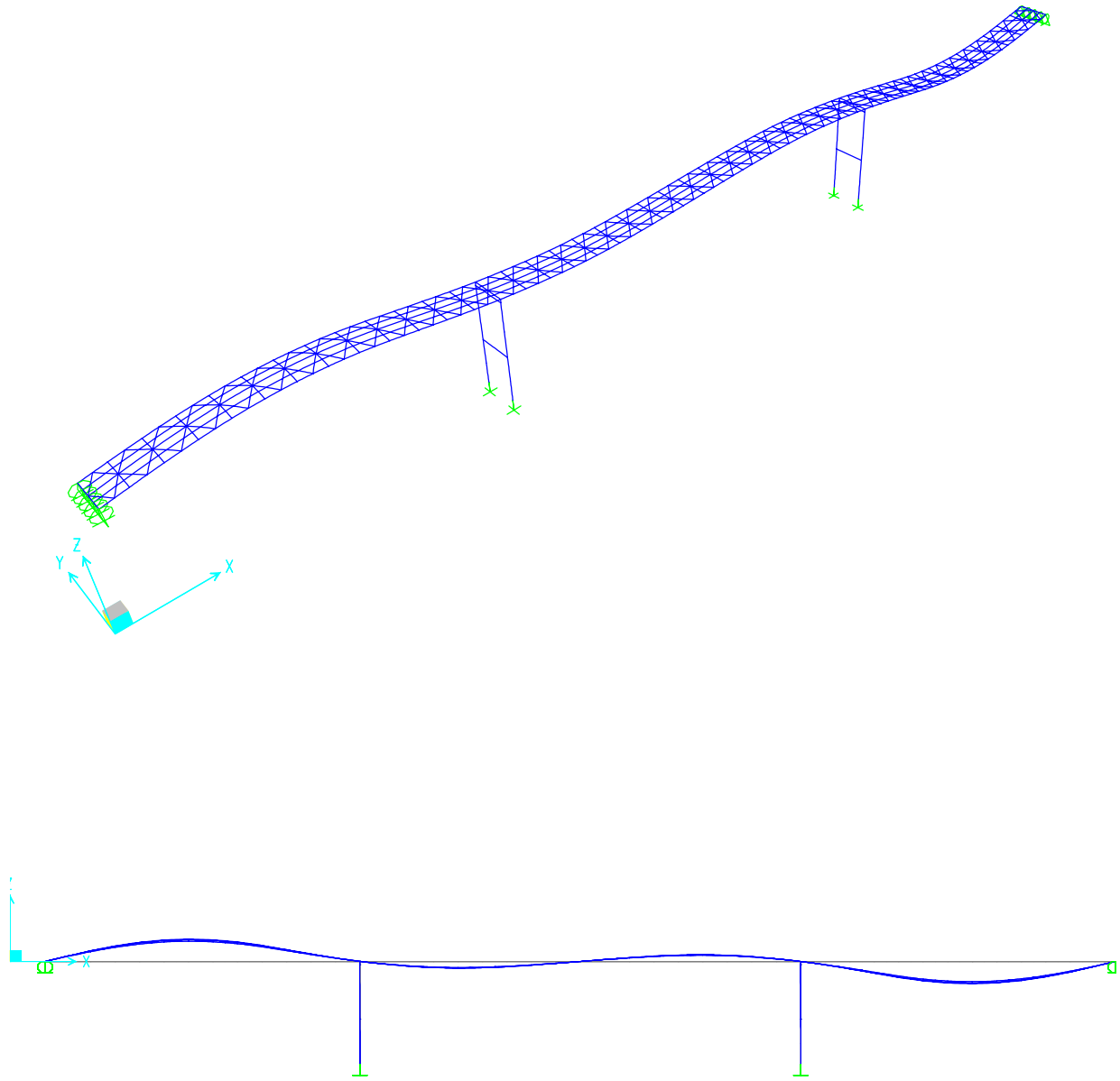
Figure 4.4 Isometric and side views of the second vertical mode shape (1.413 Hz)
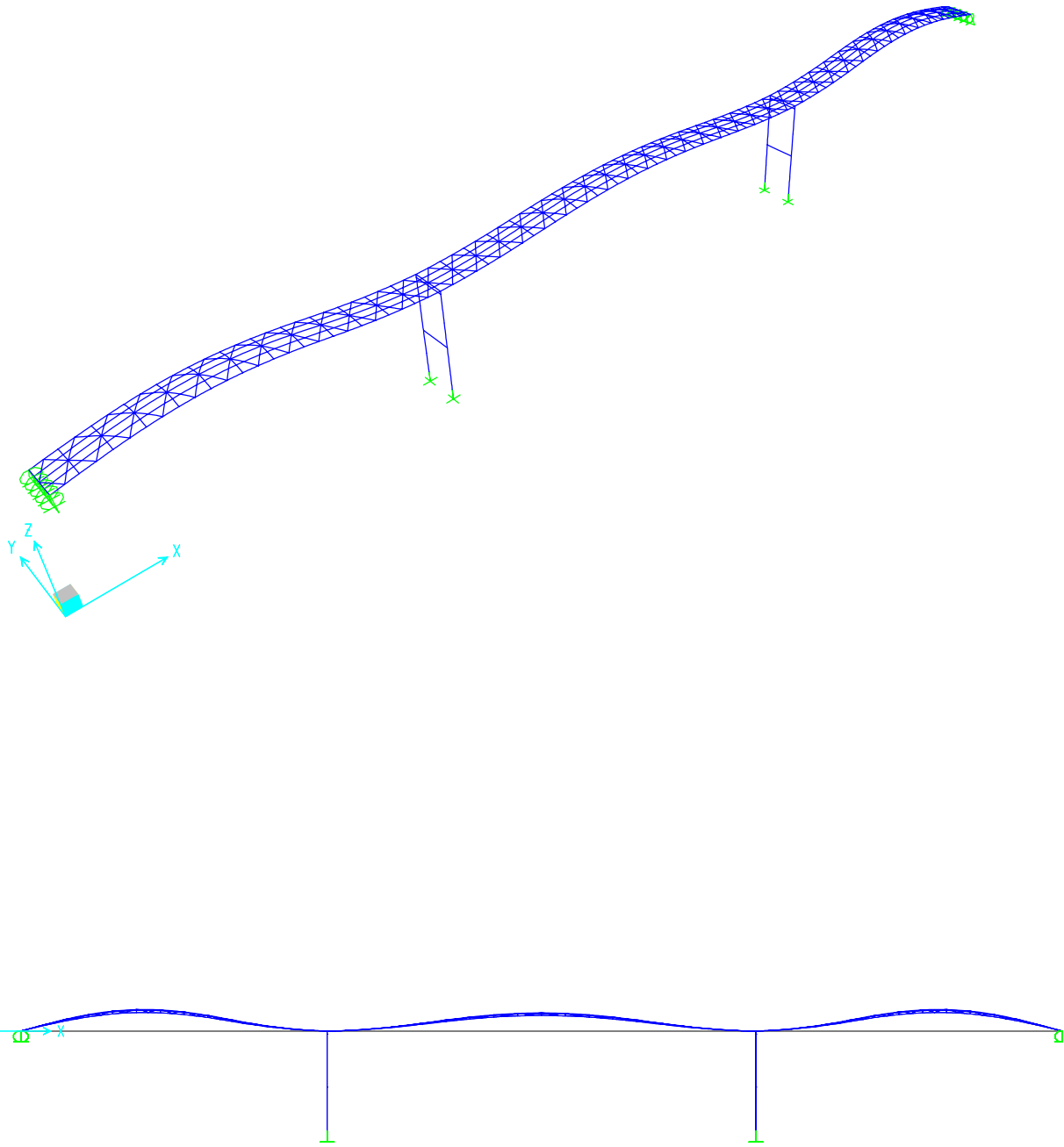
Figure 4.5 Isometric and side views of the third vertical mode shape (1.778 Hz)
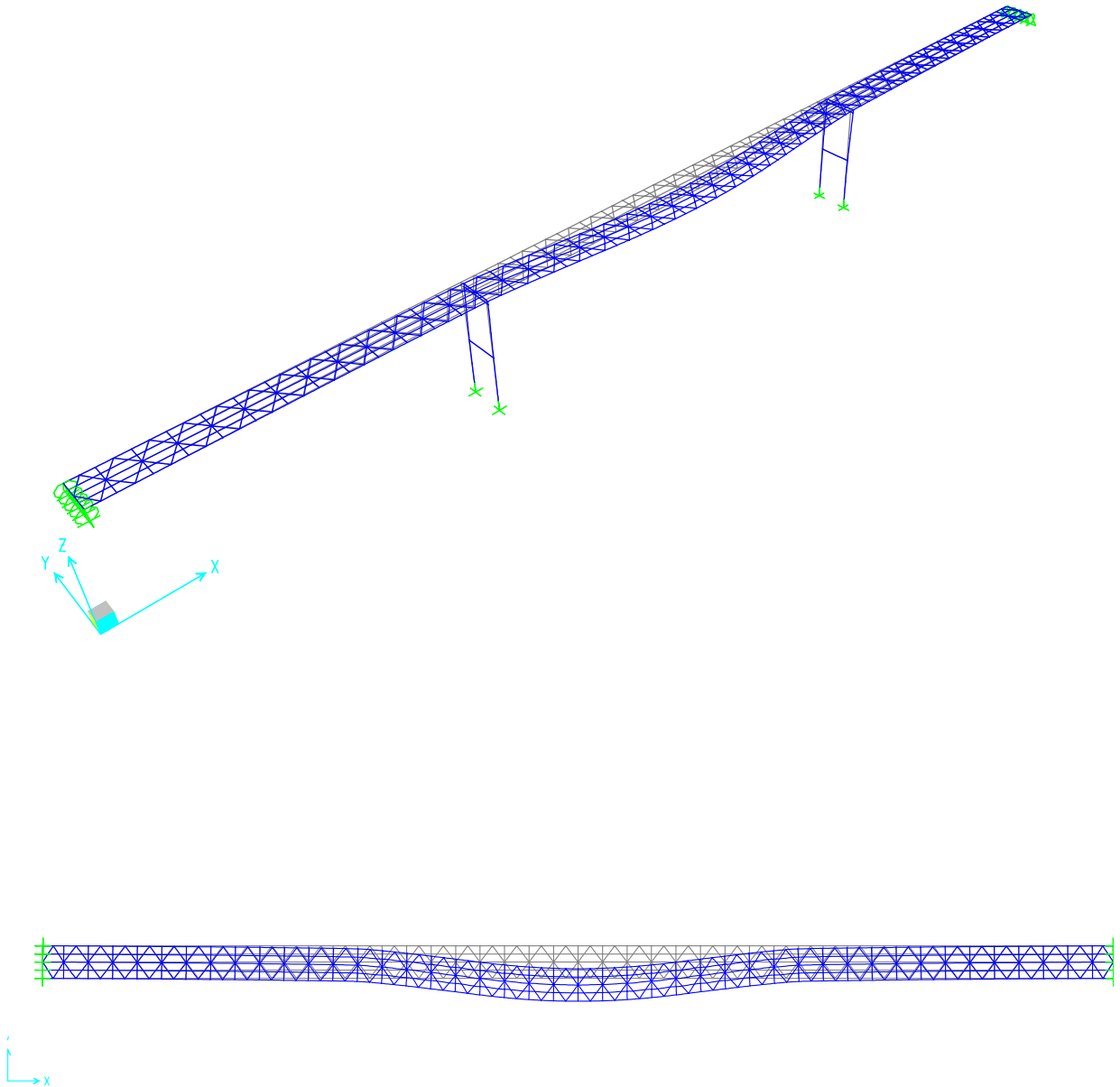
Figure 4.6 Isometric and plan views of the first transverse mode shape (1.383 Hz)
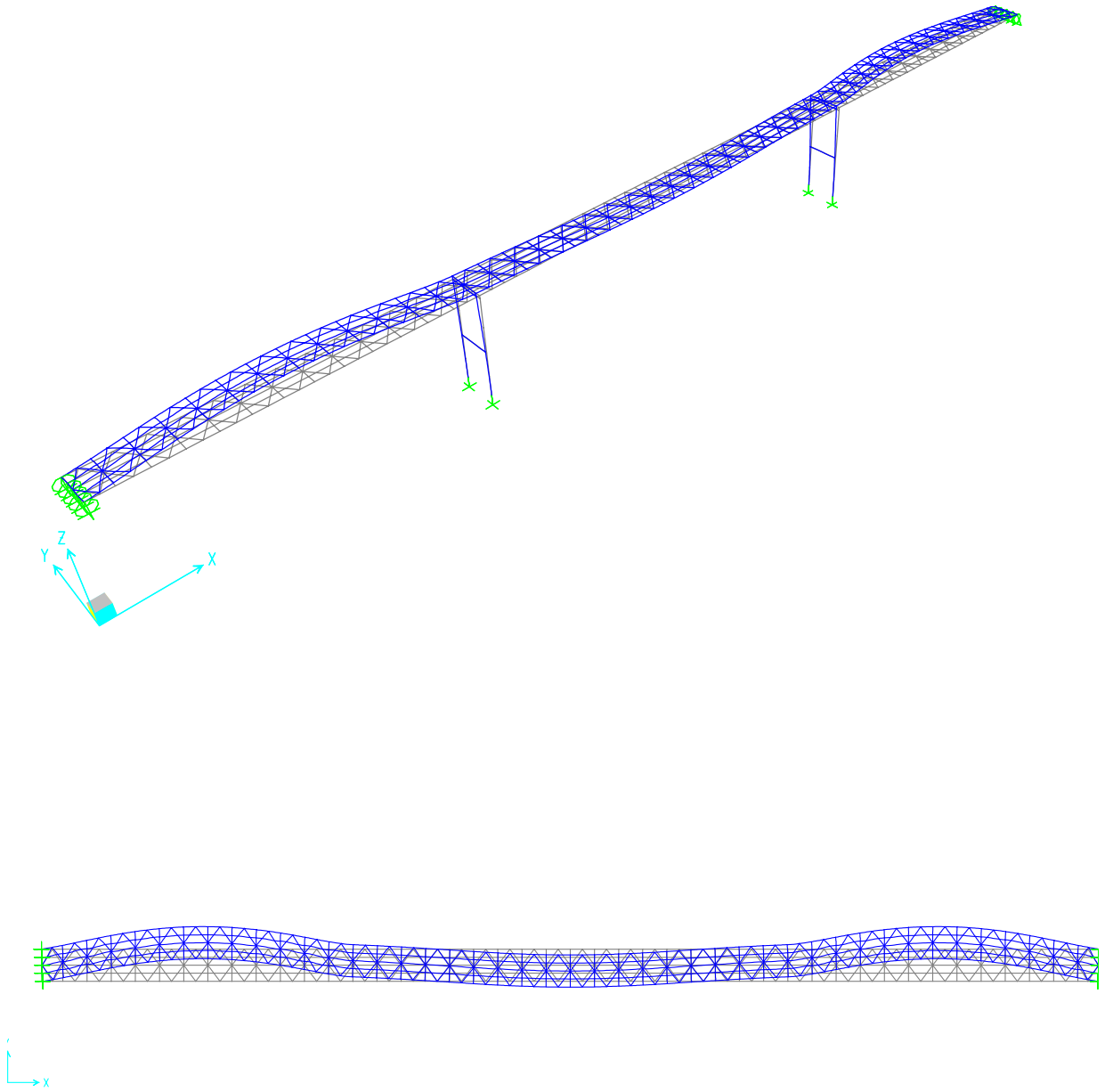
Figure 4.7 Isometric and plan views of the second transverse mode shape (1.989 Hz)
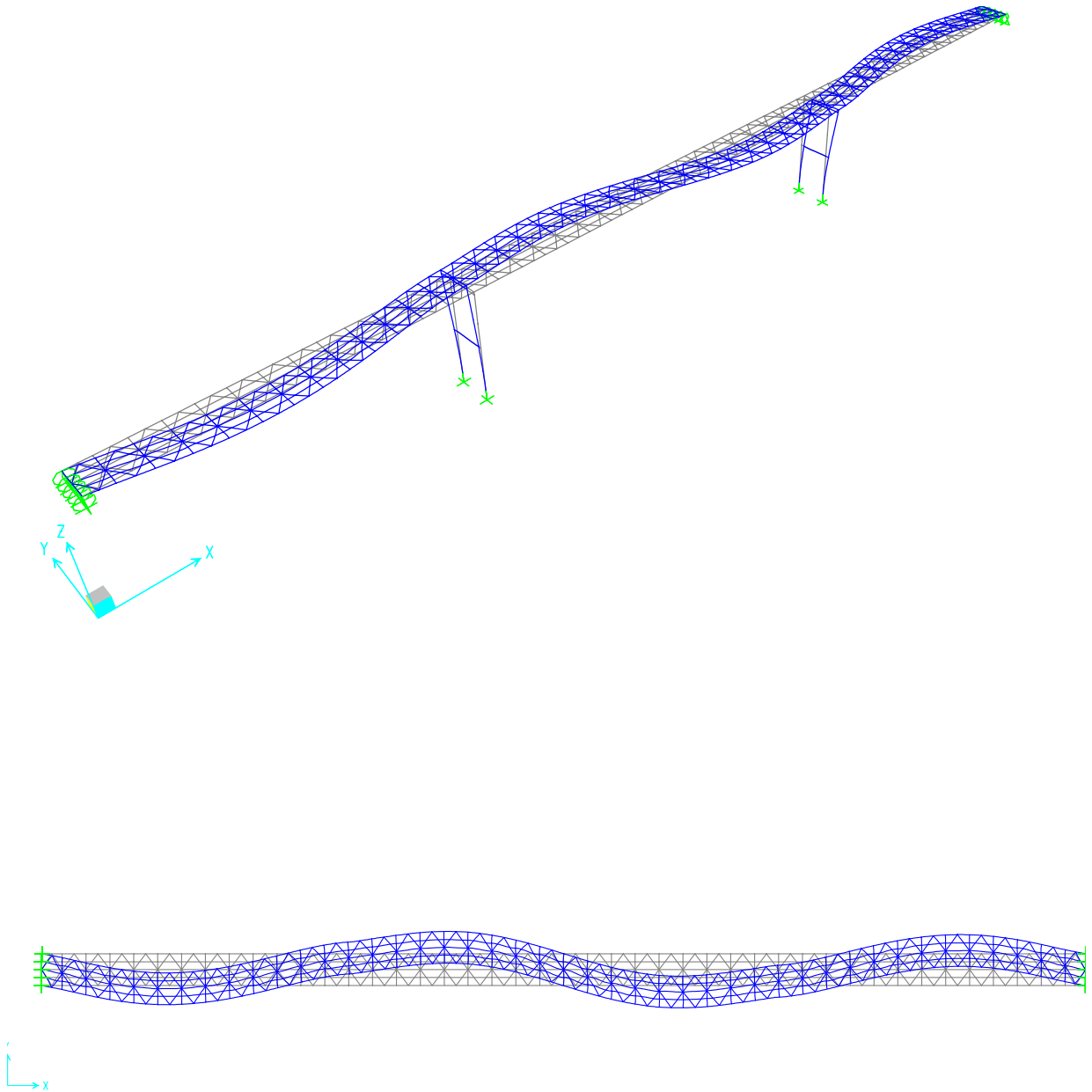
Figure 4.8 Isometric and plan views of the third transverse mode shape (2.601 Hz)
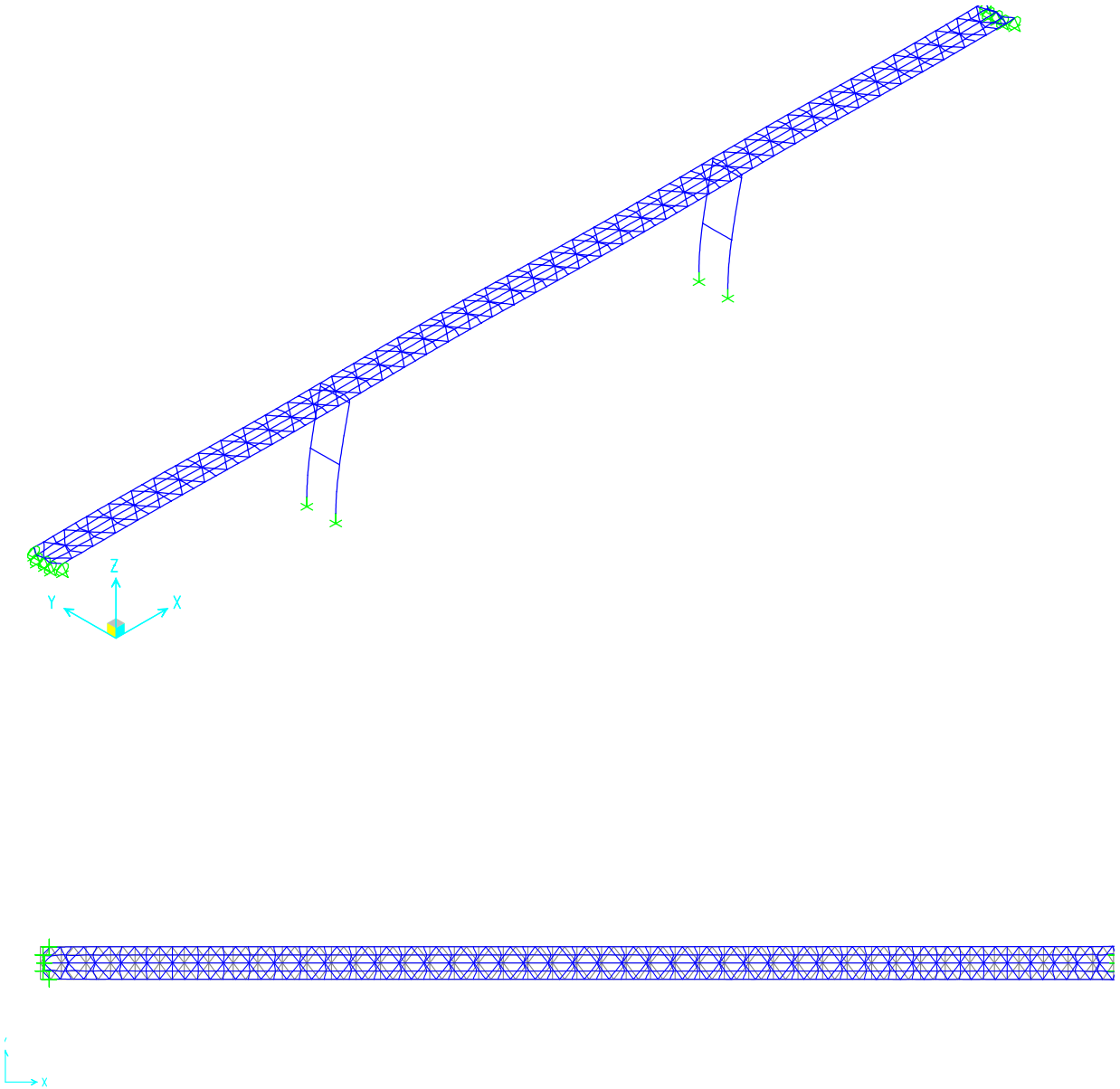
Figure 4.9 Isometric and plan views of the first longitudinal mode shape (2.853 Hz)
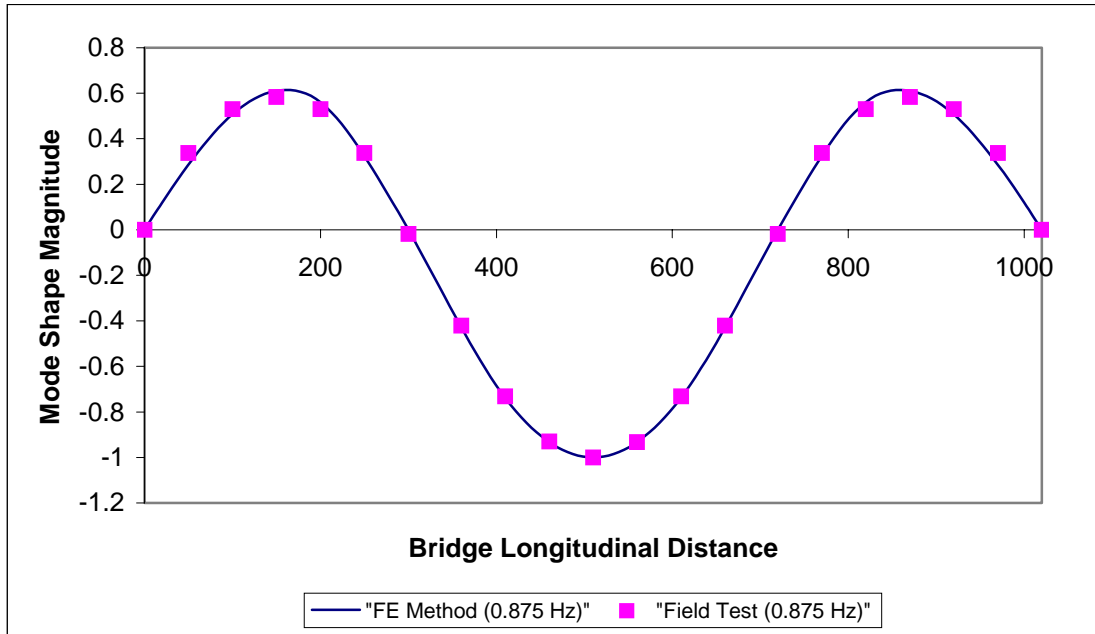
Figure 4.10 Comparison of 1st vertical mode between field test and finite element model
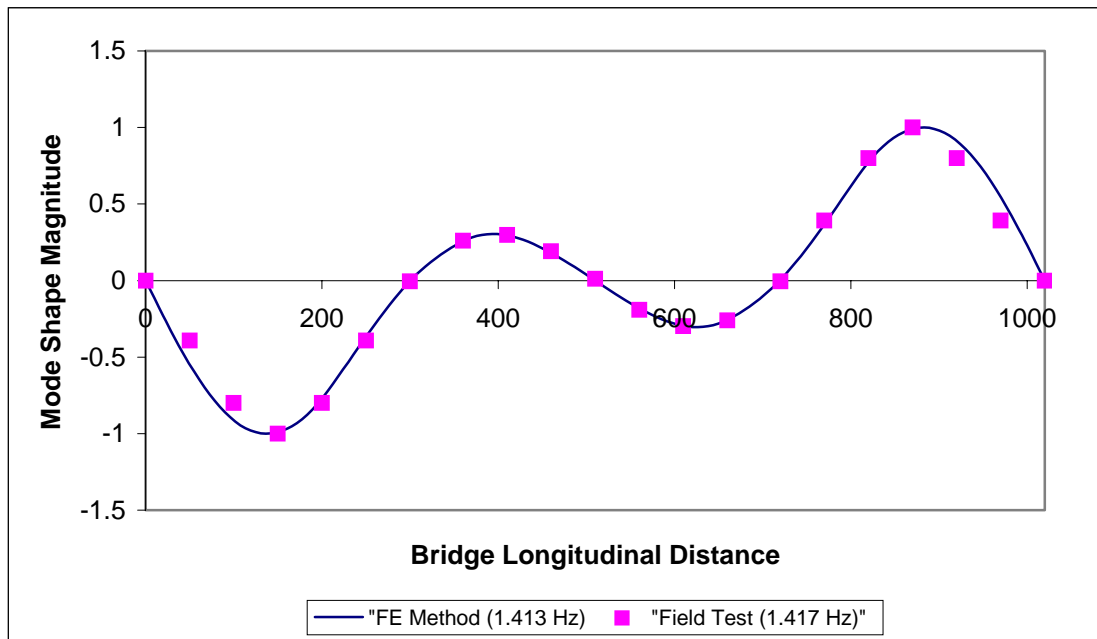
Figure 4.11 Comparison of 2nd vertical mode between field test and finite element model
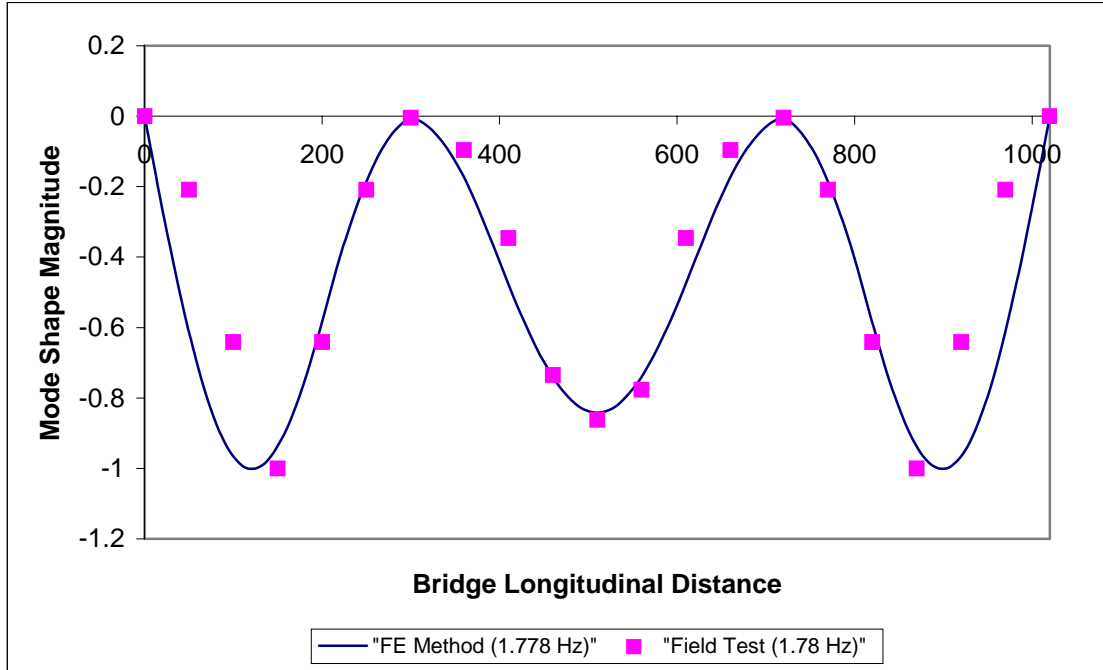
Figure 4.12 Comparison of 3rd vertical mode between field test and finite element model
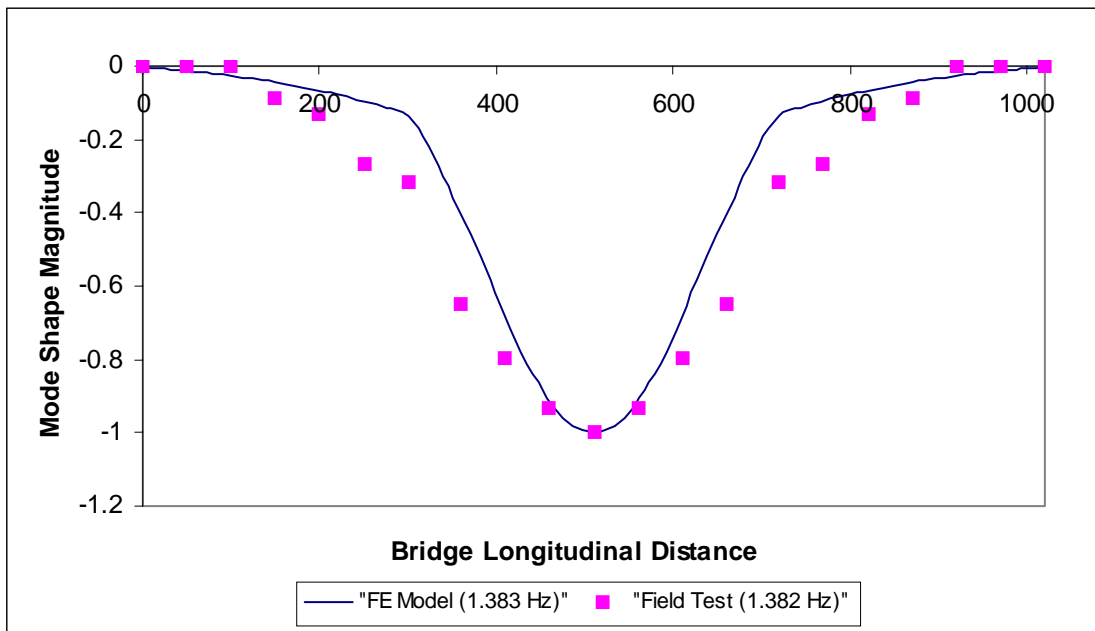
Figure 4.13 Comparison of 1st transverse mode between field test and finite element model
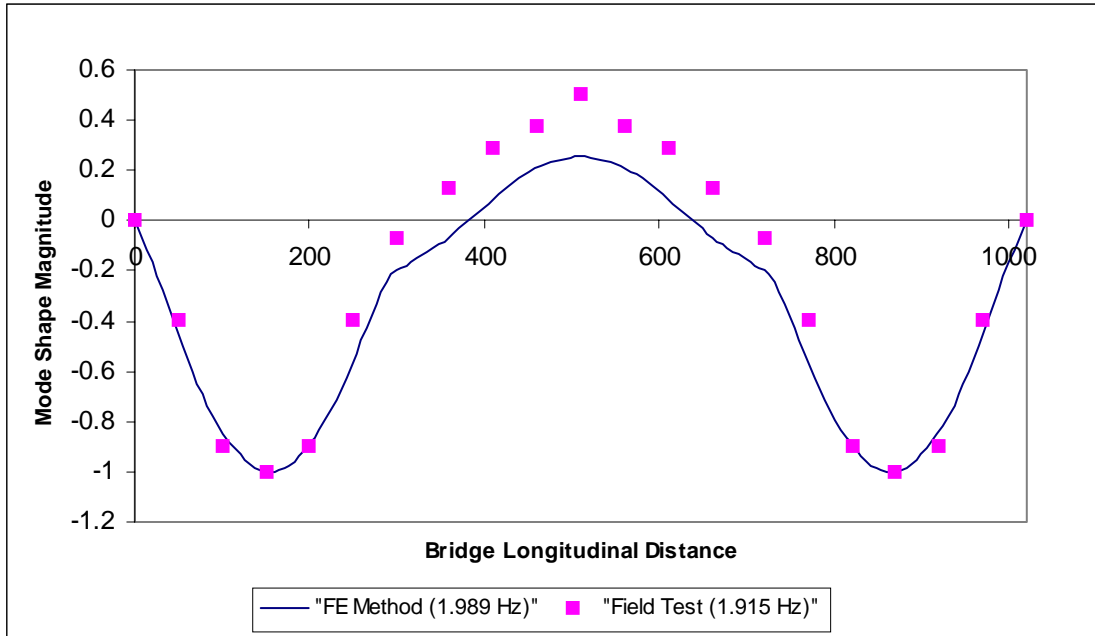
Figure 4.14 Comparison of 2nd transverse mode between field test and finite element model
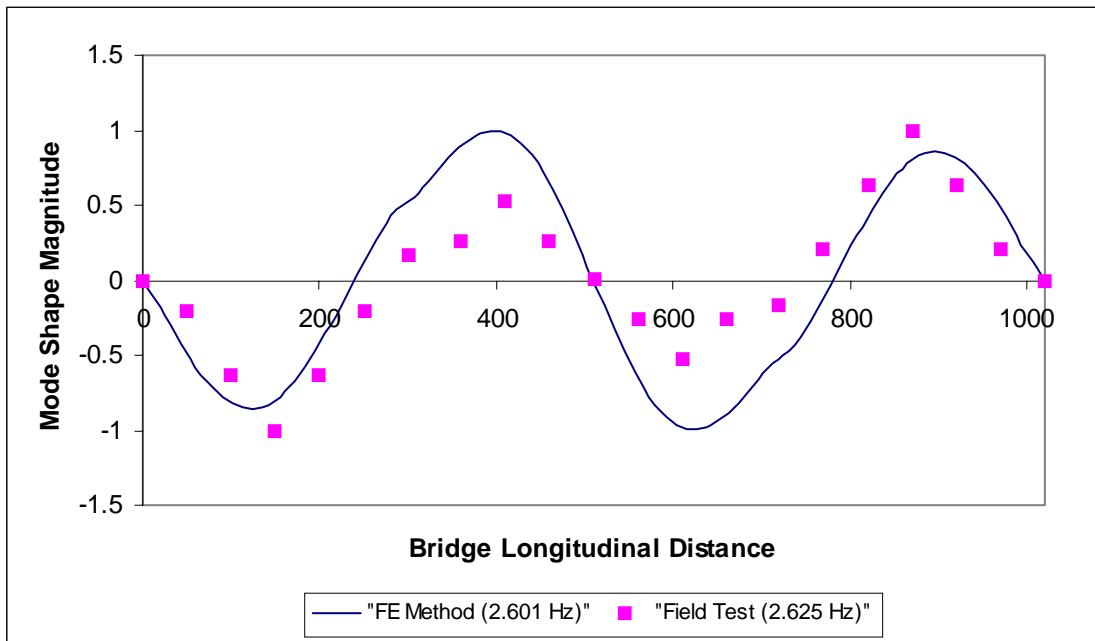
Figure 4.15 Comparison of 3rd transverse mode between field test and finite element model

Time History-Response Spectra (TR-250Y-0.xxg-x)
Identification Map for 90 Percent Probability of Not Being Exceeded in **250 Years**

▢ (blue)	0.40g-1
▢ (yellow)	0.19g-1
▢ (yellow)	0.19g-2
▢ (orange)	0.15g-1
▢ (tan)	0.15g-2
▢ (tan)	0.15g-3
▢ (white)	0.09g-1
▢ (gray)	0.09g-2

Routes

—— (red)	Interstate
—— (green)	Parkway
—— (cyan)	State

June 2001
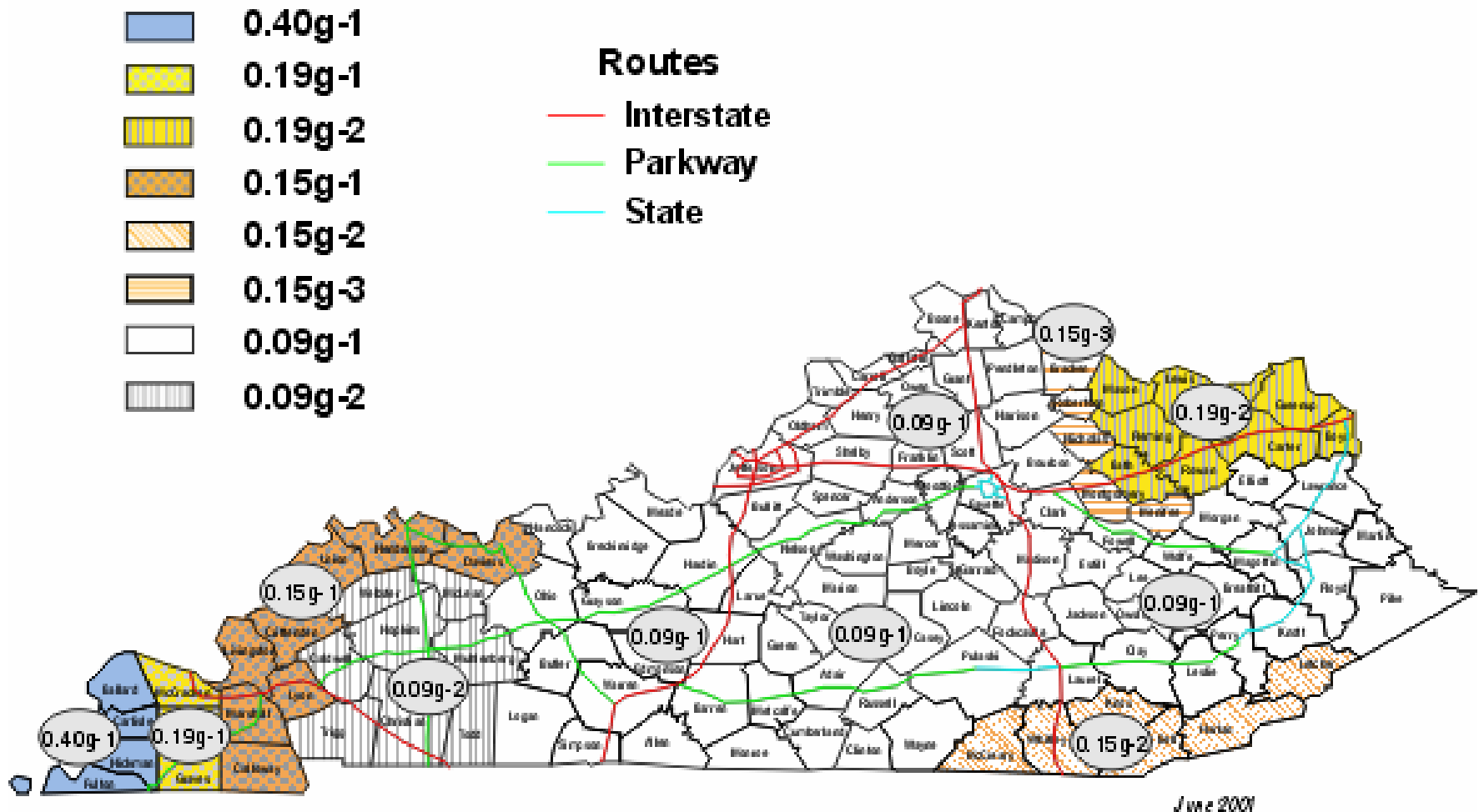
Figure 5.1 Time-history and Response spectra identification map for the Commonwealth of Kentucky (250-year event)

Time History-Response Spectra (TR-500Y-0.xxg-x)

Identification Map for 90 Percent Probability of Not Being Exceeded in **500 Years**

▦	0.60g-1	▦	0.15g-1
▦	0.40g-1	▦	0.15g-2
▦	0.30g-1	▦	0.09g-1
▦	0.19g-1	▦	0.09g-2
▦	0.19g-2	▦	0.09g-3
▦	0.19g-3	▦	0.09g-4

Routes

— Interstate
— Parkway
— State
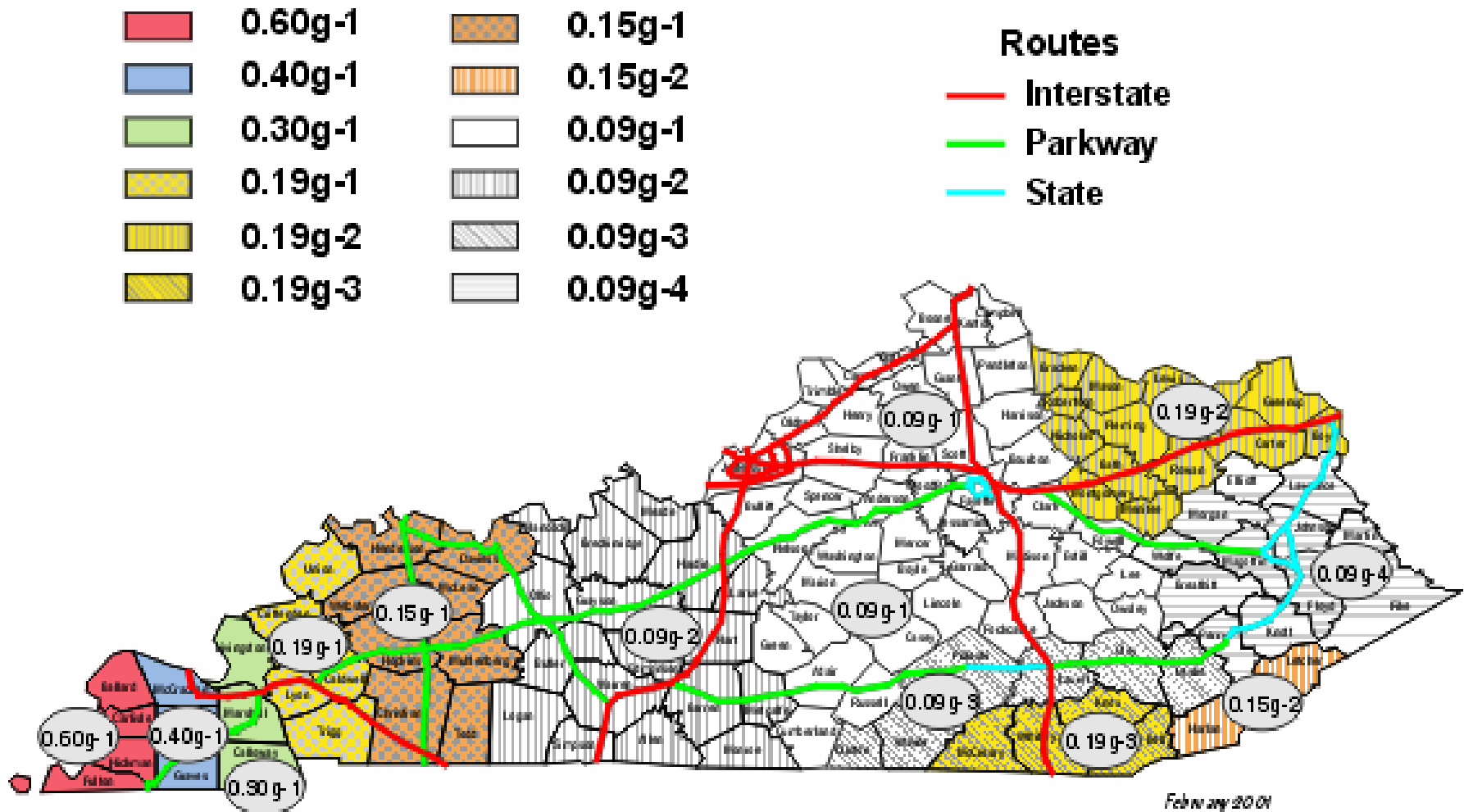
Figure 5.2 Time-history and Response spectra identification map for the Commonwealth of Kentucky (500-year event)

108
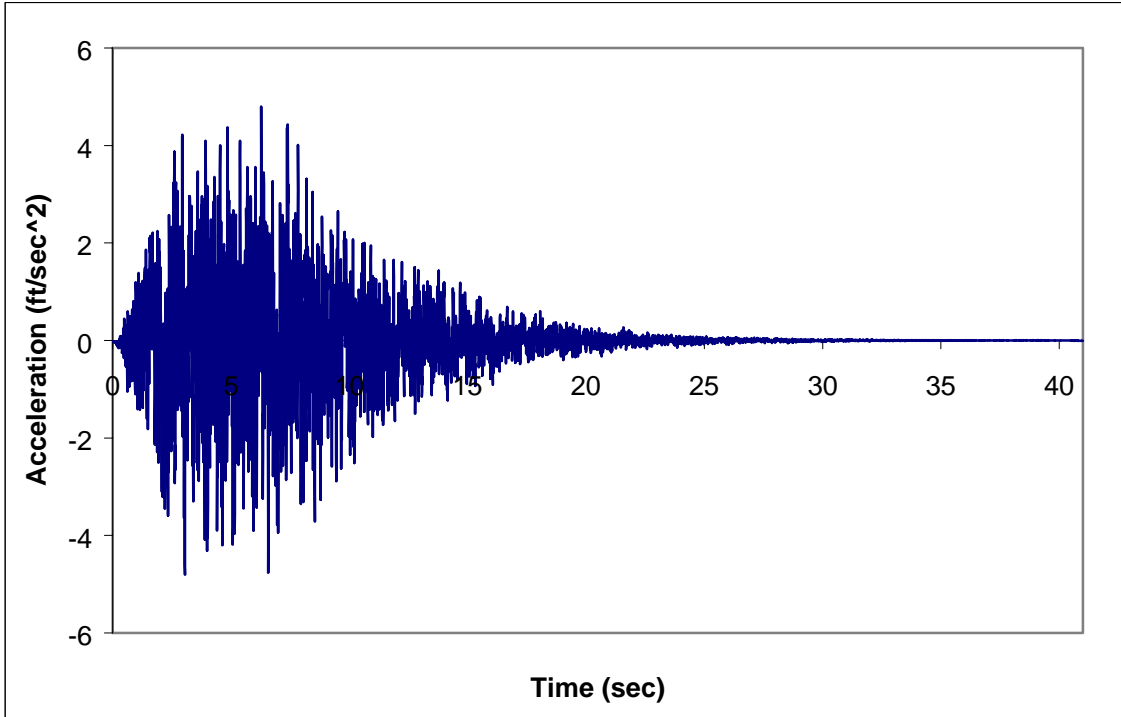
Figure 5.3 Acceleration-time history of the transverse component of the 250-year event
(Min. = –4.805 $ft/sec.^2$ at 3.050 $sec.$, and Max. = 4.800 $ft/sec.^2$ at 6.280 $sec.$)
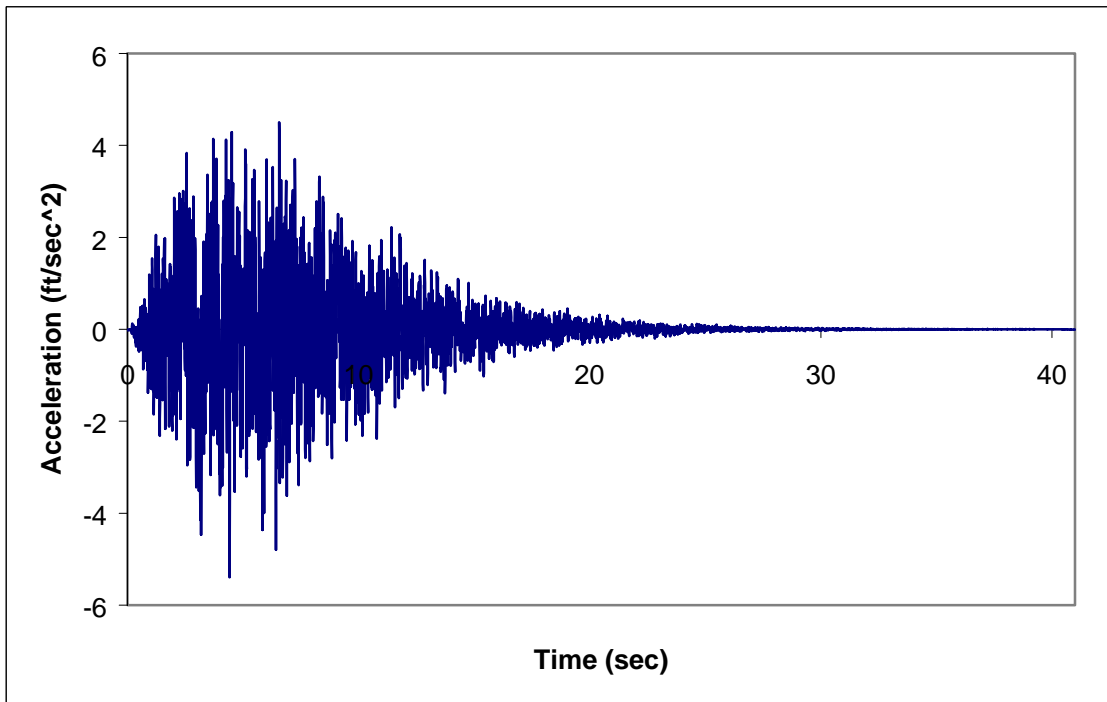
Figure 5.4 Acceleration-time history of the vertical component of the 250-year event
(Min. = –5.393 $ft/sec.^2$ at 4.420 $sec.$, and Max. = 4.506 $ft/sec.^2$ at 6.570 $sec.$)
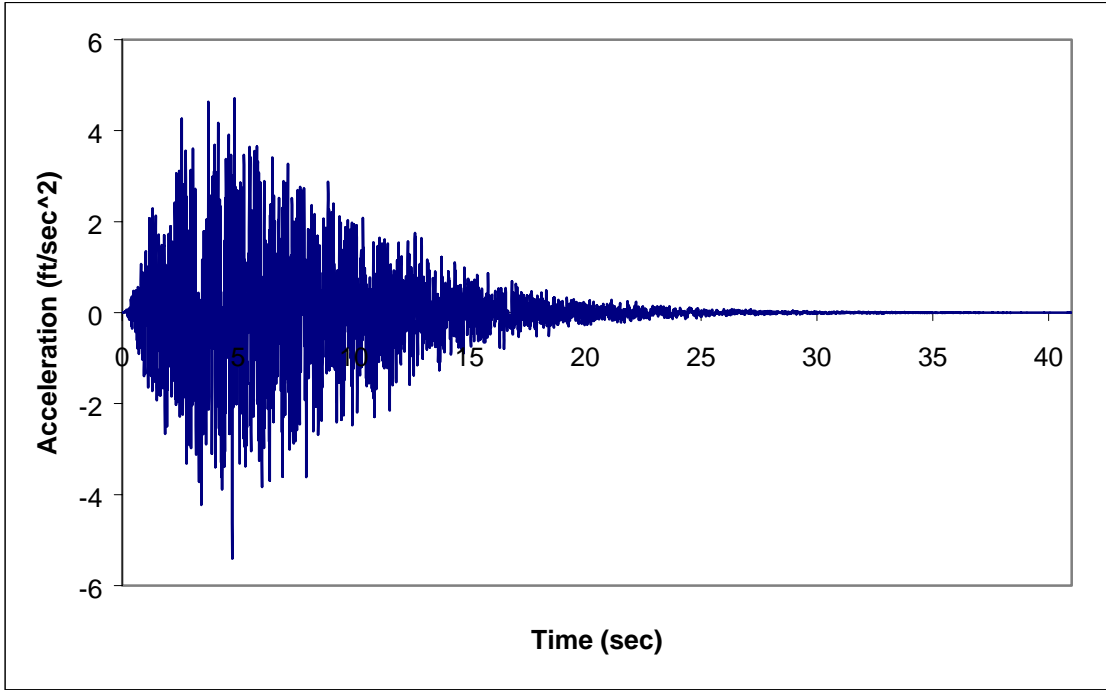
Figure 5.5 Acceleration-time history of the horizontal component of the 250-year event (Min. = –5.409 $ft/sec.^2$ at 4.750 $sec.$, and Max. = 4.704 $ft/sec.^2$ at 4.850 $sec.$)
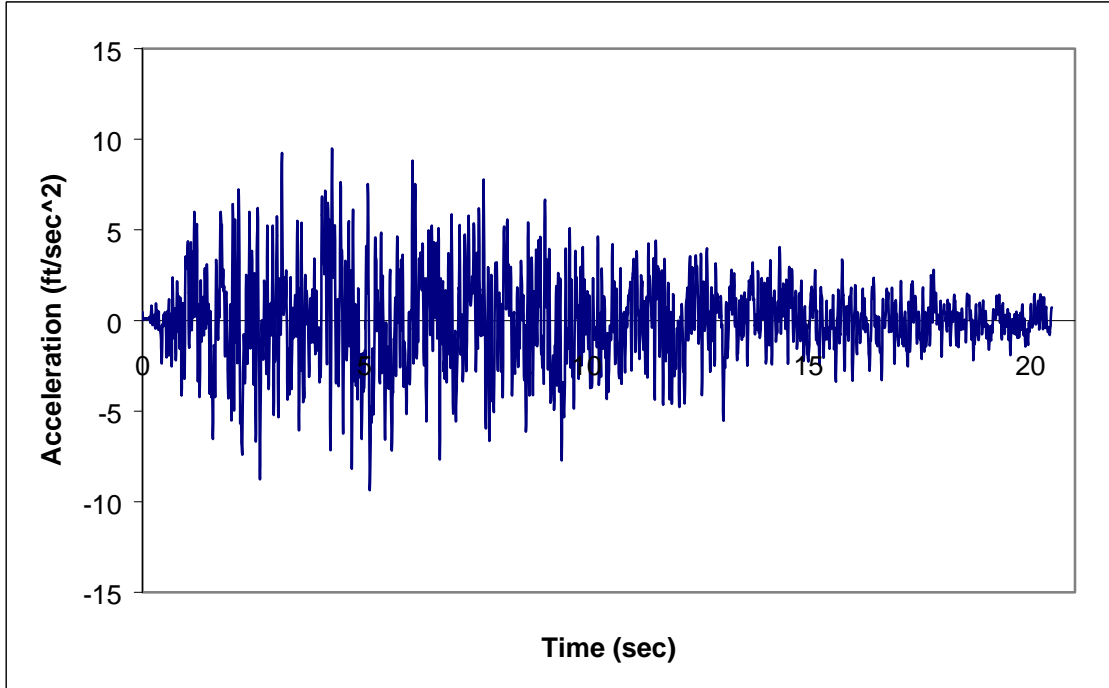
Figure 5.6 Acceleration-time history of the transverse component of the 500-year event (Min. = –9.372 $ft/sec.^2$ at 5.120 $sec.$, and Max. = 9.486 $ft/sec.^2$ at 4.265 $sec.)$
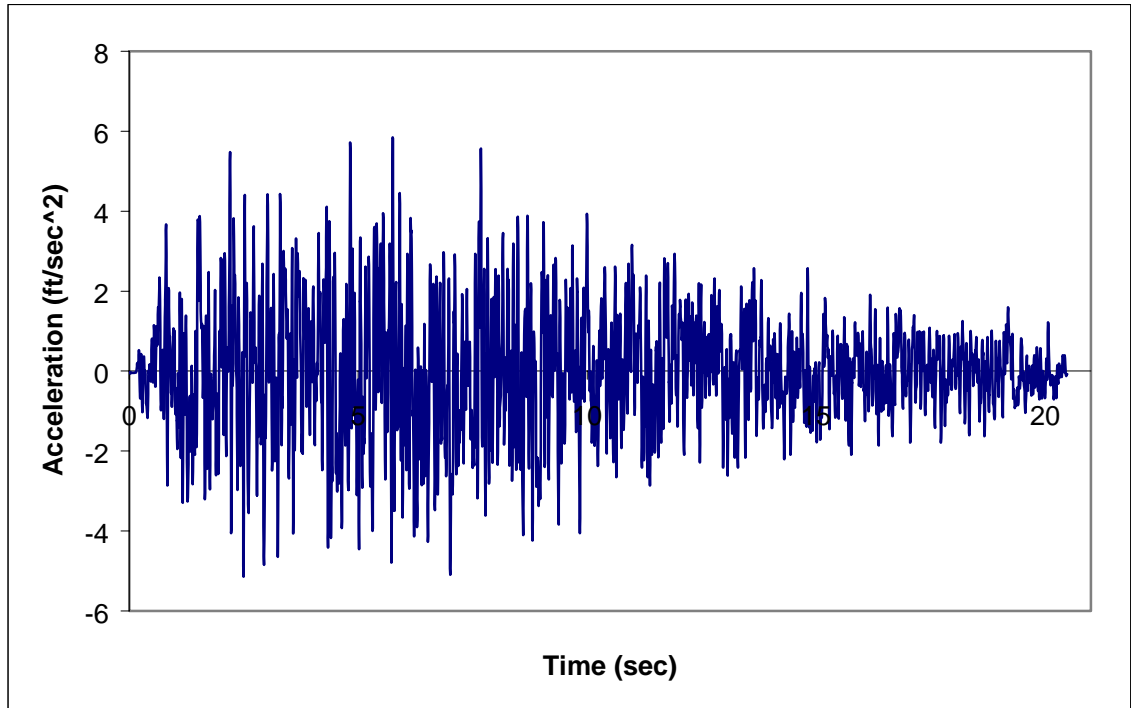
Figure 5.7 Acceleration-time history of the vertical component of the 500-year event
(Min. = –5.141 $ft/sec.^2$ at 2.495 $sec.$, and Max. = 5.850 $ft/sec.^2$ at 5.750 $sec.$)
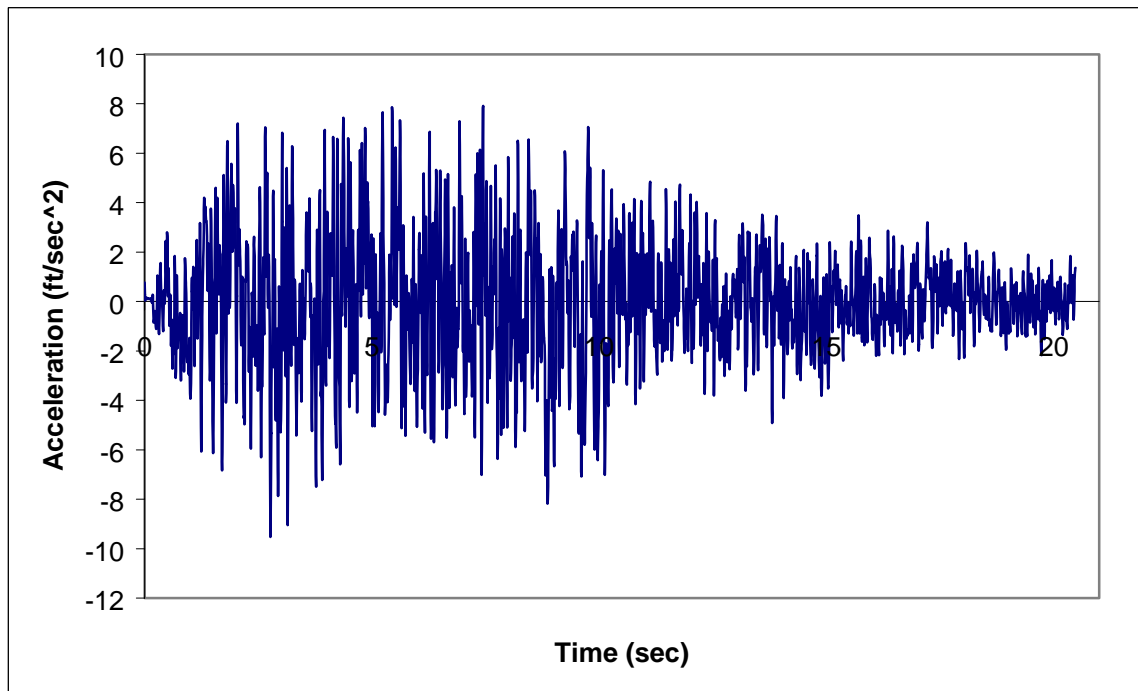
Figure 5.8 Acceleration-time history of horizontal component of the 500-year event
(Min. = –9.531 $ft/sec.^2$ at 2.770 $sec.$, and Max. = 7.917 $ft/sec.^2$ at 7.445 $sec.$)
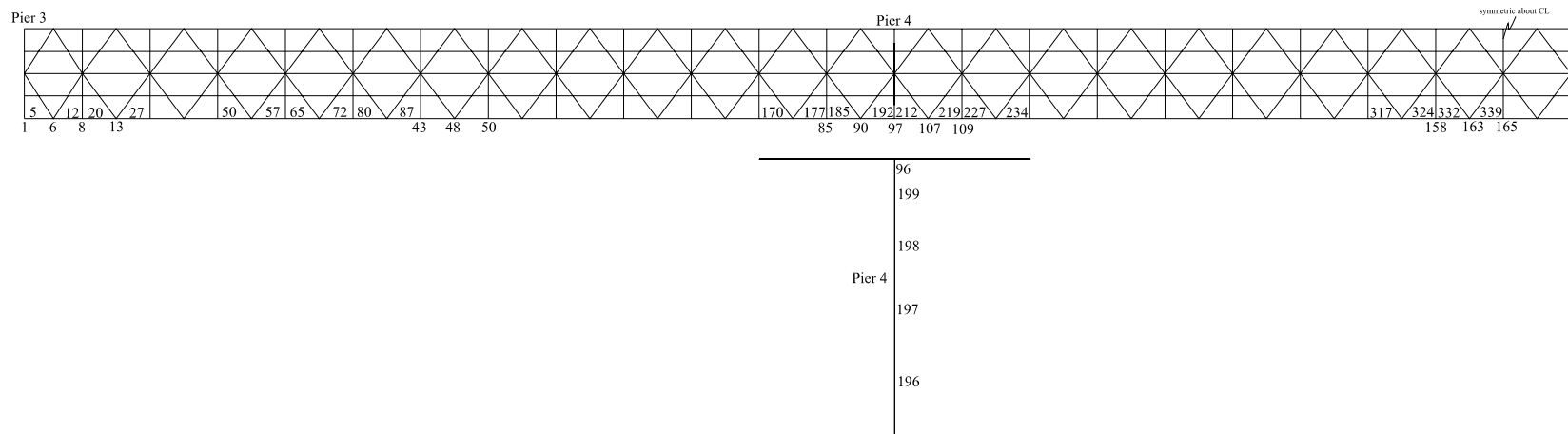
Figure 5.9 Plan and elevation views of the main bridge with frame and joint numbers

112
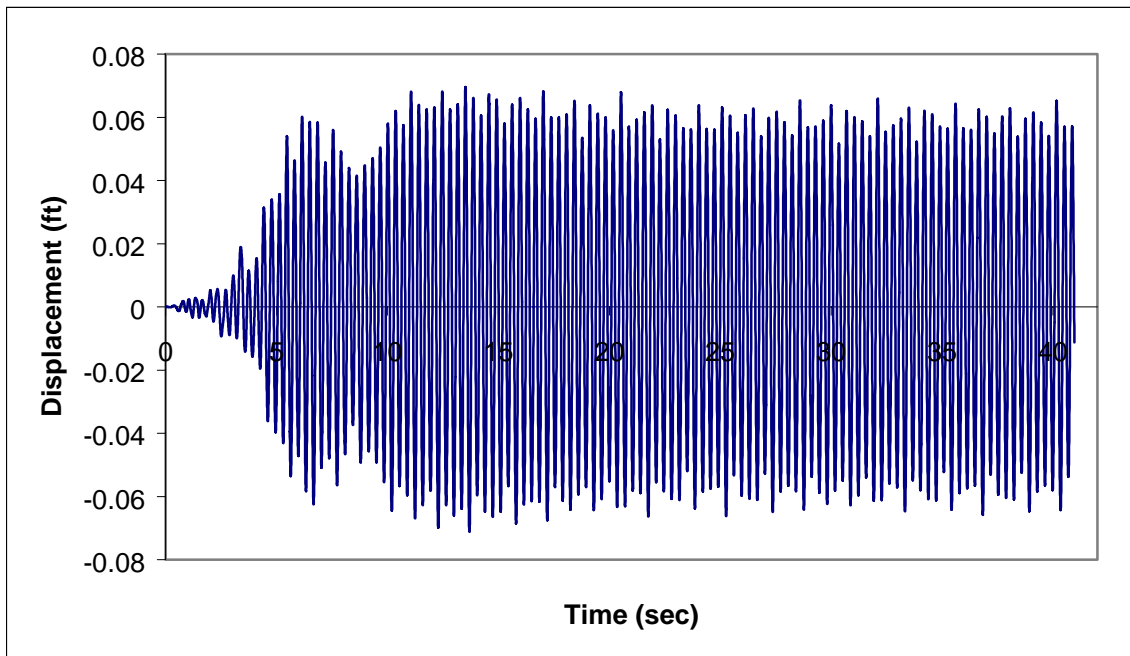
Figure 5.10 Displacement-time history in the longitudinal direction at node 90 under the *L1T2V3* excitation case (250-year event)
(Min. = –0.0712 *ft* at 13.70 *sec*., and Max. = 0.0696 *ft* at 13.52 *sec*.)
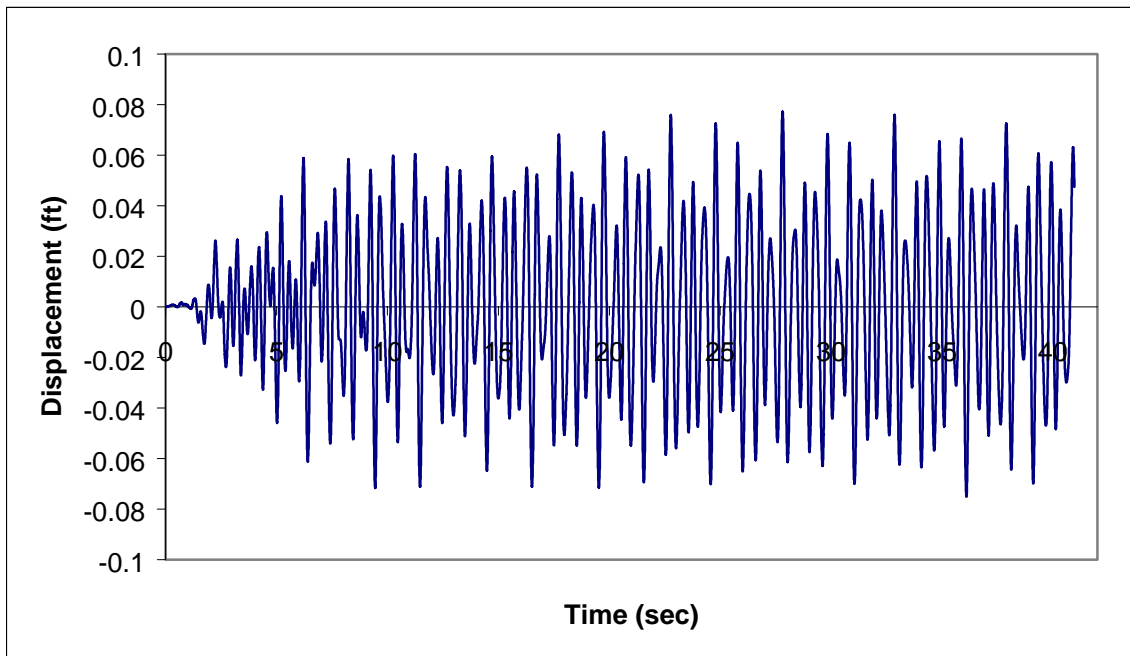
Figure 5.11 Displacement-time history in the transverse direction at node 90 under the *L1T2V3* excitation case (250-year event)
(Min. = –0.0751 *ft* at 36.10 *sec*., and Max. = 0.0772 *ft* at 27.81 *sec*.)
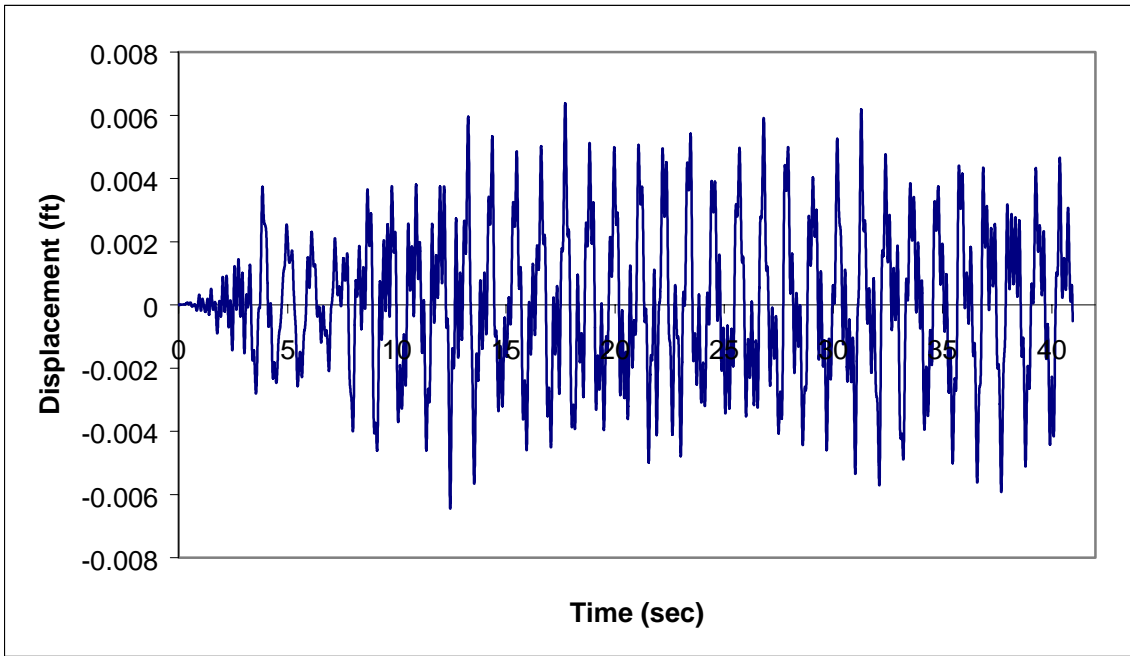
Figure 5.12 Displacement-time history in the vertical direction at node 90 under the
L1T2V3 excitation case (250-year event)
(Min. = –0.0645 *ft* at 12.44 *sec*., and Max. = 0.0639 *ft* at 17.71 *sec*.)
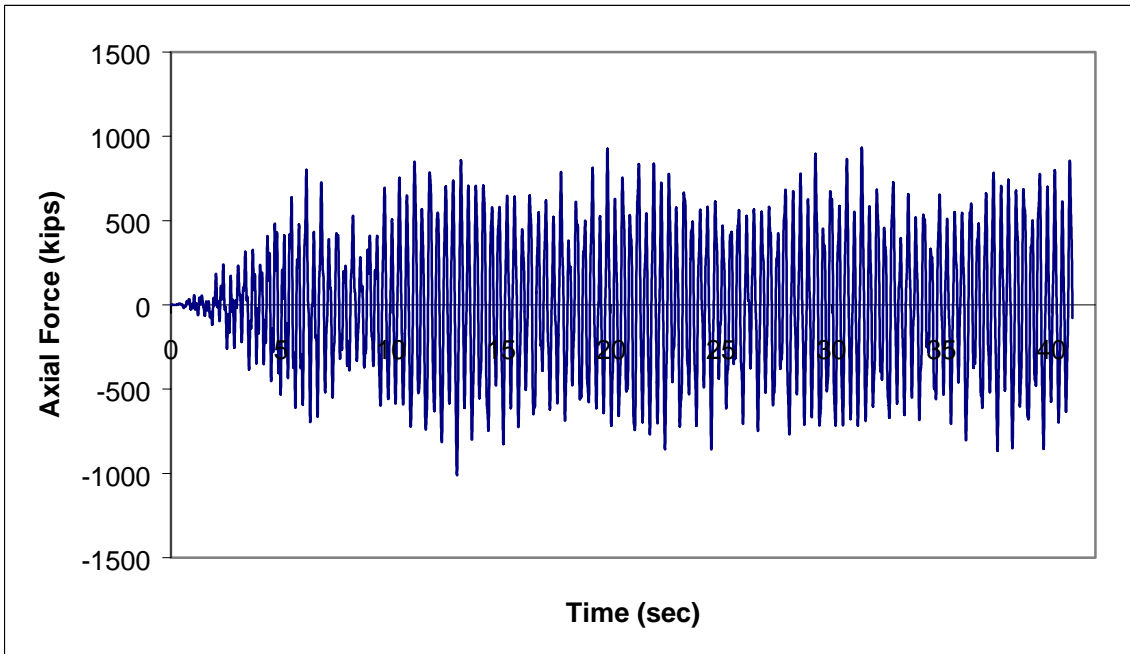
Figure 5.13 Axial force-time history of member 212 under the *L1T2V3*
excitation case (250-year event)
(Min. = –1009 *kips* at 13.00 *sec*., and Max. = 932.2 *kips* at 31.39 *sec*.)

114
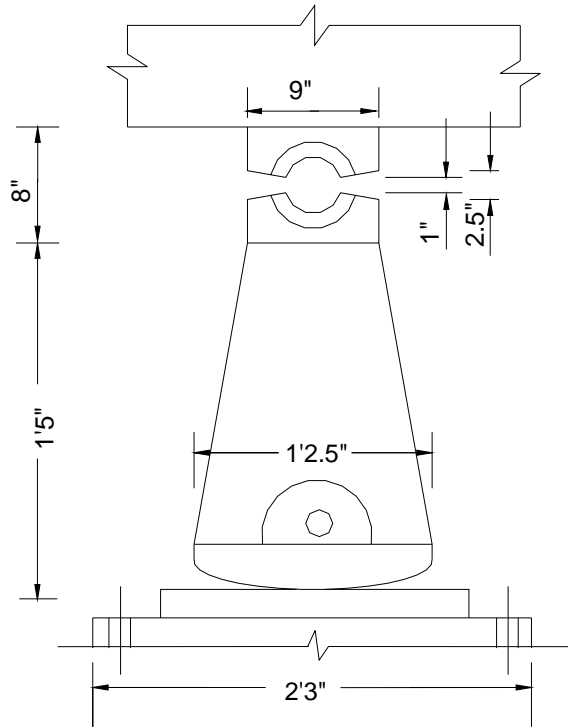
Figure 6.1 Expansion bearing for Pier 2
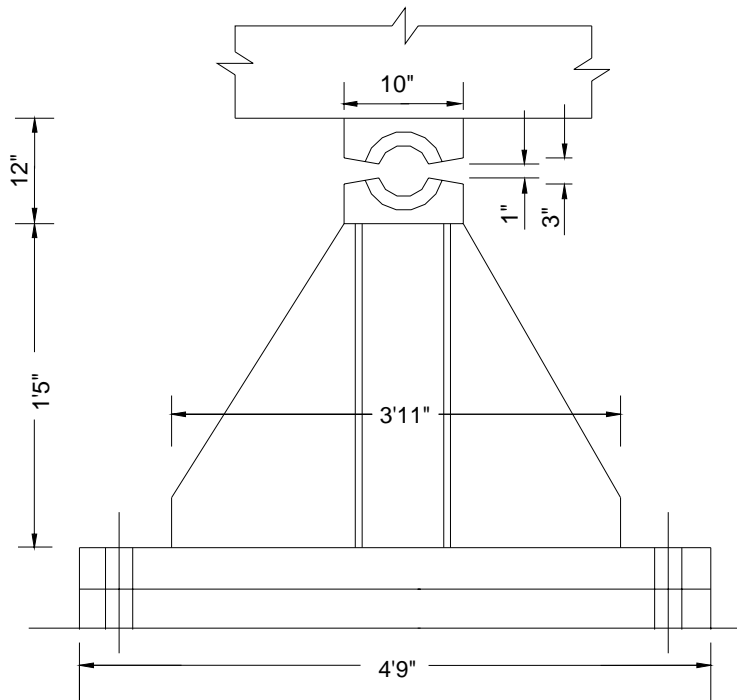
Figure 6.2 Fixed bearing for Pier 1

115
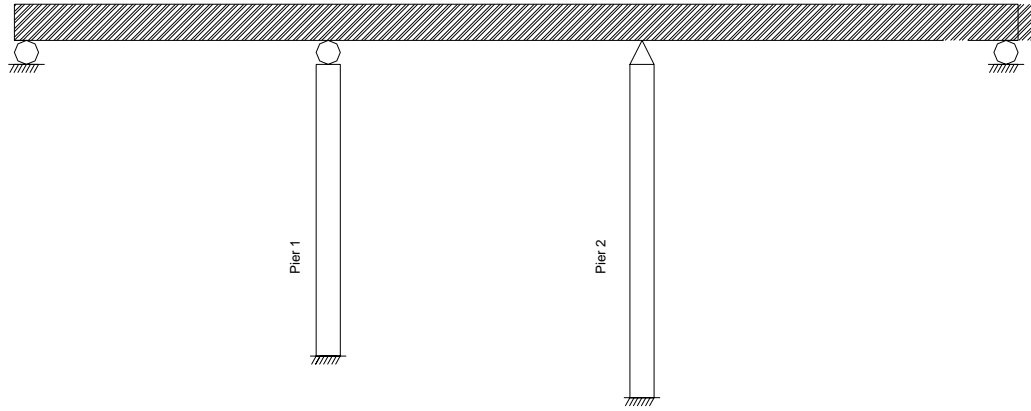
a) Piers are fixed at the bottom of pile caps
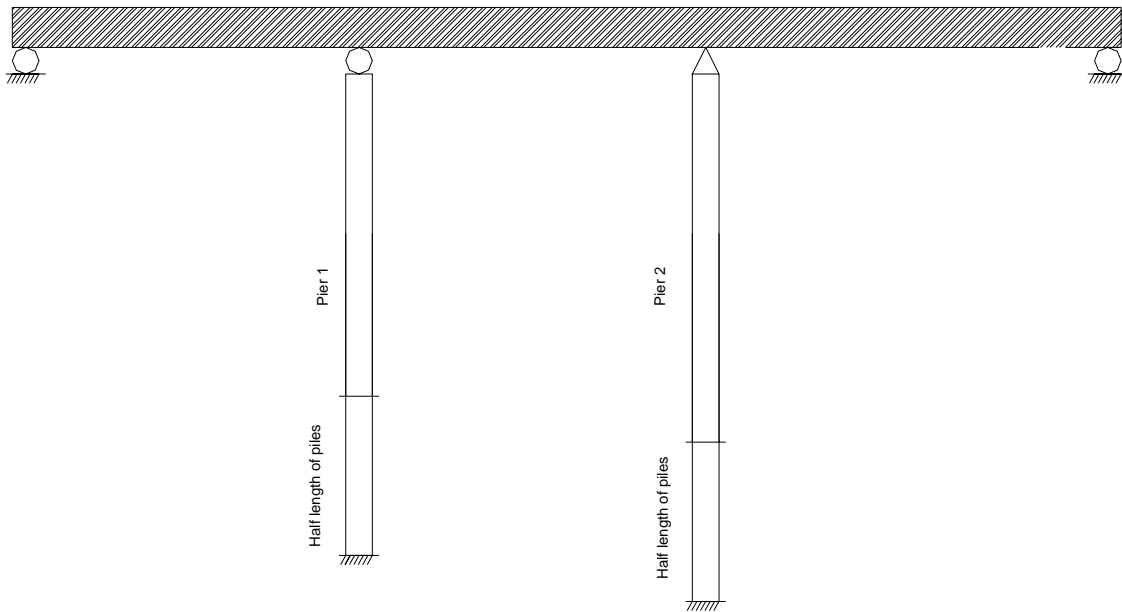
b) Piers are fixed at half-length of the piles

Figure 6.3 Analytical Model for the longitudinal direction
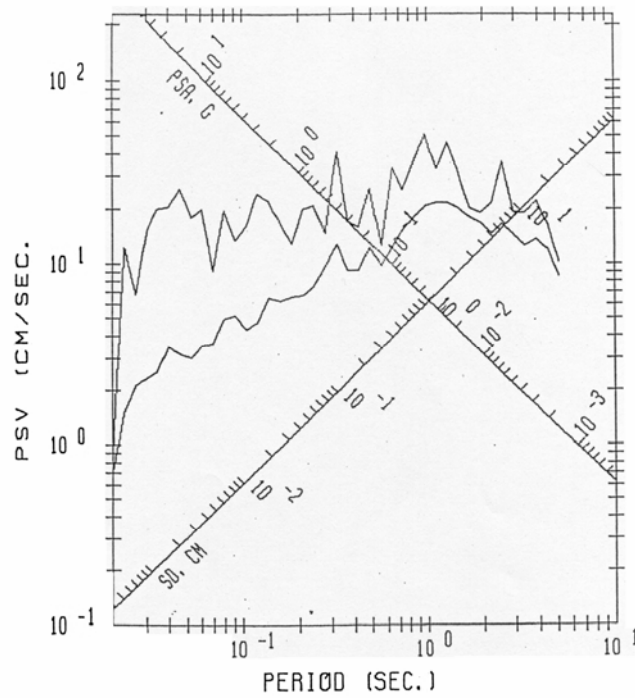
Figure 6.4 Response spectra for the horizontal component of the 250-year event (0.15g, Damping ratio=0.00 and 0.05)
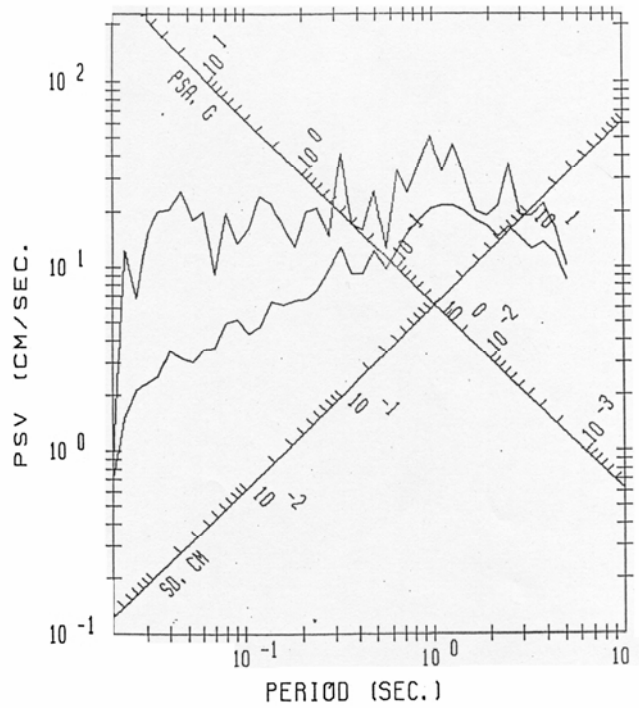
Figure 6.5 Response spectra for the transverse component of the 250-year event (0.15g, Damping ratio=0.00 and 0.05)
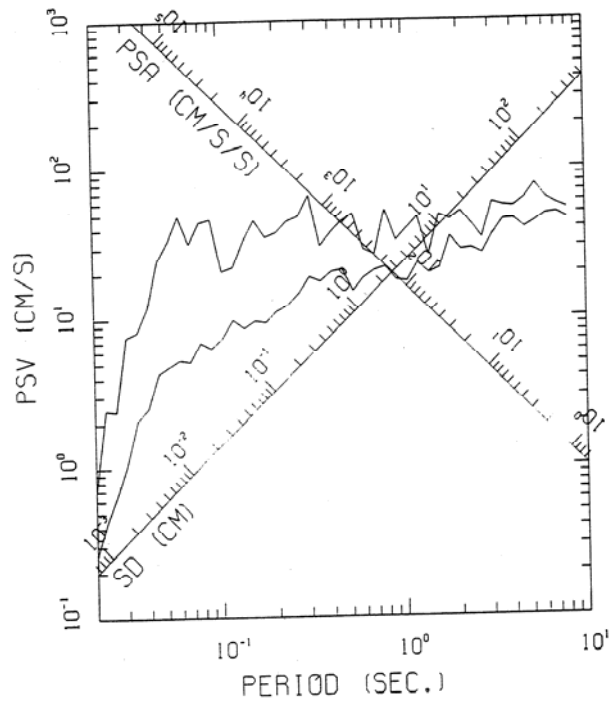
Figure 6.6 Response spectra for the horizontal component of the 500-year event (0.19g, Damping ratio=0.00 and 0.05)
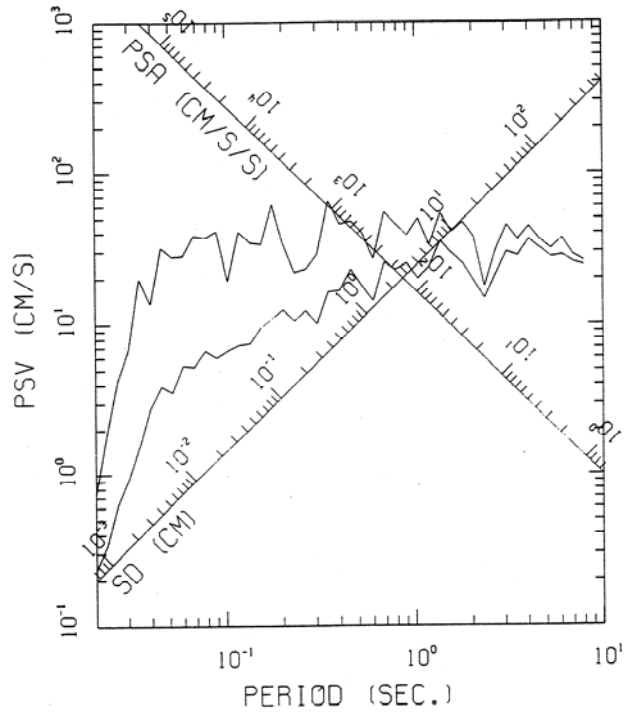
Figure 6.7 Response spectra for the transverse component of the 500-year event (0.19g, Damping ratio=0.00 and 0.05)

For more information or a complete publication list, contact us at:

KENTUCKY TRANSPORTATION CENTER

176 Raymond Building
University of Kentucky
Lexington, Kentucky 40506-0281

(859) 257-4513
(859) 257-1815 (FAX)
1-800-432-0719
www.ktc.uky.edu
ktc@engr.uky.edu